AEROSPACE REPORT NO.
ATR-74(8165-01)-1

Firebrand Phenomena

Prepared by

A. Muraszew
Vehicle Engineering Division

22 May 1974

DESIGNATED STATION REPRESENTATIVE: R. C. ROTHERMEL
NORTHERN FOREST FIRE LABORATORY
INTERMOUNTAIN FOREST AND RANGE EXPERIMENT STATION
Missoula, Montana

Prepared for
USDA FOREST SERVICE
Washington, D. C.

Engineering Science Operations

THE AEROSPACE CORPORATION

Report No.
ATR-74(8165-01)-1

FIREBRAND PHENOMENA

Prepared by

A. Muraszew
Vehicle Engineering Division

22 May 1974

Engineering Science Operations
THE AEROSPACE CORPORATION
El Segundo, California

Report No.
ATR-74(8165-01)-1

FIREBRAND PHENOMENA

Approved

E. G. Hertler, Director
Aero Engineering Subdivision
Vehicle Engineering Division

S. D. Huffman, Group Director
National Resources
Civil Programs Division

ACKNOWLEDGMENTS

The author gratefully acknowledges the assistance of his colleagues at The Aerospace Corporation, namely P. G. Crowell and J. Vasiliu in the wood heating problem, Dr. A. M. Rodriguez in the formulation of the statistical model, E. K. Weinberg in the thermochemistry problems of cellulose fuels, and P. H. Young in the programming of the trajectory model.

The section on the convection column was written under joint authorship with Dr. W. C. Kuby, of the University of California at Santa Barbara, and his valuable contributions in the formulation of a simplified model are greatly appreciated.

This program was based on the fire spread model of Rothermel, the contagion model of O'Regan, and the analytic fuel model of Philpot.

CONTENTS

CONTENTS (Continued)

TABLES

FIGURES

FIGURES (Continued)

1. INTRODUCTION

The investigation of the firebrand phenomena was a part of a broader task to provide the fire fighting agencies with an analytical tool for assessment of wild fire hazard by predicting the fire spread rate as a function of fuel type, topography, and ambient conditions (wind, temperature, moisture).

The method of calculation of a continuous progress of a fire front was given in an Aerospace Corporation computer program called Fire Spread Simulation Program. This program was based on the fire spread model of Rothermel and on the contagion modeling of O'Regan and Kourtz. However, the progress of a fire front, particularly in large fires, is often characterized by hitherto unpredicted spot fires generated at some distance from the main fire front by flying firebrands. These spot fires may in some cases spread rapidly and form unexpected and often dangerous secondary fire fronts which may entrap equipment and personnel.

The objective of this work is to provide a quantitative assessment of a firebrand-caused spot fire hazard as a function of the fire front intensity, topography, and wind. To achieve this goal, the complete history of firebrands, from their birth in a convection column to their impact in a recipient fuel array, had to be considered and expressed in analytical terms.

A graphical representation of a spot fire origin is presented in Fig. 1. The fire front is shown to generate either a two-dimensional or vortex type convection column. This convection column, with the aid of ambient winds, lifts the firebrands and carries them ahead of the main fire front. During the flight, firebrands continue to burn either by glowing or flaming until they either burn out in flight or impact the ground. After impact they will generally continue to flame or glow, and if the impact area is covered by fuel suitable for ignition, flame propagation may follow, leading to a spot fire generation. If the probability of that spot fire occurring can be expressed statistically, then this information could be fed into the Fire Spread Simulation Program and provide a more complete picture of the fire spread forecast.

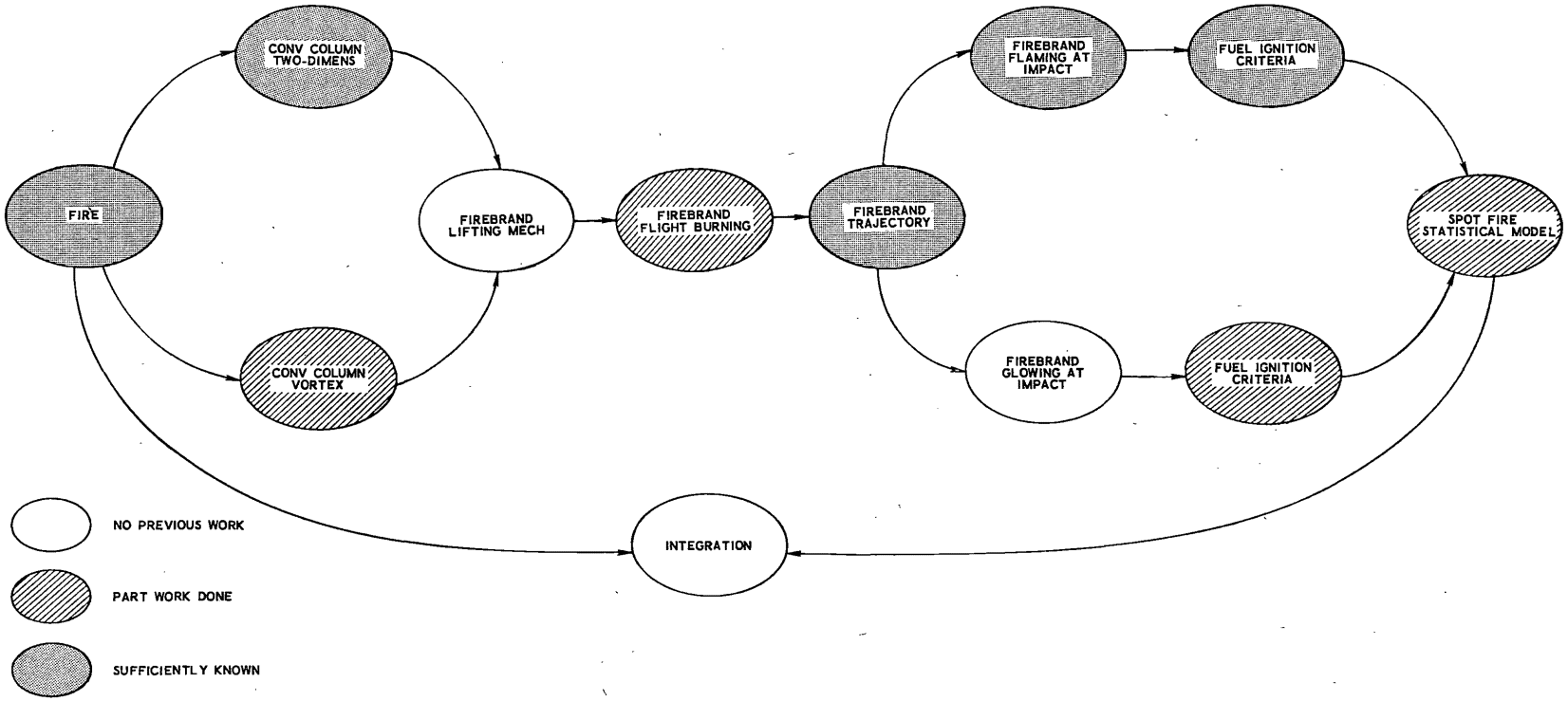

Fig. 1. Analytical Model for a Spot Fire

Figure 1 also gives an indication of the existing knowledge on firebrands. The shaded ellipses indicate areas in which a substantial amount of work on firebrands and related problems has been performed by many researchers who are quoted in this report. The blank ellipses show areas where little or no work was done. These include: firebrand lifting mechanism (firebrand generation function); heat transfer from glowing firebrands; and integration of spot fire statistical model into a general fire spread simulation model. In Section 6 work in these areas is recommended.

This report will cover the following phases of firebrand history: (1) definition of firebrand trajectory and burning process in flight; (2) characterization of two-dimensional convection column; (3) analysis of firebrand flaming process after impact; (4) definition of recipient fuel ignition criteria; (5) description of a preliminary model for prediction of spot fire probability.

Since the entire history of a firebrand is a rather complex problem, it was the author's intention to describe the various phases by means of simple analytical expressions using as inputs fuel data, topography and ambient air data usually available to the fire fighters.

Finally, conclusions are presented regarding the need for further analytical and experimental work which should be done to provide the answers still lacking in the understanding of firebrand phenomena.

2. FIREBRAND TRAJECTORIES

2.1 REVIEW OF PAST WORK

Firebrand trajectories have been investigated by several researchers, although laboratory experimental data for the verification of the analyses are scanty and any field data obtained are qualitative at best.

Most of the analyses and laboratory experiments were performed by C.S. Tarifa[1] who considered the firebrand trajectory to be a function of two forces: drag caused by the relative velocity of the firebrand with respect to the surrounding air, and gravity. Tarifa also assumed that the center of pressure of the aerodynamic drag is at any time at the center of gravity of a firebrand.

Some experimental work on firebrand fall velocity was carried out by H.P. Clements,[2] who measured the velocities of burning firebrands in a vertical wind tunnel. However, his data did not include firebrand sizes or weights; consequently, they are of limited usefulness only.

S.L. Lee and J.M. Hellman[3] studied firebrand trajectories using Tarifa's data to describe the change in firebrand density and diameter. They also presented a model of a swirling convection column. The axisymmetrical column was found to be a function of a source Froude number and a source swirling velocity parameter.

The density of the firebrand was assumed[3] to be constant during the latter part of the burning process and the variation in diameter based on Tarifa's data was defined as

$$\left(\frac{D}{D_o}\right)^2 = 1 - B[w \cdot t/D_o]^{2.5}$$

where

B = constant

D = firebrand diameter, cm

D_o = initial firebrand diameter, cm

t = burn time, sec

w = firebrand velocity relative to wind, cm/sec

Based on this burn law and the convection column model, trajectories of firebrands were calculated in a manner similar to that used by Tarifa.

In this study, it was decided to use Tarifa's trajectory model because it was correlated with his experimental data and it was at least partially verified. Tarifa's analysis was extended by the author to include the relationship for a firebrand diameter and density change with time in order to be able to define firebrand conditions at any point in the trajectory.

A trajectory model was programmed at The Aerospace Corporation, and it provides options for varying vertical velocity in the convection column, wind with altitude, and ground slope.

2.2 TRAJECTORY ANALYSIS

With Tarifa's approach, a two-dimensional model of a firebrand is considered in a vertical plane containing the wind (or convection column) and firebrand velocities (Fig. 2). Where

A = firebrand maximum cross-section, cm^2

C_D = drag coefficient

g = gravitational constant, cm/sec^2

m = firebrand mass, g

u = wind velocity, cm/sec

v = absolute velocity of a firebrand, cm/sec

α = angle between firebrand and wind velocity vector, deg

ρ = firebrand or wood density, g/cm^3

the following equation of motion can be written

$$m \cdot \dot{v}_x = m \cdot \dot{u}_x - m \cdot \dot{w}_x = \frac{1}{2}\rho C_D \cdot Aw^2 \cdot \cos\alpha = \frac{1}{2} C_D \cdot Aw^2 \cdot \frac{w_x}{w} \tag{1}$$

$$m \cdot \dot{v}_y = m \cdot \dot{u}_y - m \cdot \dot{w}_y = \frac{1}{2}\rho C_D \cdot Aw^2 \cdot \sin\alpha - m \cdot g$$

$$= \frac{1}{2}\rho C_D \cdot Aw^2 \cdot \frac{w_y}{w} - m \cdot g \tag{2}$$

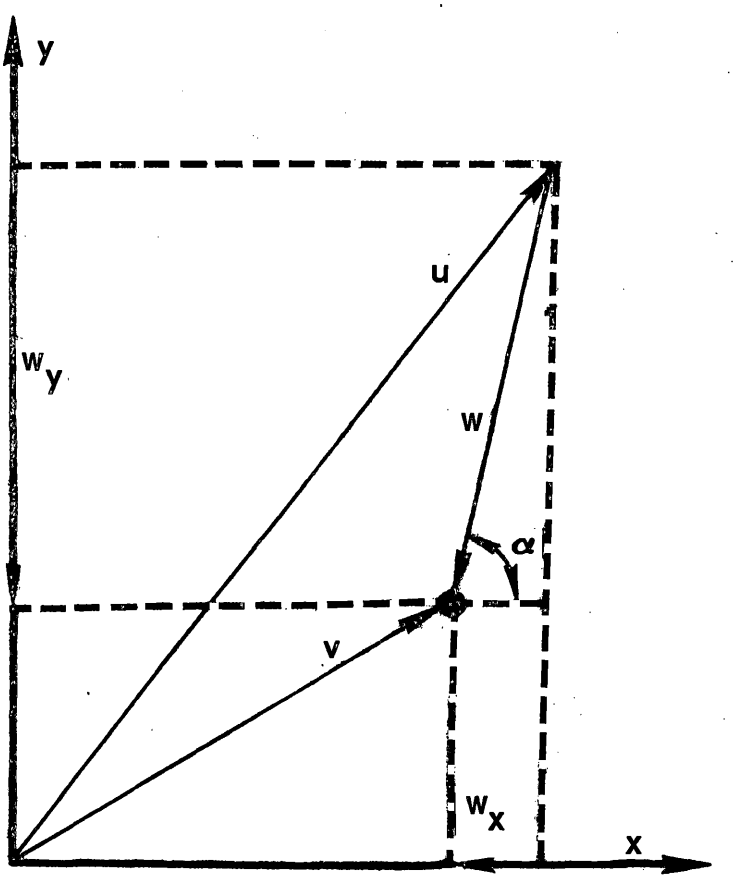

Fig. 2. Firebrand Velocity Diagram

With constant wind conditions in a given interval of time, Eqs. (1) and (2) can be written as

$$\dot{w}_x + \frac{1}{2}\left(\rho C_D \cdot \frac{A}{m}\right) w \cdot w_x = 0 \qquad (1a)$$

$$\dot{w}_y + \frac{1}{2}\left(\rho C_D \cdot \frac{A}{m}\right) w \cdot w_y - g = 0 \qquad (2a)$$

When a particle is burning, its mass, area, and drag coefficient are functions of time and relative wind speed. These functions cannot be analytically defined, and a semi-empirical approach was used by Tarifa to obtain the required relationship, as shown below.

The horizontal and vertical components of the trajectory can be defined as follows:

$$X = \int_o^t \left(u_x - w_x\right) dt \qquad (3)$$

$$Y = \int_o^t \left(u_y - w_y\right) dt \qquad (4)$$

If the components of wind velocity u are assumed to be known, then once $w_x = f(t)$ and $w_y = f(t)$ are defined, the trajectories can be calculated.

Tarifa has shown that for a constant value of the parameter $(1/2)\rho \cdot C_D \cdot A/m$, the values of w_x are converging rapidly to 0, and the value of w_y to the final fall velocity $w_{f(t)}$, which can be defined as

$$w_{f(t)} = \left(\frac{m \cdot g}{\frac{1}{2} C_D \rho A}\right)^{1/2} \qquad (5)$$

This is shown in Fig. 3, which illustrates the case of a firebrand having initial relative vertical velocity in excess of its fall velocity (solid line) and another firebrand in which initial relative vertical velocity was 0 (dotted line). In both cases the relative vertical velocity converged rapidly to the fall velocity and the relative horizontal velocity converged to 0.

The assumption of a constant initial value of the parameter $(1/2)C_D\rho(A/m)$ is a realistic one since there is a pre-ignition period in the life of a firebrand during which it can be lifted in the convection column without appreciable changes in its mass or dimension. Furthermore, since the life of a firebrand is usually measured in minutes, the initial transient condition of three to four seconds can be neglected and it can be assumed that the firebrand travels with a horizontal velocity $w_x = 0$ and a vertical relative velocity $w_y = w_{f(t)}$.

The definition of $w_{f(t)}$ as a function of time, of firebrand variables, and of the surrounding air properties was obtained by Tarifa[1] based on experimental data for various types of wood, and various sizes and shapes of firebrands comprised of square plates, cylinders, and spheres. The ratio of $w_{f(t)}/w_{fo}$ (instantaneous to initial fall velocity) was expressed by him as a function of parameter Z, where

$$Z = \frac{w_{fo} \cdot t}{D_o} \left(\frac{w_{fo} \cdot D_o \cdot \rho_a}{\mu_a} \right)^{-0.4} \cdot \left(\frac{\rho_a}{\rho_{wo}} \right)^{1.3} \cdot \left(\frac{L_o}{D_o} \right)^{-0.4} \cdot k \quad (6)$$

where ρ_a, μ_a denotes air density and absolute viscosity, respectively; ρ_{wo} is virgin wood density, L_o, D_o, w_{fo} are firebrand initial length, diameter, and fall velocity, respectively; t is burn time and k, shape factor, is a constant. The curve showing Tarifa's mean values from his experimental data is shown in Fig. 4. The calculations made by using the Aerospace model for a few sizes and shapes of wood are also plotted in the figure and show good agreement. Tarifa subsequently approximated the mean experimental curve by two exponential functions, one for $0 \leq w_{f(t)} \leq 0.9\, w_{fo}$, and the other for $0.9\, w_{fo} \leq w_{f(t)} \leq w_{fo}$.

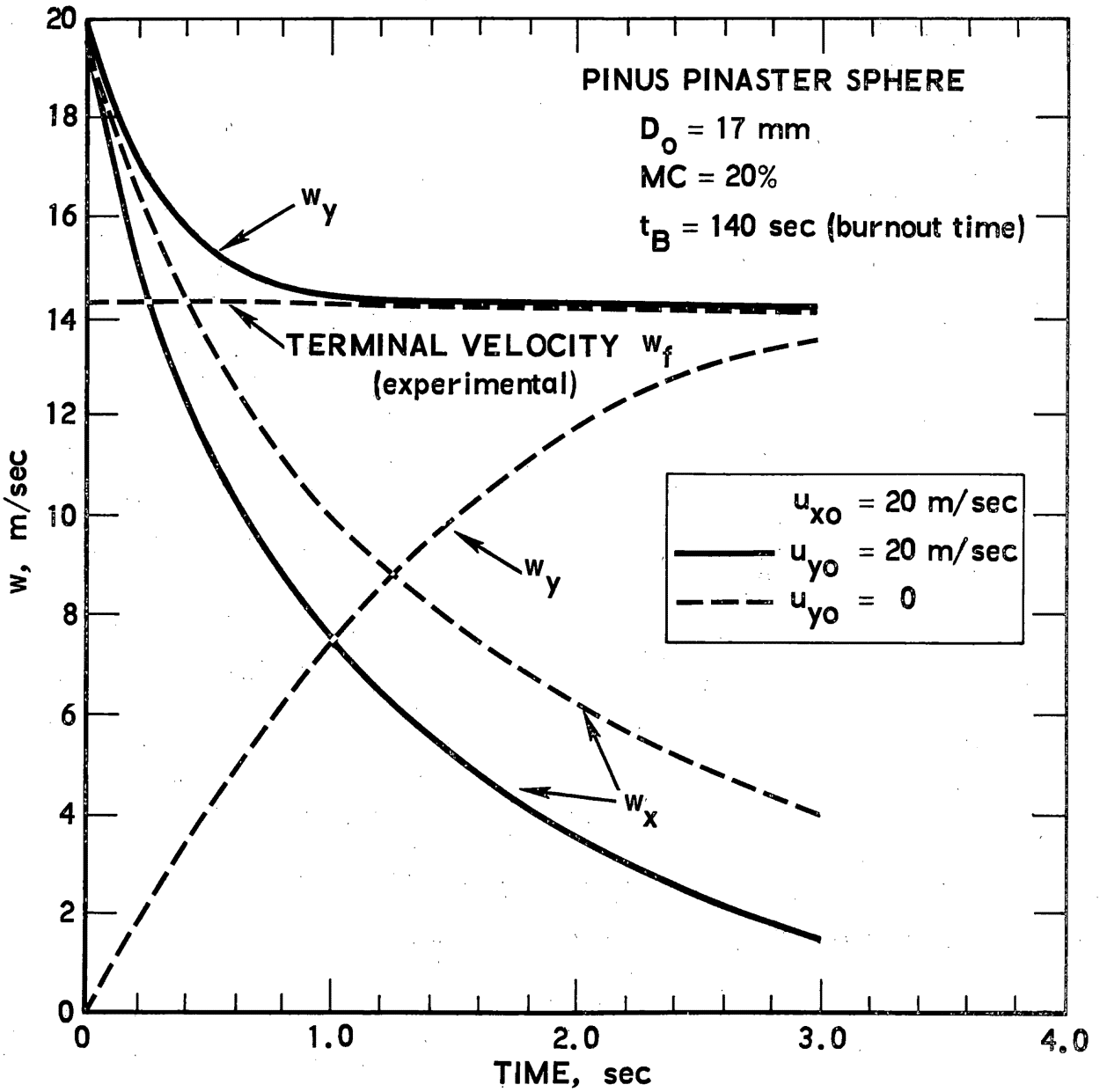

Fig. 3. Relative Velocity $w_x = 0$ and $w_y = w_{f(t)}$ in a First Few Seconds of Trajectory

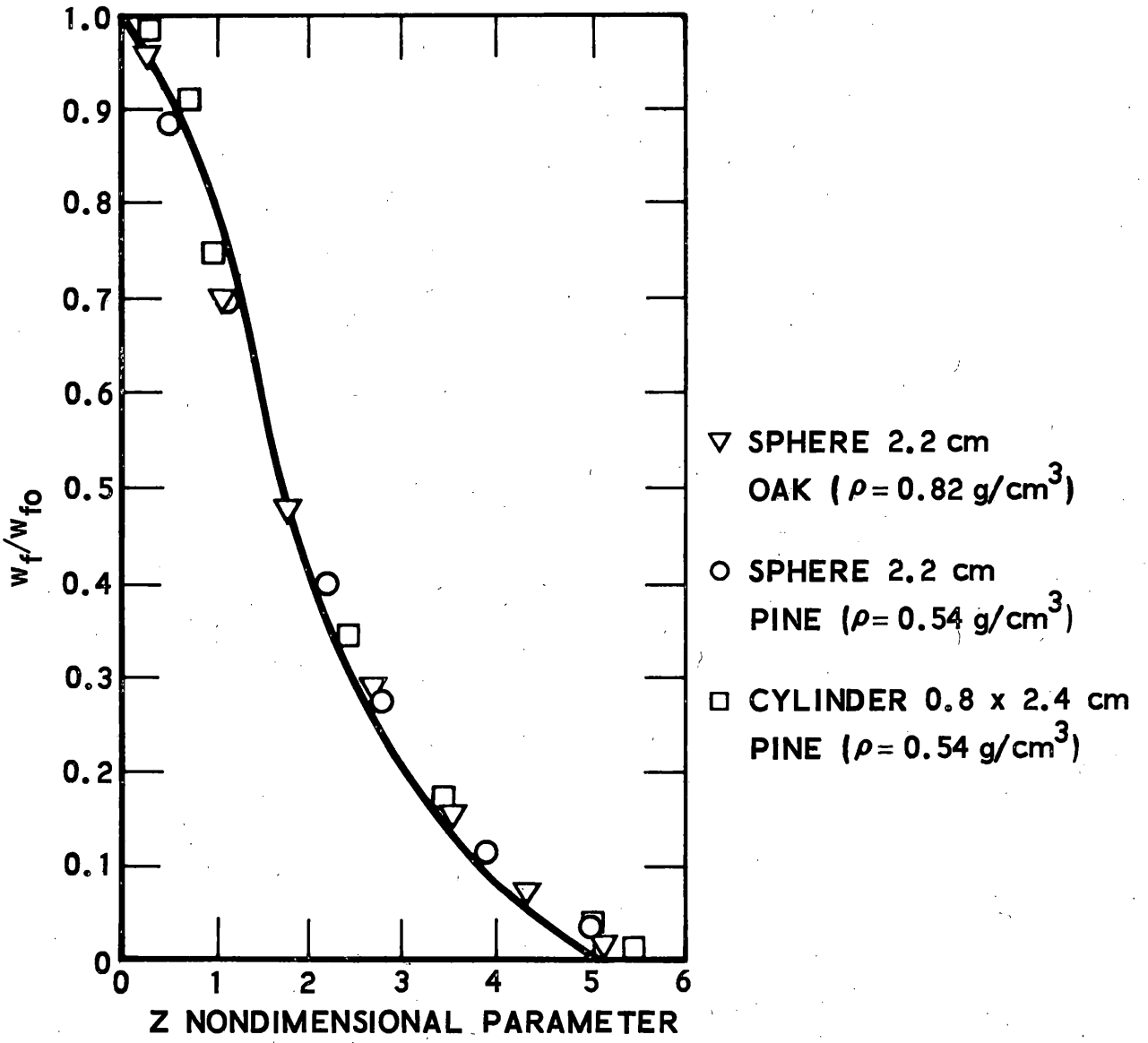

Fig. 4. Comparison of Tarifa's and Aerospace Model

Some comments can be made about this method of calculation. One of Tarifa's conclusions was that the parameter Z had a constant value of 2.6 at burnout for all firebrands. This required an introduction of a shape factor to obtain reasonable agreement between burnout time measured for various firebrands, and the burnout time resulting from Eq. (6).

Another stipulation made by Tarifa was that the variation in $w_{f(t)}$, as well as a change in the firebrand size with time for a firebrand burning in a free fall, is the same as if it was burning in a fixed position in the wind at a velocity equal to $w_{f(t)}$. This assumption requires further experimental verification to determine, for instance, how the tumbling of a non-spherical firebrand in a free fall may affect its rate of burning.

The significance of the value $L^{-0.4}$ in Eq. (6) is not clear. It would lead to the conclusion that for cylindrical firebrands the burnout time is not only a function of D, but also of L. From the writer's quiescent air experiments and other work discussed in Section 2, it appears that it is the diameter which has a predominant effect on the burning time of cylindrical firebrands. Therefore, the Aerospace model and Tarifa's data were correlated at a ratio of L/D = 3 which was used in most of his experiments. This value was left unchanged in Eq. (6) for firebrands with different values of L/D. The problem requires further experimental verification since it is quite possible that in a tumbling free fall of cylindrical firebrands there may be an effect of length on the flaming and glowing burn time.

Once the relationship between $w_{f(t)}$ and time is known (see Fig. 4), the trajectory of a firebrand can be calculated by numerical integration of Eqs. (3) and (4). Of course, the prerequisite to firebrand flight to any distance X is the existence of a convection column vertical velocity u_y, which must be greater than the firebrand initial fall velocity w_{fo}, so that the firebrand can travel to height Y before it leaves the column boundary. The Aerospace program[4], which is based on Tarifa's approach, accomplishes the trajectory calculation by determining the height and the distance at which the convection column boundary is reached. Beyond this point the vertical

velocity u_y usually becomes 0, and the firebrand trajectory is only a function of $w_{f(t)}$ and w_x.

It is tacitly assumed that the burn equations of a firebrand are the same whether it is in or out of a convection column. This is probably not correct since high temperatures of a flame surrounding the firebrand in the convection column will accelerate the rate of its burning. The model could be easily amended to account for this once experimental data become available on fuel burning under these conditions. At present the model is conservative, i.e., it predicts longer life and longer trajectories of the firebrand than may exist in reality.

To obtain information of firebrand size as a function of time, it is necessary to know not only $w_{f(t)}$, but also a change in firebrand mass and the drag coefficient $C_{D(t)}$. Fortunately, interpretation of some of Tarifa's data has shown that the drag coefficient changes very little for a burning firebrand until the diameter becomes small enough to enter the region of Reynolds number < 1000, when the lethality and importance of a firebrand becomes less significant. Consequently, it appears reasonable to assume, as Tarifa has done, C_D constant and a function of initial firebrand shape for calculation of the firebrand diameter and mass change. This assumption was also made by Lee[3]. This drag coefficient, which was found to be 0.53-0.55 for spheres, and 1.2 for cylinders, includes gas blow-off effects from the surface of the burning firebrand, although this effect is probably very small[1].

The comparison of experimental data for fall velocity of burning firebrands with the calculations performed with the Aerospace model is shown in Fig. 5 and the agreement is reasonable.

Examples of trajectories calculated using the Aerospace computer program are shown in Figs. 6 and 7. Figure 6 illustrates the trajectory of two extreme sizes of firebrands with an inclined convection column having constant vertical velocity, u_y, of 30 m/sec. The wind velocity in and out of

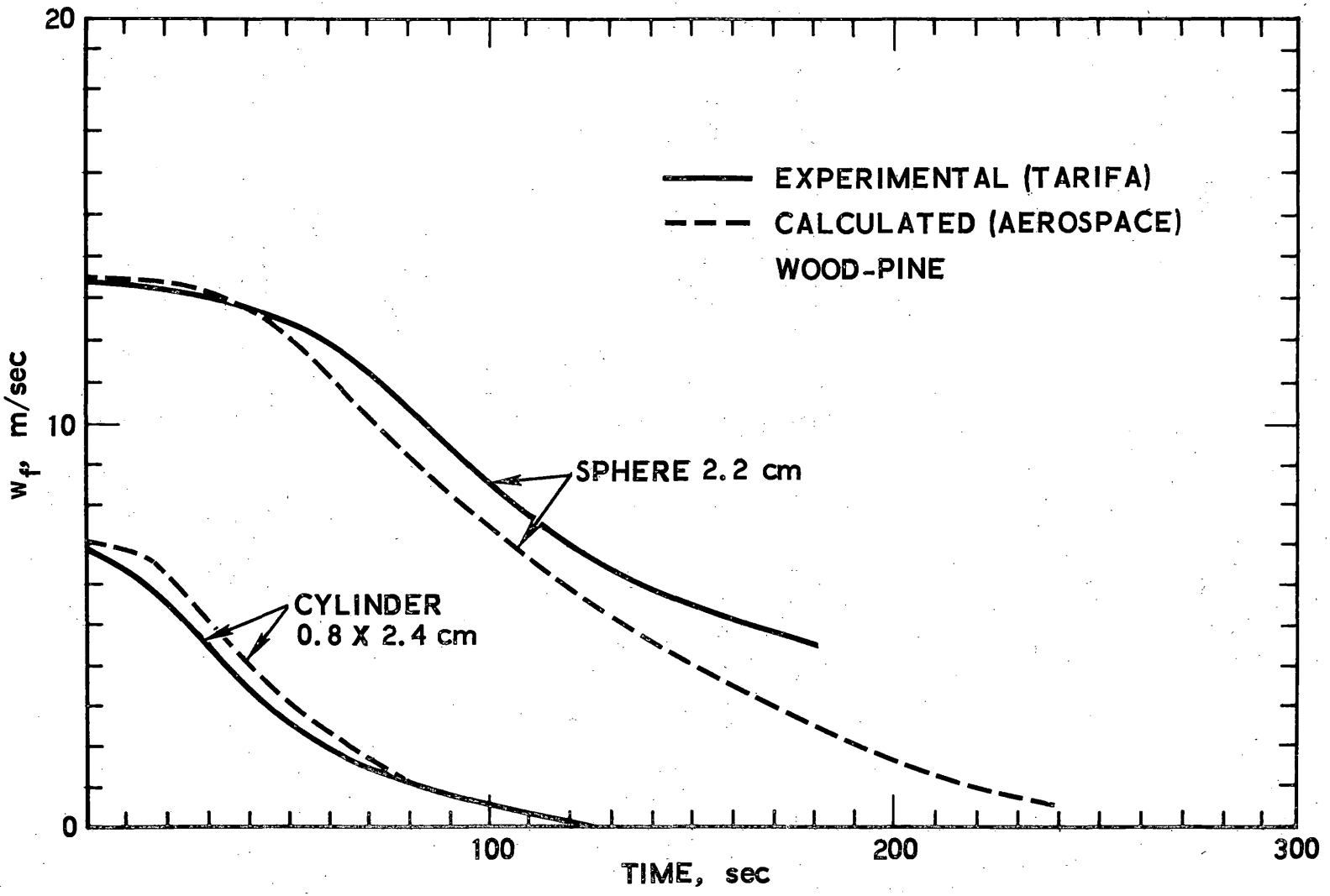

Fig. 5. Comparison of Experimental Data Tarifa and Aerospace Trajectory Model

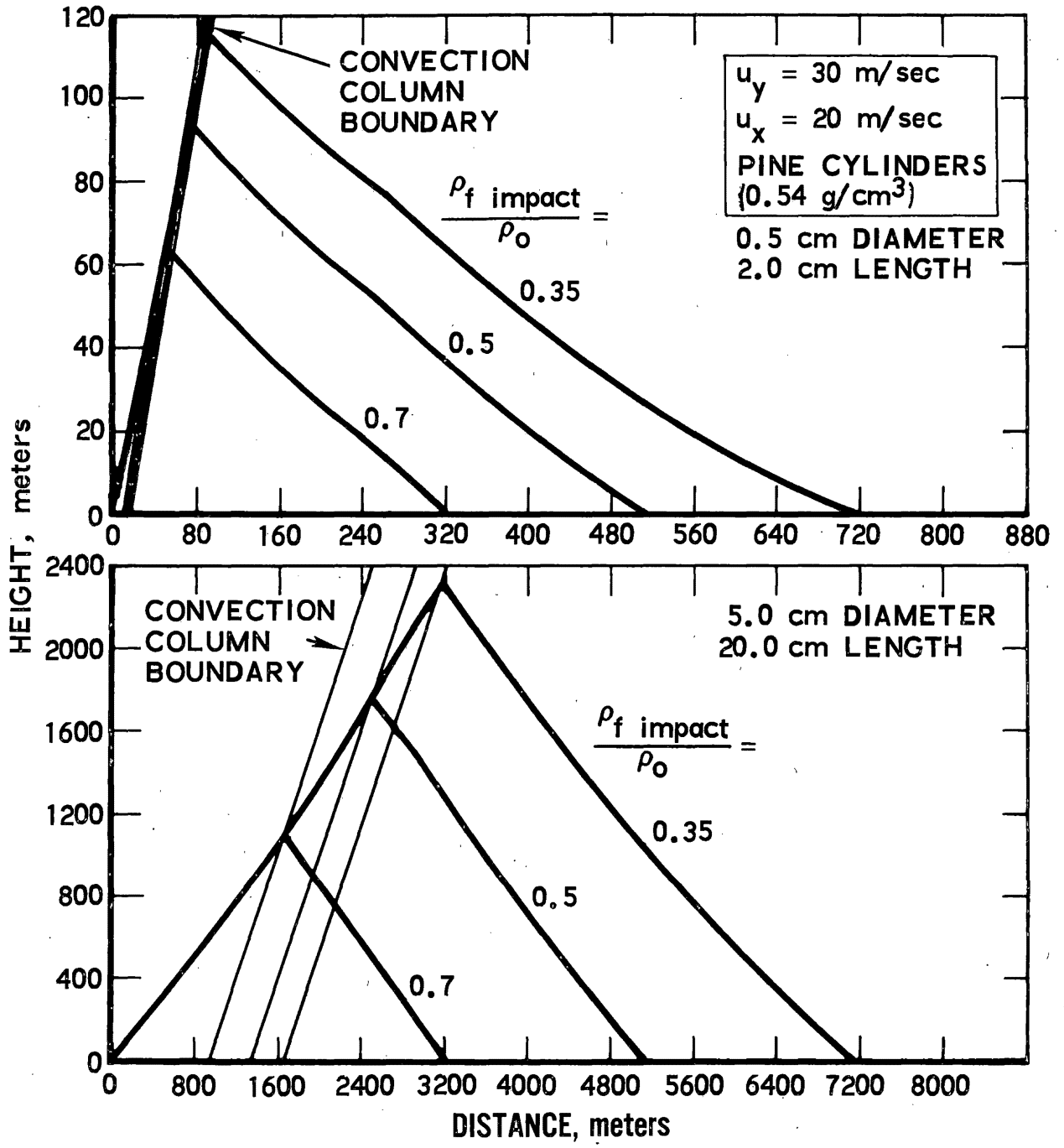

Fig. 6. Firebrand Trajectories from Aerospace Computer Program

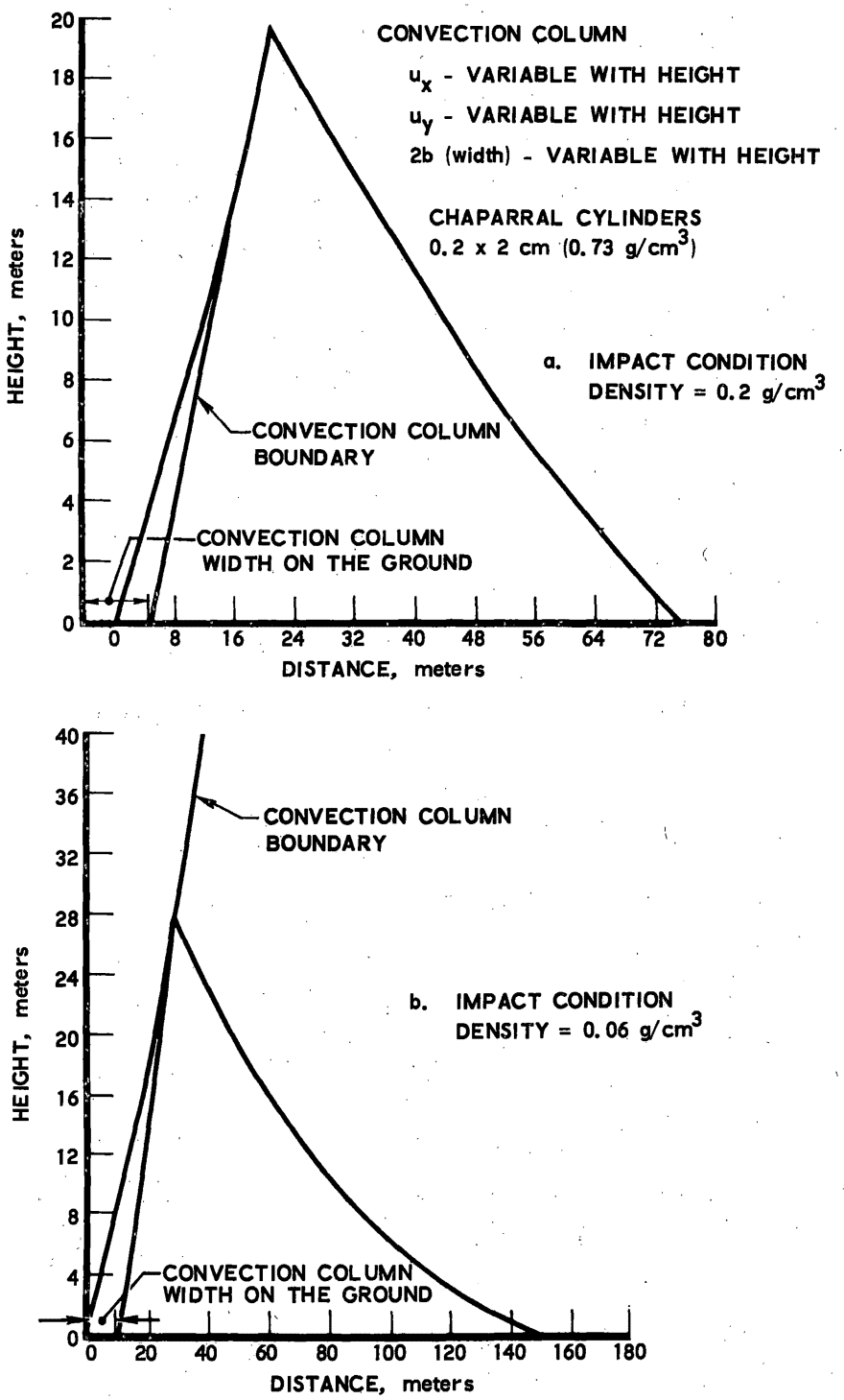

Fig. 7. Firebrand Trajectories (Romero Fire Convection Column)

the convection column u_x is also constant at 20 m/sec. The boundary of the column was "rubbery" to permit calculation of a maximum distance which could be obtained at a fixed firebrand impact condition ($\rho_{f\ impact}/\rho_o$ = defined value), where ρ_o is initial firebrand density. It can be seen that large distances can be covered with large firebrands, but then the convection column width on the ground becomes unreasonably large. To reach similar distances with a more realistic column width (10-100 meters), the vertical velocities would have to be considerably higher. Such high velocities can be obtained with a sudden flare-up or formation of a vortex in the fire line. This will be discussed further in Section 4 of this report.

Figure 7 shows a firebrand trajectory with convection column characteristics calculated and its boundary fixed for a section of the Romero Fire in California in 1971.

Examination of Figs. 6 and 7 leads to the following conclusions:

1. High uplift velocities in the convection column are necessary in order to lift larger firebrands (equivalent cylinder diameter > 2 cm) off the fuel bed and to carry them to a sufficient height for large impact distances.

2. Even large brush fires, like the Romero Fire in California (intensity ~15,000 Btu/sec-ft), may not be able to develop high uplift velocities in a two-dimensional convection column. Existence of randomly generated fire whirls or sudden flareups is necessary to provide the thermal and pressure buoyance which will be able to lift larger particles.

3. Small firebrands (equivalent cylinder diameter < 1 cm) have a relatively short burn time and even with the existence of large uplift forces they will not travel far before burnout. Consequently, one could expect a shower of smaller and not fully consumed firebrands (with $\rho_{f\ impact}/\rho_o > 0.5$) in an area up to 100 meters ahead of the flame front.

2.3 FIREBRAND SIZE AND MASS CHANGE

It is necessary in assessing the firebrand hazard to predict not only the trajectory but also to define the firebrand condition, i.e., its size and mass at impact. Obviously, firebrands which are at a near burned-out condition at impact are of a smaller hazard than those which are flaming and possess larger mass. From criteria established in Section 3, the flaming period of the firebrand on the ground will be calculated as a function of firebrand diameter and density at impact.

In seeking a solution to this problem, the aspect of mass and density change was addressed first. The density of a firebrand changes as a result of pyrolysis and outgassing, and the virgin wood is converted into char and finally into ash. From the work of many researchers and the author's experiments described in the next section, it appears that the density change associated with the pyrolysis and burning of wood can be approximated by first order Arrhenius' equation in the form

$$\frac{d\rho_{(t)}}{dt} \sim \rho_{(t)}^{a} \exp(-E/RT) \tag{7}$$

where

a = pre-exponential constant, sec^{-1}
E = activation energy, cal/g-mole
R = universal gas constant = 1.987 cal/g-mole-^{o}K
T = pyrolysis temperature, ^{o}K
$\rho_{(t)}$ = the variable wood density, g/cm^3

The experimental data of $\rho = f(t)$ were obtained[1] for various sizes of spherical firebrands of oak and pine. These data are plotted on a semi-log scale in the form of ρ/ρ_o versus t/D_o in Fig. 8. It appears that the results correlated fairly well with a straight line with the exception of a few points at values $\rho/\rho_o \leq 0.35$. The reason for this is at present not clear, but it corresponds to the break point in the pyrolysis of cellulose discussed in the

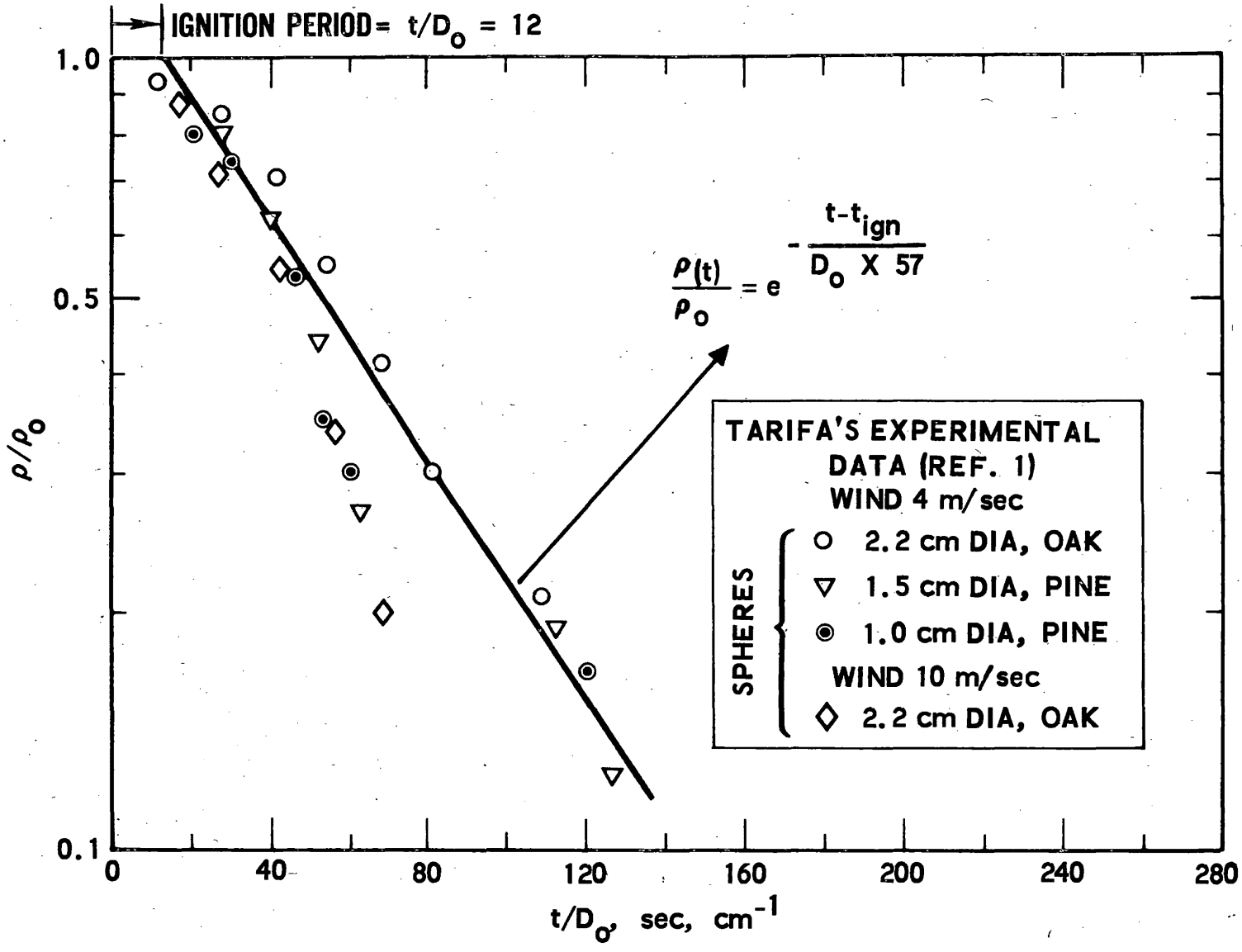

Fig. 8. Correlation of Density-Time Function

next section. For the flaming conditions, the density ratio below 0.3 is of small interest. The equation of the function from Fig. 8 is

$$\frac{\rho_{(t)}}{\rho_o} = \exp\left(-\frac{t-t_{ign}}{57\,D_o}\right) \tag{8}$$

for

$$t_{ign} \leq t \leq 80\ D_o$$

where

$$t_{ign} = 12 \cdot D_o$$

One can calculate the density beyond the value of $t = 80 \cdot D_o$ and this was done for some of the trajectories, but there is a possibility of greater errors, particularly with large firebrands burning in a strong wind. In practice, this will seldom occur since with the density change down to a value of $\rho/\rho_o = 0.3$ (corresponding to $t/D_o = 80$) the fall velocity of the firebrands will be low also, around 2-4 m/sec (see Fig. 5).

It is interesting to compare Eqs. (7) and (8) and note that differentiation of Eq. (8) leads to $d\rho_{(t)}/dt = -\rho_{(t)} \cdot 1/KD_o$ and that the main difference between the two equations is in the factor $1/D_o$, since it can be assumed that $1/K = a \exp(-E/RT)$, where K is a constant, cm/sec.

The factor $1/D_o$ can be considered for spheres and cylinders as proportional to a ratio of surface (S) to volume (V). Consequently, it could be assumed that self-pyrolysis or burning of wood can be approximated by first order reaction, which is also controlled by the ratio of the rate of heat soakback into the fuel ($\sim$S) to the rate of fuel heat absorption ($\sim$V). The heat soakback will depend also on other factors such as flame temperature and thermal characteristics of the fuel, while the heat absorbed will be a

function of particle density and specific heat. However, for the cellulose type of fuels the variation in these parameters (except density) is not appreciable.

Equation (8) does not include wind effect, although Ref. 1 shows an increase in burn rate when experiments were carried at constant, but varying magnitude, wind velocities.

The difficulty in assessing wind effect is that the firebrand flies with a relative velocity equal to its fall velocity which decreases rapidly with decreasing firebrand mass. From the few experimental points reproduced in Fig. 8, it appears that the scatter of points due to wind effect is not greater than that caused by other parameters.

The available experimental data do not permit in-depth evaluation of the effect of relative velocity and other parameters, and the problem requires further experimentation with firebrands burning in free fall with well-defined fuel properties and accurate instrumentation.

Once the density and the fall velocity functions versus time are known, the instantaneous size of the firebrands can be calculated assuming that the drag coefficient determined for the initial firebrand shape is constant.

The question also arises: What will be the effect of tumbling in flight on non-spherical bodies such as cylinders and plates? Experiments carried out[1] led to the conclusion that the measured fall times of cylinders under tumbling conditions were of the same magnitude as those calculated for the attitude of maximum drag and that the errors between the two sets of experiments were less than 10 percent.

From a drag-mass equality equation in a free fall, the diameter of a cylinder or sphere can be calculated

$$\frac{D_{(t)}}{D_o} = \left(\frac{w_{f(t)}}{w_{fo}}\right)^2 \cdot \left(\frac{\rho_o}{\rho_{(t)}}\right) \qquad (9)$$

where D_o, ρ_o, w_{fo} are firebrand initial diameter, density, and fall velocity, respectively; $w_{f(t)}$ and $\rho_{(t)}$ are calculated at any time t, in a manner previously described.

The Aerospace model performs and plots these calculations. An example is given in Fig. 9 for the same firebrands whose trajectories were shown in Fig. 6. From the type of data shown in Fig. 9, a series of curves illustrating the change in firebrand density as a function of flight time and initial diameter can be calculated. These curves are presented in Fig. 10. It can be seen that small firebrands burn out quickly and only those with initial diameters greater than 2.5 cms will have a life of 400 sec or more and be able to cover large distances. A similar family of curves could be drawn to illustrate the change in firebrand size.

There are few experimental data available in the literature[1] on the rate of change of a firebrand size in a free fall to compare against the model predictions. Figure 11 shows a comparison of a 22-mm diameter oak sphere for which Ref. 1 gives the size change at two constant wind velocities of 4 and 10 m/sec, and the values calculated from the Aerospace model for free fall velocities. At first glance, the correlation appears poor. However, if one considers that the initial fall velocity of this firebrand is higher than 10 m/sec, and that it drops rapidly to a value which will, in terminal stages, be less than 4 m/sec, one would expect the free fall data to fall between the other two curves.

The rapid decrease in firebrand size with time shown in Ref. 1, and also calculated from the Aerospace model, appears to be inconsistent with the results of experimental work performed by the author, and others. During experiments on burning of wooden dowels and spheres in quiescent air, only a small dimensional change was observed throughout the flaming range (typically, 10 percent reduction in diameter). It is possible, however, that even low relative air velocity may dislodge char formed at the surface, resulting in an effective reduction in diameter. It is also possible that

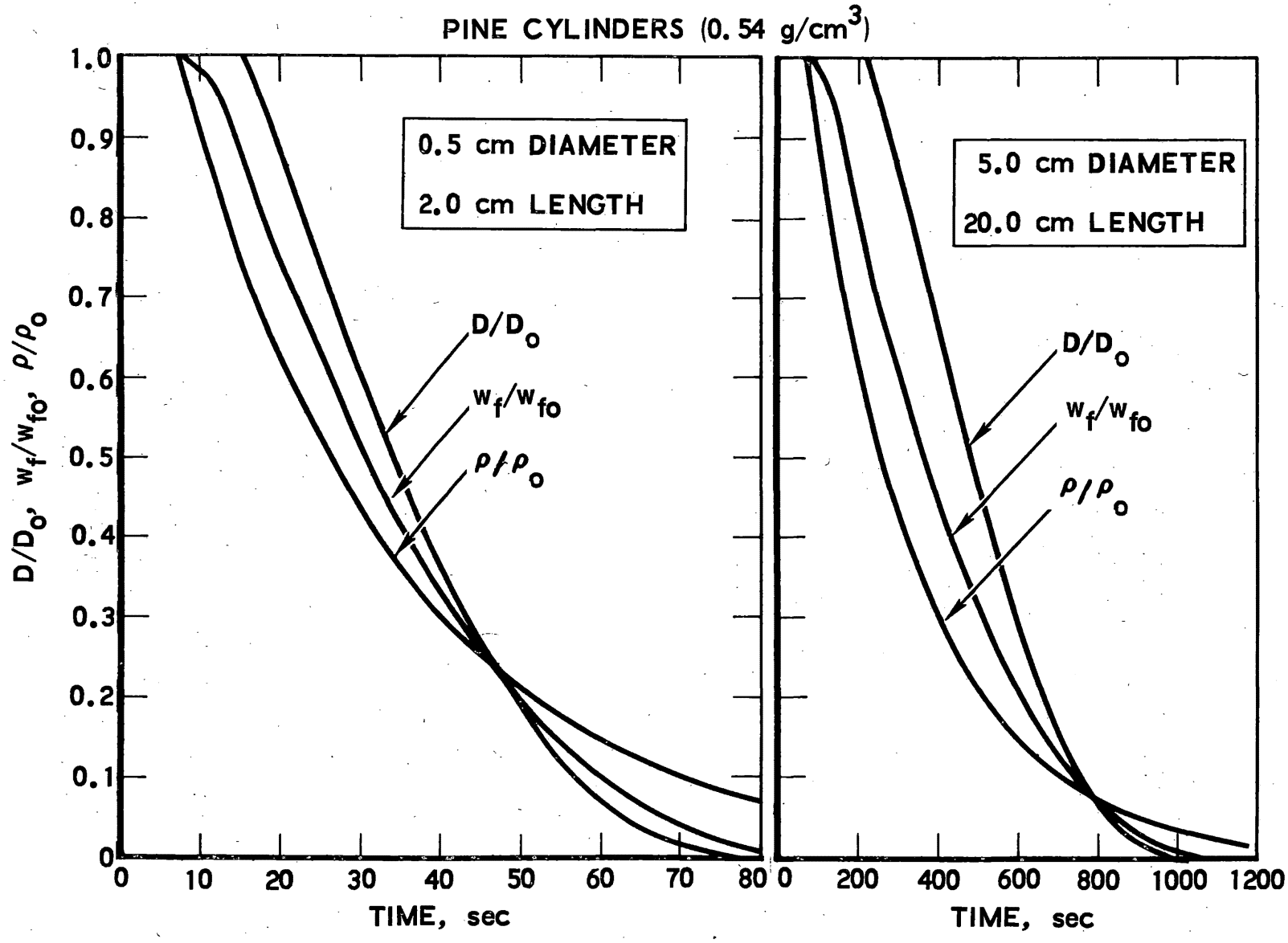

Fig. 9. Time History of Firebrand Diameter, Fall Velocity and Density

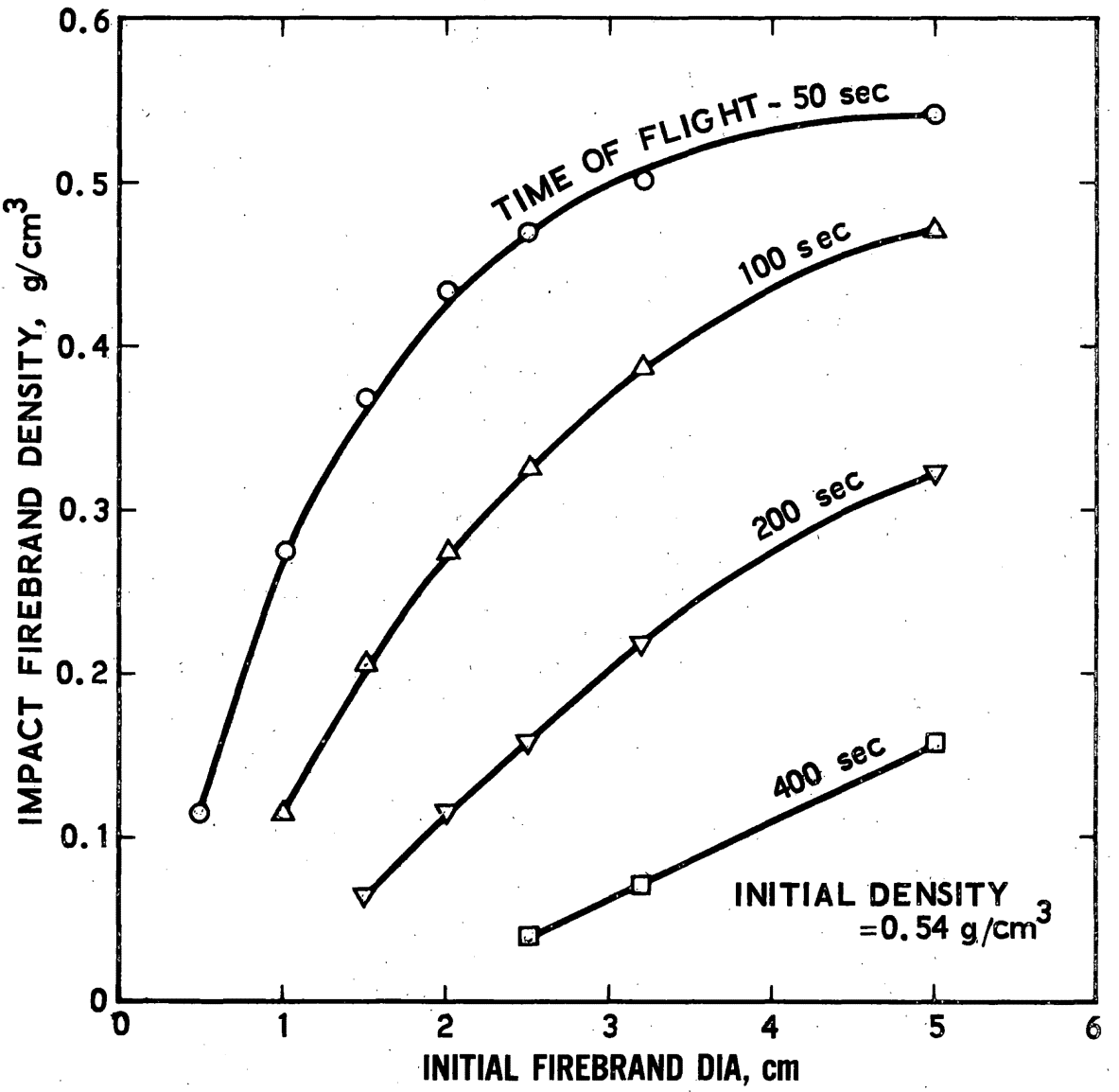

Fig. 10. Change in Firebrand Density as a Function of Flight Time and Initial Diameter

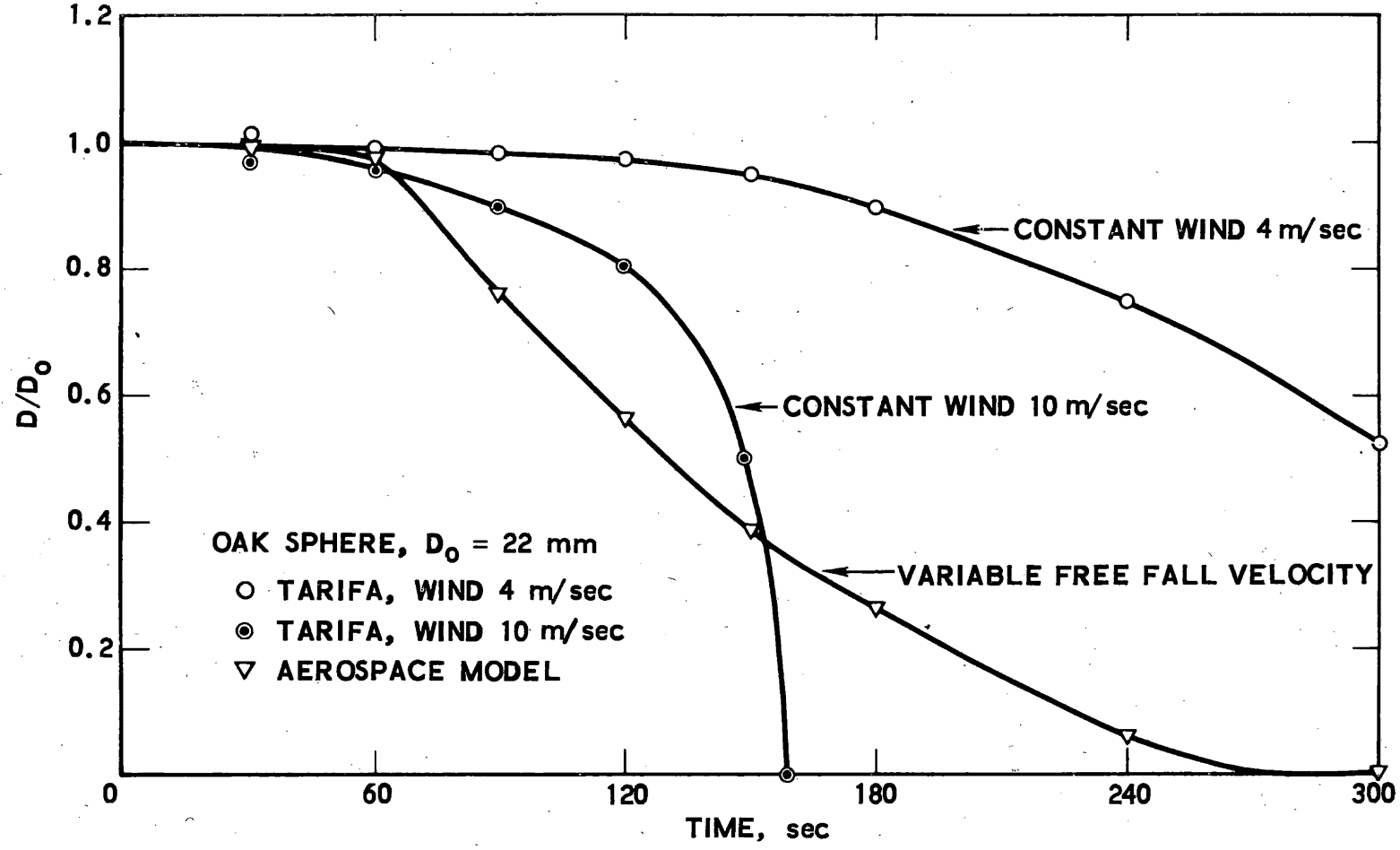

Fig. 11. Comparison of Experimental and Analytical Data on the Firebrand Size Change

because of difficulties in measuring the size of a burning firebrand in a dynamic environment, the experimental data presented are of a limited accuracy only. This fact stresses the need for further experimentation on the change in firebrand density and size with varying relative air velocities.

The ignition time of firebrands was deduced from experiments[1] to be of the order of 12 · D_o sec (see Fig. 8). This value will increase, as shown later in Section 3, with an increase in firebrand moisture content. Most of the experiments[1] were performed with 2 percent moisture content.

While this study concerns itself mainly with the flaming period of the firebrands after they impact the ground, it is not clear from the interpretation of the data[1] if, or for what duration, the firebrands were flaming in flight. One would expect a reduced rate of mass loss in the glowing, as opposed to the flaming stage, but perusal of data in Fig. 8 does not indicate a change in the slope of the ρ/ρ_o function. It is stated in Ref. 1 that at low air speeds a flame exists in the first part of the combustion process and changes later into a glowing combustion. At high air speeds there is no flaming at all and all combustion occurs as a glowing process. Clements[2] made observations on various types of pine cones in free fall and found the flaming period to be relatively short compared to the subsequent glowing period.

Certain criteria were developed for the flaming period of firebrands burning on the ground in quiescent air (see Section 3), but whether these criteria apply to firebrands in free fall is open to further investigation.

The effect of moisture content was not studied in detail in Ref. 1 beyond a statement made that the moisture has a strong effect on the ignition process, but after ignition its influence is not important, particularly for smaller and medium-size firebrands. The author's own experiments on moisture effect with burning in quiescent air have shown that there appears to be a decrease in the rate of mass loss with increasing moisture content, although this effect was not quantitized.

In practice, the firebrands with moisture content greater than, say, 10 percent would be of small interest because of greatly increased ignition time and sluggish burning. Nevertheless, it is necessary to define experimentally the effect of 0-10 percent moisture on firebrand ignition, flaming, glowing time, and on burning rate in a dynamic environment. This information is at present not available.

The Aerospace trajectory model[4] was computerized on the CDC 7600 computer and, together with a yet-to-be-developed convection column model, is to be used as a subroutine to the Forest Fire Simulation Program[5], thus providing a more complete picture to the fire fighters of the fire spreading rate and the hazards involved.

3. CONVECTION COLUMNS

3.1 REVIEW OF PAST WORK

In the phenomenology of firebrands, the convection columns producing the uplift force are an important factor in lifting the potential firebrands off the fuel bed to some altitude where they can be picked up by the wind and carried over varying distances. These distances are a function of altitude, wind velocity, and of firebrand size.

The uplift force will be, generally, created by the thermal buoyancy of the air entrained in and heated by the burning fuel bed. The process is a complex one. The heated fuel pyrolysis generates combustible gases which, after mixing with the air above them, begin combustion so that a heated column of air rises and causes entrainment of the cool air from outside and a turbulent mixing in the diffusion zone. The combustion process continues in the high buoyancy, high temperature zone; and although it is completed at a certain height, the convection plume continues to rise in a low buoyancy zone, its temperature drops progressively and finally reaches the ambient air values. The process is further complicated by a nonuniform fuel distribution over the fire area which will cause reduction or flare-up in the fire intensity and in the convection column characteristics. Countryman[6] distinguished six zones in a fire plume: (a) fuel bed zone, (b) combustion zone corresponding to high buoyancy zone ($\leq$100 ft), (c) turbulence zone with undefined boundaries (100-200 ft above the combustion zone), (d) thermal convection zone corresponding to low buoyancy zone (1000-15,000 ft) and (e) a thin smoke fallout zone; and condensation-convection zone deriving its energy mainly from condensed water vapors.

A random appearance of fire whirls, generated either by uneven terrain and wind, or by unstable conditions of ambient air on flat terrains, is another factor adding complexity to the convection column phenomena. These fire whirls are important, as mentioned previously in Section 2, in

providing updraft forces capable of lifting large embers to high altitudes from which they can then be carried for large distances.

Finally, there is the presence of wind which adds another parameter to the shape and behavior of a convection column. The effect of wind cannot be neglected in the firebrand investigation since it is mainly responsible for firebrand behavior outside of the convection column.

This report will deal with two-dimensional convection columns generated by line source. Fire whirls will not be considered here because they pose a separate problem by themselves and will be dealt with in our future work.

The convection columns generated from line or point source have been a subject of analysis and experimentation for many years. Some of this work will be reviewed here because the methods and assumptions made by various investigators will be used in our simplified treatment of the problem.

W. Schmidt[7], one of the early investigators, used Prandtl's turbulence mechanism of heat and momentum transfer to determine the upward force on an element due to its buoyancy. Schmidt found analytically, and then confirmed experimentally, that a heated column of air spread out in such a manner that both the distribution of temperature and vertical velocity were similar at all heights, and that the width of the column increased uniformly with height.

H. Rouse[8] considered both the point and the line source convection column. We will limit ourselves to his conclusions regarding the line source. His analysis was based on the assumption that "whereas the unit buoyancy force (local density change) is sufficiently great to produce vertical acceleration, the corresponding variation in the mass density of fluid undergoing acceleration is sufficiently small in comparison with the density itself to be neglected." This assumption is particularly applicable to a low buoyancy zone where the changes in density could be considered small.

From the solution of equations of continuity, momentum-buoyancy, and energy conservation, Rouse concluded that for a line source the convection column width will expand linearly with altitude, that the upward velocity is a constant value independent of altitude, and that the density decrease increment will vary inversely with altitude. Rouse and his coworkers also performed experiments with a linear gas burner to obtain the convection column temperature and velocity profiles. The results have shown that the distribution of both can be approximated by a Gaussian distribution

$$\exp\left(-\frac{ky^2}{x^2}\right)$$

where x was the height above the line source, y horizontal distance from the line source, and k a constant of different value for temperature or velocity with a maximum temperature and velocity in the line source plane.

G. I. Taylor[9] reviewed the work of Schmidt and Rouse which, while carried out independently, agreed in the conclusions. Taylor applied Schmidt's turbulent energy transfer to a scaling law for buoyant plumes with side wind, which he expressed as a ratio, R, of linear scale to full size model

$$R^{-1/2} = \frac{u_{model}}{u_{full\ size}} \text{ and } R^{-3/2} = \frac{H_{model}}{H_{full\ size}}$$

where u is the wind velocity and H is the heat release per unit length of source. The convection plume would tilt with the wind and would be bounded by an angle $\tan^{-1}(u \pm \alpha w/w)$, where w is the vertical velocity in the plume and α is the air entrainment coefficient.

B. R. Morton[10,11] addressed himself to low buoyancy point source plumes. His main assumptions were that the rate of air entrainment at a given height is proportional to some characteristic velocity at that height, the distribution of vertical velocity and buoyancy force (temperature) are of

similar form at all heights, and the local density variations are small in comparison with ambient air density at a given height. From equations of conservation of volume, momentum and energy, Morton arrived at similar conclusions regarding plume width, vertical velocity, and buoyancy to those of Schmidt's and Rouse's for point source of heat. Morton carried out experiments in which he released low density fluid (methylated spirit colored with methyl violet) in higher density water/salt solution. Photographs taken give data on the rate of growth and spread of the plume and they are in good agreement with the analytical predictions.

Assuming "top hat" distribution for the vertical velocity and temperature, Morton suggested a value of $\alpha = 0.116$ for air entrained coefficient and $\lambda = 1.08$ for the spreading ratio (if the top hat velocity is over a radius R, similar temperature top hat will be taken of a radius λR).

In Ref. 12, Morton added the consideration of highly buoyant plumes. He utilized the weakly buoyant plume theory but modified the ratio of air entrainment to vertical velocity by a factor of $(\rho/\rho_o)^{1/2}$, where ρ and ρ_o are air density inside the plume, and ambient, respectively. The pressure was assumed constant within and without the plume. Consequently, from gas law equations $\rho/\rho_o = T_o/T$. With this assumption and an assumption of top hat vertical velocity distribution, Morton used the equation for conservation of mass, momentum and energy leading to a set of differential equations from which plume radius, vertical velocity, and temperature as a function of altitude could be calculated by means of numerical integration.

P. H. Thomas[13-15] performed analytical and experimental work on flames and the high buoyancy plumes generated by them. From the interpretation of the data of others he concluded that the maximum vertical velocity, w, in highly buoyant plumes at any height, z, is equal to $w = 0.36\sqrt{2gz(\Delta T_{fl}/Ta}$ when T_{fl} and T_a are flame and ambient air temperatures, respectively. The height or the length of the flame, L, from Thomas' experiments for a line source was expressed by $L = 400\,\dot{m}^{2/3}$, where $\dot{m}$ is the burning fuel weight flow rate per unit of flame front in cgs units. Flame height was defined as

that beyond which a certain temperature drop was observed. Thomas calculated air entrainment coefficient assuming that a sideways air entrainment velocity $v = \alpha(\rho_{fl}/\rho_a)^{1/2} \cdot w$ and found $\alpha = 0.16$ for line source flames (ρ_a and ρ_{fl} are ambient air and gas density, respectively). Thomas also performed experiments on the effect of wind on flame length and concluded that this effect was relatively small.

A. A. Putnam[16] investigated the effect of wind on flame from a multi-spud gas burner and from data on wood cribs. Under the influence of a crosswind, the flame deflects from vertical by an angle, θ, which is a function of Froude number expressed as u^2/gL, where u is the crosswind velocity, L the flame length in no-wind condition, and g the gravitational constant. Putnam found that for line source flames $\tan\theta = K \cdot (u^2/gL)^{1/2}$, where K is a constant of 1.3 to 1.4. He found that the length of windblown flames, L_s, is shorter than that of no wind ones, L, and that the ratio of L_s/L was approaching a constant value of 0.7 at Froude numbers greater than 0.3.

Shao-Lin Lee and H. W. Emmons[17] investigated analytically and experimentally with a channel burner the characteristics of no-wind, low buoyancy convection plumes. In their analysis, Morton's and Thomas' assumption of air entrainment being proportional to the vertical velocity, and Rouse' assumptions of Gaussian distribution of velocity and temperature in the plume, were applied. Three regimes of modified (by factors for Gaussian distribution of velocity and temperature, and effective density distribution) Froude number $(u^2/gb_o) < 1$, $= 1$ and > 1 were evaluated using equations of mass, momentum and energy conservation. The characterization of plumes for Froude number = 1 were similar to those of Schmidt and Rouse. According to the authors, rigorous analysis of flame is extremely complicated, but with simplifying assumptions of uniform velocity and temperature distribution, plume characteristics (width, velocity, and buoyancy) can be expressed as a function of source energy flux.

In our analysis, the two-dimensional convection plume from a line source will be divided into two zones: high and low buoyancy. The analysis will define, with certain simplifying assumptions, the convection column characteristics (velocity, temperature, and width) at a zero plane corresponding to flame tip (see Fig. 12) and then, using the known conditions at the zero plane, the low buoyancy above it will be defined.

3.2 HIGH BUOYANCY ZONE

The high buoyancy zone, which usually extends to less than 50 meters in altitude, will be characterized by top hat distribution of vertical velocity and of gas temperature. The mixing of the entrained air with the combustible products of fuel pyrolysis continues in the high buoyancy zone until at an assumed flame tip plant (0 plane, see Fig. 12) all reactions are completed. We shall assume a constant "characteristic" gas temperature through that zone. The zone has a unit length along the z axis perpendicular to the x-y plane and a width defined by A.

Where

A_o = $2\,b_o$ - convection column width at height L, air

c_p = air (gas) specific heat (cal/g-^oC)

c_r = radiation loss factor

g = gravitational constant = 981 cm/sec^2

H_{comb} = heat of fuel combustion (cal/g)

L = flame height or length (cm)

$\dot{M}_{air}$ = entrained air mass flow rate per unit of flame front (g/cm-sec)

$\dot{M}_f$ = fuel mass flow rate per unit of flame front (g/cm-sec)

$\dot{M}_t$ = total mass flow rate per unit of flame front (g/cm-sec)

$\bar{r}$ = mean fuel radius (cm)

R = flame spread rate (cm/sec)

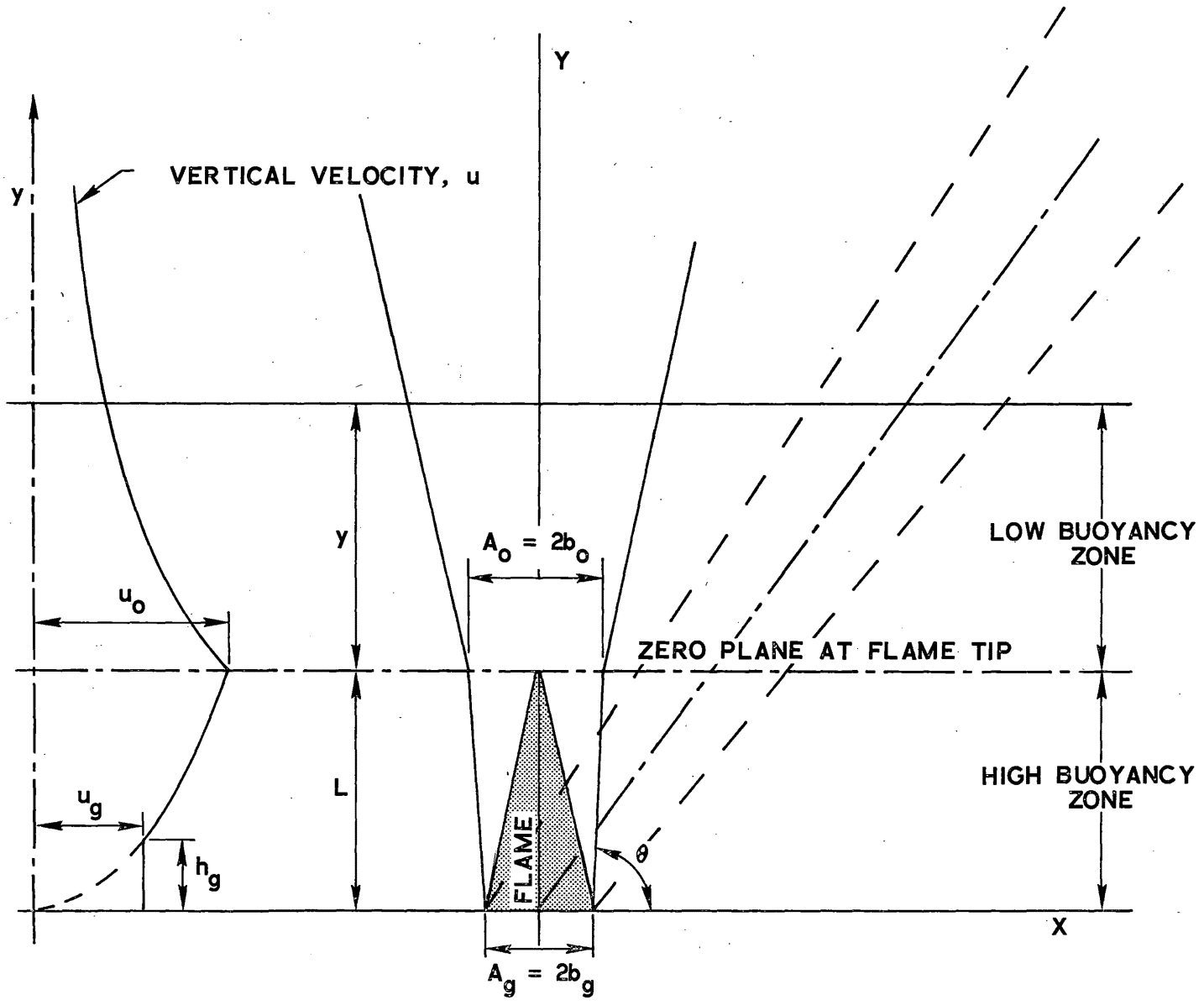

Fig. 12. Convection Plume Schematic

T_{fl} = characteristic flame temperature (^{o}K)

T_{l} = ambient air temperature (^{o}K)

u = vertical gas velocity at height y (cm/sec)

v = entrained air velocity at height y (cm/sec)

w = wind velocity (cm/sec)

α = air entrainment coefficient

α_{f} = fuel thermal diffusivity (cm^2/sec)

θ = angle of plume tilt from vertical (deg)

ρ_{fl} = gas density (g/cm^3)

ρ_{l} = ambient air density (g/cm^3)

τ_{res} = flame residence time (sec)

from Thomas[13,14]

$$L = 400 \cdot \dot{M}_{f}^{2/3} \tag{10}$$

and

$$u = 0.36 \left[\frac{2gy(\rho_{l} - \rho_{fl})}{\rho_{fl}} \right]^{1/2} \tag{11}$$

Since the pressure in and out of the flame zone can be assumed constant, the universal gas equation gives $\rho_{fl}/\rho_{l} = T_{l}/T_{fl}$, and Eq. (11) becomes

$$u = 0.36 \left[\frac{2gy(T_{fl} - T_{l})}{T_{l}} \right]^{1/2} \tag{11a}$$

The entrained air velocity from Thomas[14]:

$$v = \alpha \cdot u \left(\frac{\rho_{fl}}{\rho_{l}} \right)^{1/2} = 0.16 \cdot 0.36 \cdot \left[2gy \frac{T_{fl} - T_{l}}{T_{fl}} \right]^{1/2} \tag{12}$$

Air flow rate per unit of flame length and for a height dy:

$$d\dot{M}_{air} = 2 \cdot 0.16 \cdot 0.36 \cdot \rho_1 \left[2gy \frac{T_{fl} - T_1}{T_{fl}} \right]^{1/2} \cdot dy \qquad (13)$$

Total entrained air flow rate in the high buoyancy zone:

$$\dot{M}_{air} = \int_o^L 2 \cdot 0.16 \cdot 0.36 \cdot \rho_1 \left[2gy \frac{T_{fl} - T_1}{T_{fl}} \right]^{1/2} \cdot dy$$

$$\dot{M}_{air} = \frac{2}{3} \cdot 2 \cdot 0.16 \cdot 0.36 \cdot \rho_1 \left[2g \frac{T_{fl} - T_1}{T_{fl}} \right]^{1/2} \cdot L^{3/2} \qquad (14)$$

$$\dot{M}_{air} = 3.4 \cdot \rho_1 \left[\frac{T_{fl} - T_1}{T_{fl}} \right]^{1/2} \cdot L^{3/2} \qquad (14a)$$

Since at plane 0 combustion is completed, equations for conservation of mass and energy apply for solution of $A_o = 2b_o$ and T_{fl}.

Mass conservation:

$$\dot{M}_t = \dot{M}_f + \dot{M}_{air} = u_o A_o \cdot \rho_{fl} = u_o \cdot 2b_o \cdot \rho_1 \frac{T_1}{T_{fl}} \qquad (15)$$

Substituting u_o from Eq. (11a) with y = L, one finds

$$\dot{M}_f + \dot{M}_{air} = 0.36 \left[2g \frac{T_{fl} - T_1}{T_1} \cdot L \right]^{1/2} \cdot \rho_1 \frac{T_1}{T_{fl}} \cdot 2b_o$$

$$\dot{M}_f + \dot{M}_{air} = 31.9 \cdot \rho_1 \left[\frac{T_{fl} - T_1}{T_{fl}} \cdot \frac{T_1}{T_{fl}} \cdot L \right]^{1/2} \cdot b_o \qquad (15a)$$

Energy conservation:

$$(\dot{M}_f + \dot{M}_{air}) \cdot c_p \cdot (T_{fl} - T_1) = \dot{M}_f \cdot H_{comb} \cdot c_r \qquad (16)$$

If Eqs. (14a) and (16) are combined

$$3.4\rho_1 \left[\frac{T_{fl} - T_1}{T_{fl}}\right]^{1/2} \cdot L^{3/2} + \dot{M}_f = \frac{\dot{M}_f \cdot H_{comb} \cdot c_r}{c_p (T_{fl} - T_1)} \qquad (17)$$

This equation can be solved with respect to T_{fl} (cubic function) by substituting L from Eq. (10) and provides an answer which is not a function of $\dot{M}_f$ (or L) but of the remaining parameters.

Assuming $c_p = 0.26$ cal/g-^oC, $T_1 = 300^oK$, $H_{comb} = 4500$ cal/g, $c_r = 0.95$ and $\rho_1 = 1/2 \times 10^{-3}$ g/cm^3, one finds the solution for $T_{fl} = 857^oK$. This value may be considered typical and will vary little with small variation in the above parameters. The area $A_o = 2b_o$ can be found from Eqs. (15a) and (16).

$$b_o = \frac{\dot{M}_f \cdot H_{comb} \cdot c_p}{31.9 \cdot \rho_1 [(1-Z) \cdot Z \cdot L]^{1/2} \cdot c_p \frac{T_1}{Z} (1-Z)} \qquad (18)$$

where $Z = T_1/T_{fl}$.

For the numerical values assumed above and the T_{fl} calculated

$$b_o = 81\dot{M}_f^{2/3} \simeq 0.2\ L \text{ [see Eq. (10)]} \qquad (19)$$

u_o can be calculated from Eq. (11a) substituting for y the value for L.

$$u_o = 434 \cdot \dot{M}_f^{1/3} \qquad (20)$$

The value of $A_g = 2b_g$ (width of column on the ground) cannot be calculated from the above equations since at y = 0, u and v = 0. In reality, there is some air entrainment at ground level and pyrolysis plus partially burning fuel generated fuel-rich gases are lifted up with some velocity u_g.

We can assume that at the ground the convection column is equal to flame width which can be calculated from Albini's[18]

$$A_g = 2b_g = \tau_{res} \cdot R = \frac{\bar{r}^2}{\alpha_r} \cdot R \tag{21}$$

The vertical velocity, u_g, at ground level can be calculated from

$$\dot{M}_f = 2b_g \cdot u_g \cdot \rho_{fl} \tag{22}$$

Equation (22) is an approximation in that for the fuel to burn some air must be entrained into the fuel bed at some distance from the ground. Thus, the total flow rate > $\dot{M}_f$ and the density $\rho_g > \rho_{fl}$. However, these two errors tend to compensate one another with respect to u_g, and the distance from the ground when $\dot{M}_t \simeq \dot{M}_f$ is considered small.

It is also assumed that this velocity will be constant through a height, h_g (see Fig. 12). The height, h_g, can be calculated by equating u_g from Eq. (22) to u from Eq. (11a) for a height, $y = h_g$.

$$h_g^{1/2} = \frac{\dot{M}_f}{2 \cdot b_g \cdot \rho_1} \frac{T_f}{T_1} \cdot \frac{1}{0.36\left[2g \frac{T_{fl} - T_1}{T_1}\right]^{1/2}} \tag{23}$$

For the value T_{fl} calculated, and other values assumed above

$$h_g = 3000 \cdot \left(\frac{\dot{M}_f}{b_g}\right)^2 \tag{23a}$$

velocity, u_g, can be calculated from Eq. (22) by substituting values for ρ_{fl}

$$u_g = 1190 \cdot \frac{\dot{M}_f}{b_g} \qquad (22a)$$

To satisfy the continuity equation with the new value, u_g, the air entrainment factor has to be corrected over the height, h_g, to $\alpha' = (2/3)\alpha = 2/3 \cdot 0.16 = 0.106$.

The width of the convection column at any height y can be calculated from an equation similar to Eq. (15), once T_{fl} is known, by substituting for u_o the value for u from Eq. (11a) and by integrating $\dot{M}_{air}$ to height, y, [Eq. (15)] rather than L.

With the characteristics of the convection column (u_o, b_o, T_{fl}) defined at the 0 plane, the low buoyancy zone will now be characterized.

3.3 LOW BUOYANCY ZONE

The low buoyancy zone extends from 0 plane to an altitude which for large fires can be measured in thousands of meters. In characterizing this zone, Morton's approach[10] was utilized with modifications of his equations from a point source plume to a line source and retention of the variable gas density, ρ, in the differential equations. Morton's equations for conservation of mass, momentum and energy result in

$$\frac{d}{dy}(uA\rho) = 2\alpha' u \rho_l \qquad (a)$$

$$\frac{d}{dy}(u^2 A\rho) = Ag(\rho_l - \rho) \qquad (b) \qquad (24)$$

$$\frac{d}{dy}\left(uAg\,\frac{\rho_l - \rho}{\rho_l}\right) = 0 \qquad (c)$$

where A and ρ are plume width and density, respectively, at any height, y, above the 0 plane, α' is the low buoyancy zone air entrainment coefficient, u vertical velocity at height, y, and ρ_1 ambient air density assumed constant between plane 0 and y.

These equations have a closed form solution if one assumes that A and u are monotonic functions of y. From Eq. (24c)

$$uAg \frac{\rho_1 - \rho}{\rho_1} = Q \tag{25}$$

The constant Q can be determined from 0 plane conditions where u_o, A_o, ρ_o are known.

The solution for u, A, and ρ is

$$u = \left(\frac{Q}{2\alpha'}\right)^{1/3} \tag{26}$$

$$A = 2\alpha' y + \frac{Q}{ug} \tag{27}$$

$$\rho = \rho_1\left(1 - \frac{Q}{uAg}\right) \tag{28}$$

The relationship between the height, y, and column width, density and velocity is similar to that of Rouse' which is to be expected since similar assumptions were made. Thus, the vertical velocity is constant, A increases and ρ decreases with increasing y. The conditions at plane 0 must be matched with regard to u_o, A_o and ρ_o.

From Eq. (26), α' can be defined such that $2\alpha' = Q/u_o^3$; and from Eq. (27) an imaginary line source can be postulated at a distance y' below the 0 plane such that $2\alpha' y' = A_o - Q/u_o g$. Density, ρ, at height, y', will then become equal to ρ_o.

Using the method described above for the low and high buoyancy zone, a convection column was calculated for the Romero Fire in California in October 1971. Fuel in the area selected for calculation was coastal chaparral (Type 4), the fire spread rate was obtained from the Rothermel model adapted in the Aerospace Corporation Fire Spread Simulation Program[21]. The results of convection column calculation are presented in Table 1.

It is of interest to note that the entrainment coefficient $\alpha' = 0.274$ is greater than $\alpha(0.16)$ which is in agreement with Morton's observations that "rate of entrainment into very hot plumes is substantially less than that into cool plumes."

The temperature can be substituted for density assuming constant pressure so that $T\rho = T_1\rho_1 = T_o\rho_o$.

3.4 WIND EFFECT

The effect of wind on the rate of fire spread and flame shape was studied by various investigators such as Albini, Anderson, Byram, Putnam, Rothermel, Thomas, and others. We shall not consider here the effect of wind on the rate of burning, but confine ourselves to its effects on the flame shape since from these the effect on the convection column shape will be deduced.

Thomas[14] and Putnam[16] observed that flamed subjected to crosswind tilt from a vertical by an angle, θ. This angle can be calculated using Putnam's approach

$$\tan\theta = k\left(\frac{w^2}{gL}\right)^{1/2} \tag{29}$$

or

$$\tan\theta = \frac{w}{u_o} \tag{29a}$$

If one substitutes $(gL)^{1/2}$ by u_o for $y = L$ from Eq. (11a) and uses the value for $T_{fl} = 857^oK$, Eq. (29a) becomes equivalent to Eq. (29) with a constant $k = 1.44$, which is close to the value of 1.3 to 1.4 arrived at by Putnam.

Table 1. Romero Fire Convection Column

Fire spread rate, R = 73.01 ft/min = 37.1 cm/sec. Fuel loading, ΣW_n = 1.604 lb/ft^2 = 0.783 g/cm^2.

$\dot{M}_f = \Sigma W_n \times R$ = 29.05 g/cm sec; Mean fuel diameter, $2r = \frac{4\Sigma V_n}{\Sigma S_n} = \frac{4\Sigma W_n}{\Sigma \sigma_n \times W_n}$ = 0.263 cm.

$L = 400 \times \dot{M}_f^{2/3}$ = 3780 cm; Wind velocity, w = 12 mph = 536.4 cm/sec; $\alpha_f = 2 \times 10^{-3}$ cm^2/sec.

	y, m	h, m	T, °K	u, m/sec	v_c, m/sec	A, m	$\tan^{-1}$ w/u
High Buoyancy	0	0	857.0	2.15	0.86	3.21	21.9°
	10.00	10.00	857.0	6.87	2.76	4.51	21.9°
	37.80	37.80	857.0	13.34	5.36	15.30	21.9°
Low Buoyancy	0	37.80	857.0	13.34	5.36	15.30	21.9°
	10.00	47.80	574.0	↓	↓	20.80	↓
	50.00	87.80	391.0			42.70	
	100.00	137.80	350.0			70.00	
	300.00	337.80	317.6			179.70	
	600.00	637.80	309.0			344.00	
	1000.00	1037.80	305.4			563.30	

h = column height from ground level

v_c = lateral velocity in the column

θ = $\tan^{-1}$ w/u - angle of column tilt from vertical

α' = 0.274

y' = 978 cm

Note: In Eqs. (26) and (27) use: y + 978

We shall describe, therefore, the convection column with a crosswind as being tilted in the high buoyancy (flame) zone at a constant angle θ. We shall neglect any changes in flame length and regard the height of the 0 plane as remaining unchanged. The lateral velocity inside the convection column at any height, y, in the high buoyancy zone can be defined by

$$v_c = u_y \cdot \tan\theta \tag{30}$$

where u_y is the vertical velocity at height y calculated from Eq. (11a).

At the 0 plane, lateral velocity in the column equals crosswind velocity w and will remain at this value (or any other value defined for the crosswind) throughout the low buoyancy zone. Since the vertical velocity, u, remains constant in the low buoyancy zone and if the crosswind velocity also remains constant, the convection column tilt will remain constant at the angle θ.

The tilt angle for the Romero Fire column was calculated in Table 1, and Fig. 13 depicts this convection column as calculated. Assumption of a constant ambient air density and temperature introduces errors above, say, 300 meters, and for better accuracy the integration height interval should be limited to 200-300 meters, starting each time with initial conditions at a new plane.

Figure 14 compares the normalized column height and width (h/L, A/A_o), for the Romero Fire and columns from Tarifa (Ref. 1a). Considering the difficulties in measurement of column boundaries and the simplified approach taken, the agreement is surprisingly good. The convection column temperature data from Fons[20] are also in reasonable agreement with the data of Table 1, showing a rapid drop in temperature with height.

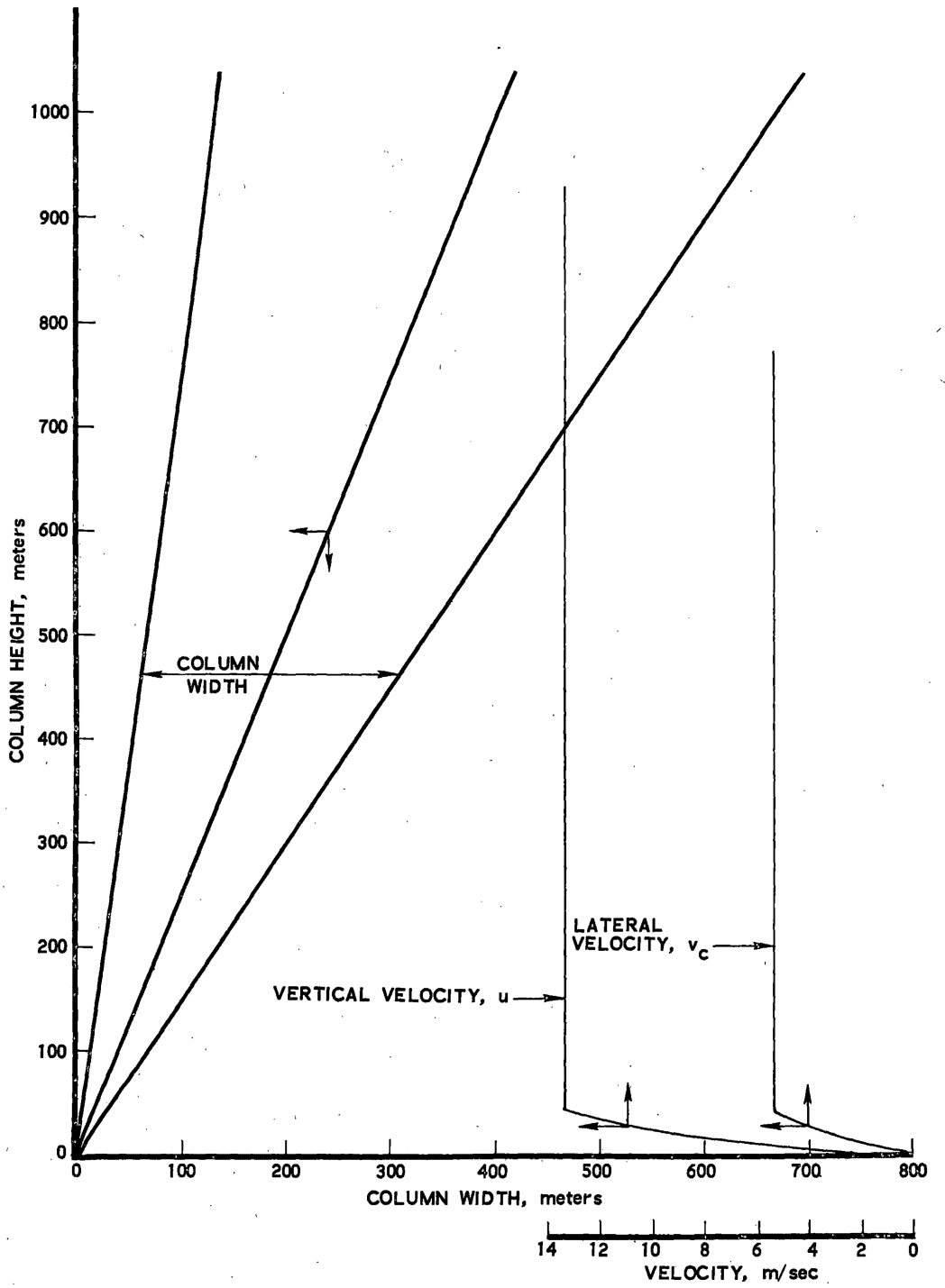

Fig. 13. Romero Fire Convection Column

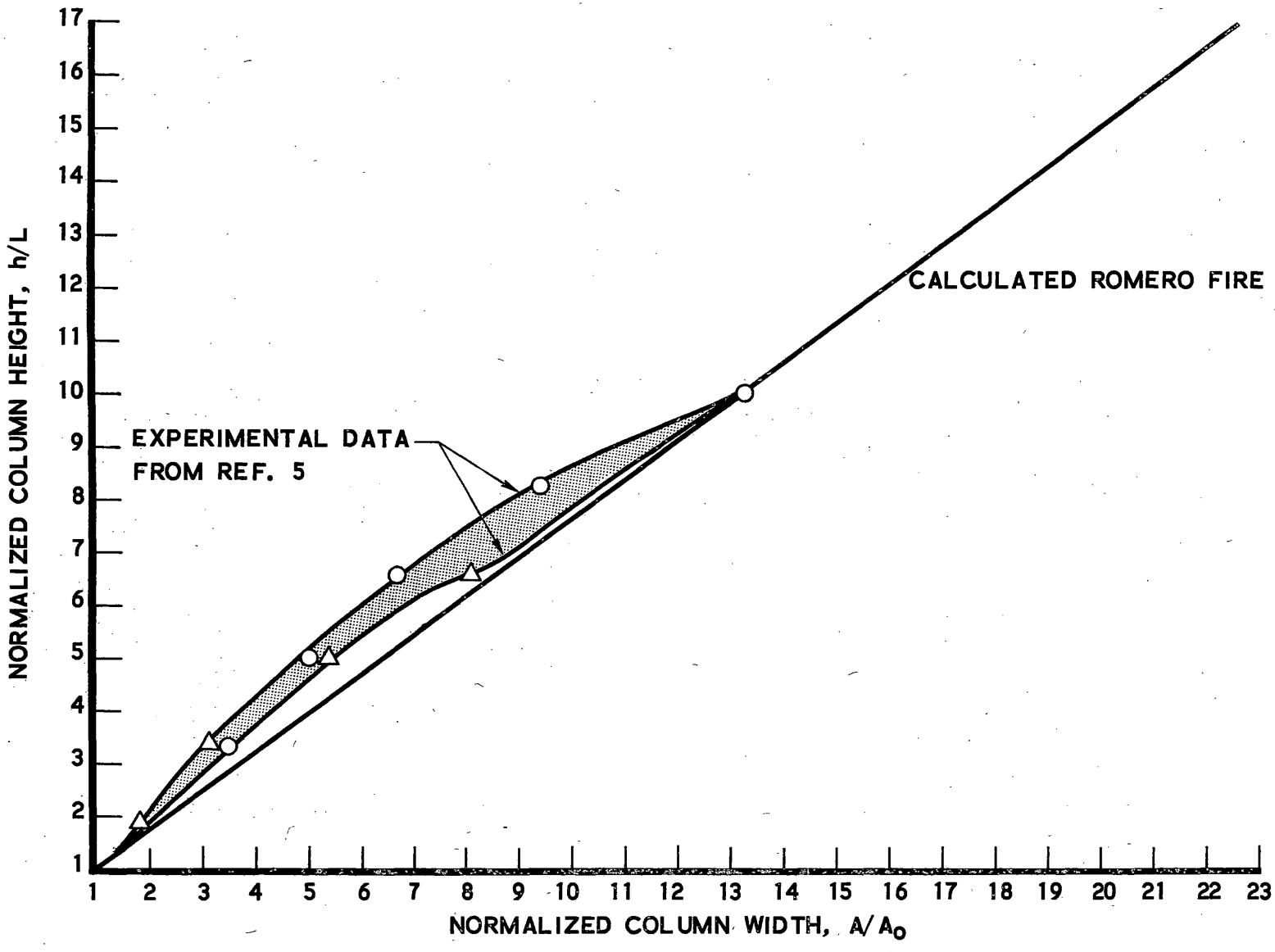

Fig. 14. Convection Column Comparison

4. FIREBRAND GROUND BURNING AND FUEL IGNITION

4.1 REVIEW OF PAST WORK

In the previous sections we have analyzed the firebrand trajectory and convection columns, and have also developed equations based on experimental data defining the changes in firebrand mass and volume during its burning period in flight. Upon impact on the ground, the firebrand will continue to burn in flaming or glowing combustion, transferring heat by either radiation, convection, or conduction, or a combination of the three, to the surrounding fuel particles. We shall consider primarily the case of flaming combustion of a firebrand with a fuel particle being close enough to be enveloped in the flame since this is a condition most likely leading to a spot fire. The questions to be answered therefore are: What is the duration of the flaming combustion as a function of firebrand impact size and its previous flight history? What are the criteria for the fuel particle ignition? What is the probability that a fuel particle of a certain size will be close enough to a firebrand?

The burning of wood is a complex process. Wood is composed mainly of cellulose (50 percent), hemicellulose (25 percent) and lignin (25 percent). Upon addition of external heat, the wood particle temperature increases by heat conduction, and once local temperatures above approximately 200°C are reached, a process of pyrolysis starts. The hemicellulose, which is the most reactive constituent, decomposes first between 200-260°C, followed by cellulose (240-350°C) and, finally, by lignin (280-500°C)[22]. As a result of pyrolysis, which is an endothermic reaction[23], gases including vaporized water moisture are generated which diffuse through the hot and charred surface layer, being further heated during this passage, and escape into the surrounding air. There they mix with oxygen, ignite and burn, provided the gas temperature is high enough. Some of the pyrolysis products diffuse into the virgin fuel ahead of the pyrolysis wave and cause alteration of its physical

and chemical structure prior to subsequent pyrolysis. A good pictorial representation of the wood burning process is shown in Fig. 15 reproduced from Ref. 24. Further complexity to the pyrolysis process is added by the catalytic effect of a small percentage of inorganic salts present in the wood. Roberts[22] quotes Broido's experiments in which as little as 0.15 percent of inorganic matter had an appreciable effect on the cellulose pyrolysis rate.

We will consider here a process of burning in which wood ignited by an external flame source (piloted ignition) continues to burn by being heated by its own flame without any other heat source. The process of burning will be principally controlled by the rate of pyrolysis generating the combustible gases.

A considerable amount of work was done in the past on cellulose ignition and pyrolysis. Kanury[25] reviewed work on ignition of cellulosic materials which included both piloted ignition and spontaneous ignition, the latter induced usually by radiative heat. The definition of the two types of cellulose ignition is quoted from Ref. 25:

> "For piloted ignition the mixture of fuel vapors and air in the proximity of the exposed wall is within the flammability limits of composition, but it needs an external source of heat (such as pilot flame, electrical filament, glowing embers, etc.) to initiate combustion. For spontaneous combustion, on the other hand, the mixture in addition to being within flammability limits is also in such a thermal condition that it can automatically react in an accelerating exothermic manner to yield a flame without the aid of any external, local energy sources."

It is of interest to note that experimental data indicated surface temperature criteria for piloted ignition of 300-410°C, while for spontaneous ignition it was approximately 600°C.

The temperature history and mass loss of wooden dowels (white fir) heated in a constant temperature furnace were reported by Tinney[26]. Alvares and Martin[27] studied the ignition time of radiatively heated thin sheets of blackened alpha cellulose in a furnace with varying oxygen partial pressure.

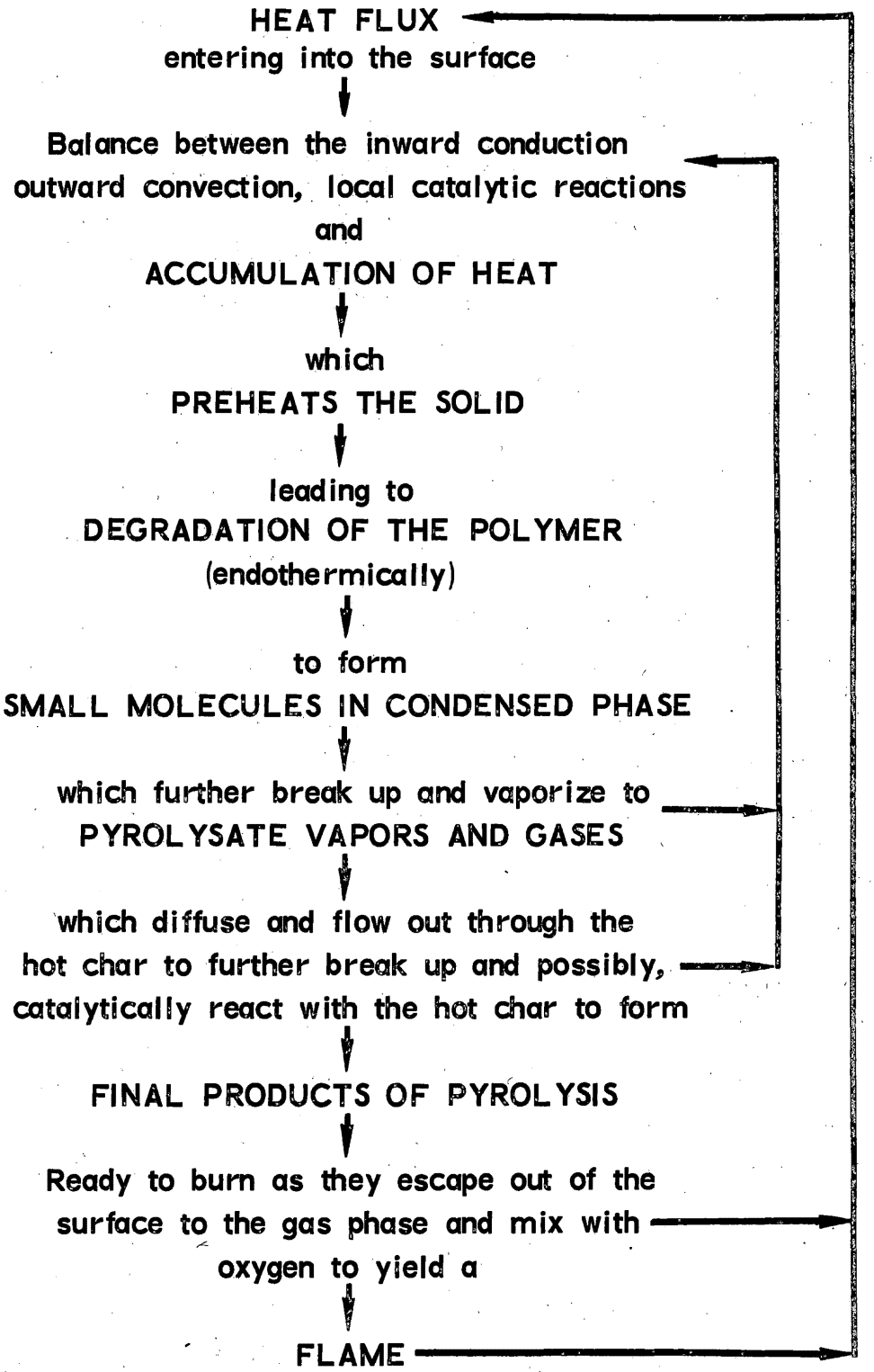

Fig. 15. Flow Diagram for Events in Burning Wood

They observed that surface temperature of about 600°C was consistently achieved with the onset of ignition regardless of the value of heat flux. Simms[28] subjected cellulose materials in the form of thin sheets (0.02 to 0.065 cm) or slabs with thickness > 1 cm to radiation heating by radiant panels or carbon arc. Analytical equations for ignition temperature were developed and the best fit between analytical and experimental data was obtained with surface temperature of 525°C.

Blackshear and Kanury[29,30] performed experiments with fuel-soaked cylindrical wicks and cellulose cylinders of various diameters burning in air and measured the mass loss as a function of burn time. A relationship $M/M_o \propto t/D_o^{1.563}$ gave a good correlation of all data. These and other data quoted in Ref. 29 suggested "insensitivity of the burn rate to factors other than the fuel element diameter." They also found that the orientation of the plates or cylinders had relatively small effect on the rate of mass loss.

Martin[31,32] studied ignition of alpha cellulose sheets by radiative heating. He distinguished a region of transient flaming, persistent flaming, and glowing as a function of Fourier number and normalized heat input value. Kosdon, Williams and Buman[33] burned alpha cellulose and birch wood cylinders vertically oriented and developed an expression for flame height and stand-off distance.

Clements[34] ignited and burned in air, square and circular dowels of white fir and mixed hardwoods, as well as square sheets of white fir. All samples were burned in methanol flames and mass loss was measured as well as rate of mass loss and burning time. An agreement was observed with Blackshear and Kanury data in that the ratio of instantaneous to initial mass $M/M_o \propto t/D^{1.58}$.

The effect of moisture was investigated by various researchers. Simms and Law[47] found, for instance, that the minimum intensity radiation required for ignition with pilot flame is increased only slightly with moisture content but that the increase in time at the same level of heat flux was more pronounced. This is in agreement with observations made by the author.

In Ref. 50, experiments were performed on ignition of slash pine needle litter of varying moisture content by means of flaming firebrands. There was a small difference in the percentage of needles ignited with moisture up to 20 percent, but a substantial reduction in ignitability occurred above that level.

Fons[51] presented data on ignition of ponderosa pine cylinders in a heated oven. His data are compared later with the calculated values.

4.2 FIREBRAND BURNING AFTER IMPACT

Since it was postulated that in the process of self-burning the combustion rate was controlled by wood pyrolysis, i.e., the rate of generation of combustible gases, it appeared logical to consider the first order pyrolysis reaction which is generally accepted as a good representation of complex phenomena*. After review of the literature, the author concluded that while a lot of experimental work was done on cellulose material pyrolysis, relatively few data were available on the rate of auto-burning of wood elements without another heat source. Consequently, experiments were conducted as a part of this work in which a variety of wood dowels, spheres, plates, as well as natural fuels, were burned in quiescent air with measurements taken of the rate of mass loss, flaming time, flame height, and flame temperature. In all of these tests, the moisture content of the fuel was kept between 0 and 3 percent of the dry fuel weight, although a few tests were made with moisture content up to 10 percent. In most of the tests, the fuel samples were held in a horizontal position, although the effect of vertical orientation on the rate of mass loss was examined briefly on a few specimens. Ignition in all cases was obtained by means of a gas burner and the sample was considered ignited when it was flaming uniformly along its length. It was observed in these experiments that there was a small change in the volume of the sample during the flaming combustion (diameter change $\leq$ 10 percent), and that the major

*Refs. 22, 24, 26, 29, 31, 32, 35

changes in the structure of the sample (fissures, cracks, peeling), as well as in the volume, occurred in the subsequent glowing period. A similar observation was made in Ref. 33 in which the change in the diameter of alpha cellulose cylinders was less than 25 percent. Consequently, a constant sample volume was assumed during the flaming period and the rate of mass loss could be interpreted directly as the rate of density loss defined by

$$\frac{d\rho_{(t)}}{dt} = - (\rho - \rho_c) \cdot a \exp\left(- \frac{E}{RT}\right) \tag{31}$$

Designation of the symbols is the same as noted for Eq. (7), with ρ_c being the final density of the sample on completion of combustion (g/cc).

The tests carried out by the author, as well as observations made in Ref. 30, indicated a strong influence of the initial diameter or thickness of the sample on the rate of burning. Equation (31) was amended therefore to include the size effect

$$\frac{d\rho_{(t)}}{dt} = - (\rho - \rho_c) \frac{1}{D_o} \cdot \frac{1}{K} \tag{32}$$

Integration of Eq. (32) results in

$$\frac{\rho_{(t)} - \rho_c}{\rho_o - \rho_c} = \exp\left(- \frac{t}{D_o} \cdot \frac{1}{K}\right) \tag{33}$$

This equation is similar to that derived for firebrands burning in flight [see Eq. (8)]. If we assume that the $1/D_o$ is a volume-to-surface ratio, then for cylinders $S/V = 4/D_o$ it can be postulated then that

$$\frac{1}{K} \simeq 4 \cdot a \exp\left(- \frac{E}{RT}\right)$$

or

$$K = \frac{1}{4a} \exp\left(\frac{E}{RT}\right) \tag{34}$$

The values of a, E and T were estimated in various references. For instance, review of Refs. 22, 26 and 35 indicates that there is a break point in the pyrolysis of wood. In the first stage of the pyrolysis, the value E = 30 Kcal/mole and $a = 6 \cdot 10^7 - 7 \cdot 10^8$ sec^{-1}. The second stage of pyrolysis which starts at density $\rho_{(t)}/\rho_o = 1/3$ and continues to the final density is defined by E = 37 - 43 Kcal/mole and $a = 4 \cdot 10^8 - 2 \cdot 10^9$ sec^{-1}. The $\rho_{(t)}/\rho_o = 1/3$ break point may correspond to the completion of cellulose pyrolysis and continuation of lignin decomposition. The temperature of pyrolysis varies depending upon the wood constituents, as was mentioned before, and for cellulose it has been estimated to lie between 250-350°C. Since our interest in flaming combustion implies mainly cellulose pyrolysis before the break point, we shall assume an average value of $a = 3.5 \cdot 10^8$ sec^{-1}, E = 30 Kcal/mole and T = 600°K. Substituting these values for Eq. (34) results in K = 60.6 sec/cm for cylindrical wood samples.

Experiments described above were conducted to check the proposed relationship. It was observed that small diameter samples ($D_o < 1$ cm) burn out completely, first flaming and then glowing, so that the final density ρ_c/ρ_o is of the order of 0.03-0.06, while larger diameter samples flame for a period of time, glow briefly and extinguish, leaving unburned material with high average density. Measurements of final density plotted in Fig. 16 for machined wood samples and in Fig. 17 for natural fuels, indicate that relationship

$$\rho_c = \rho_o \cdot 1.35\left(\frac{V_o}{S_o}\right)^2 \tag{35}$$

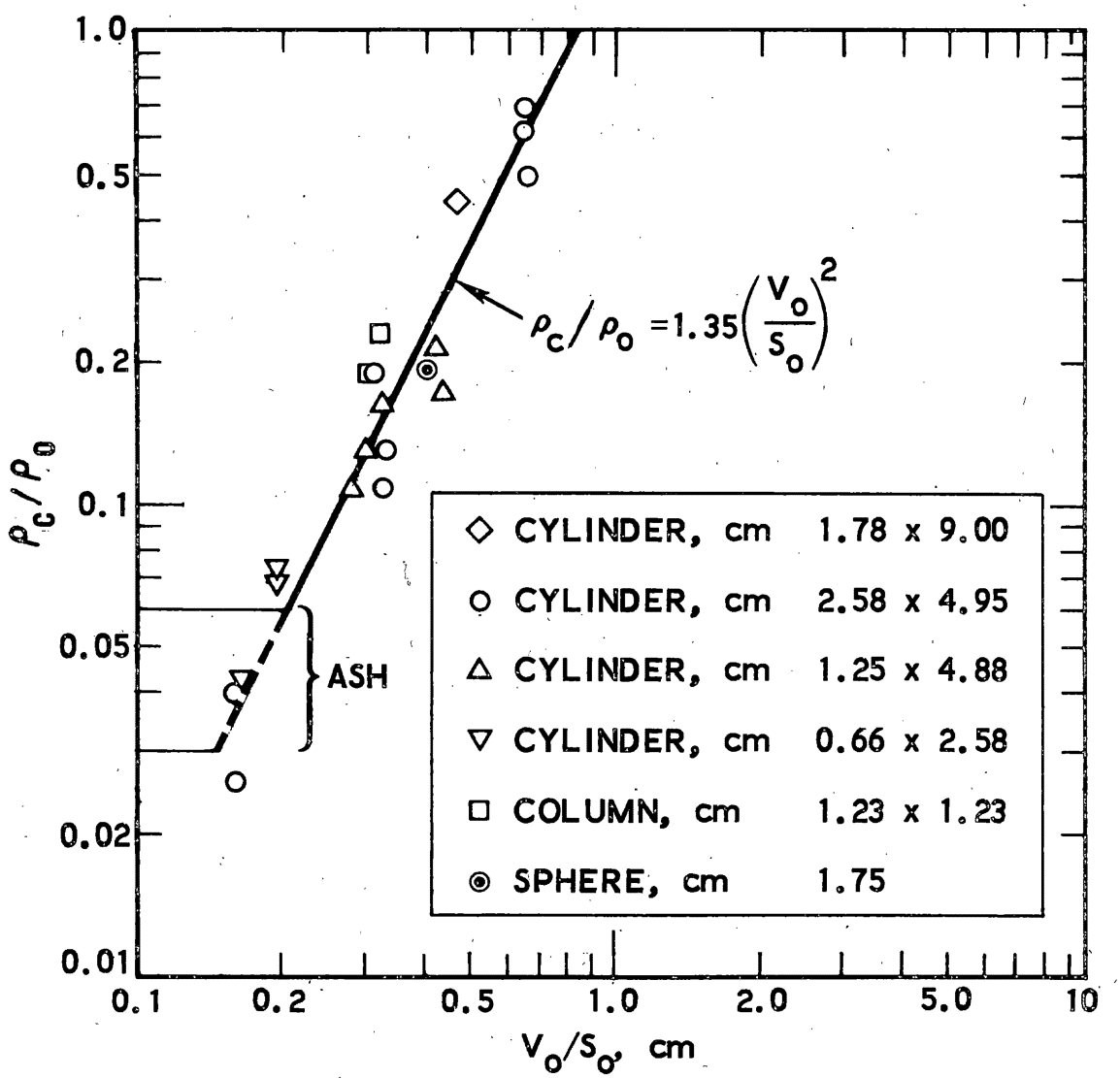

Fig. 16. Burnout Density for Wood Cylinders and Spheres as a Function of V_o/S_o

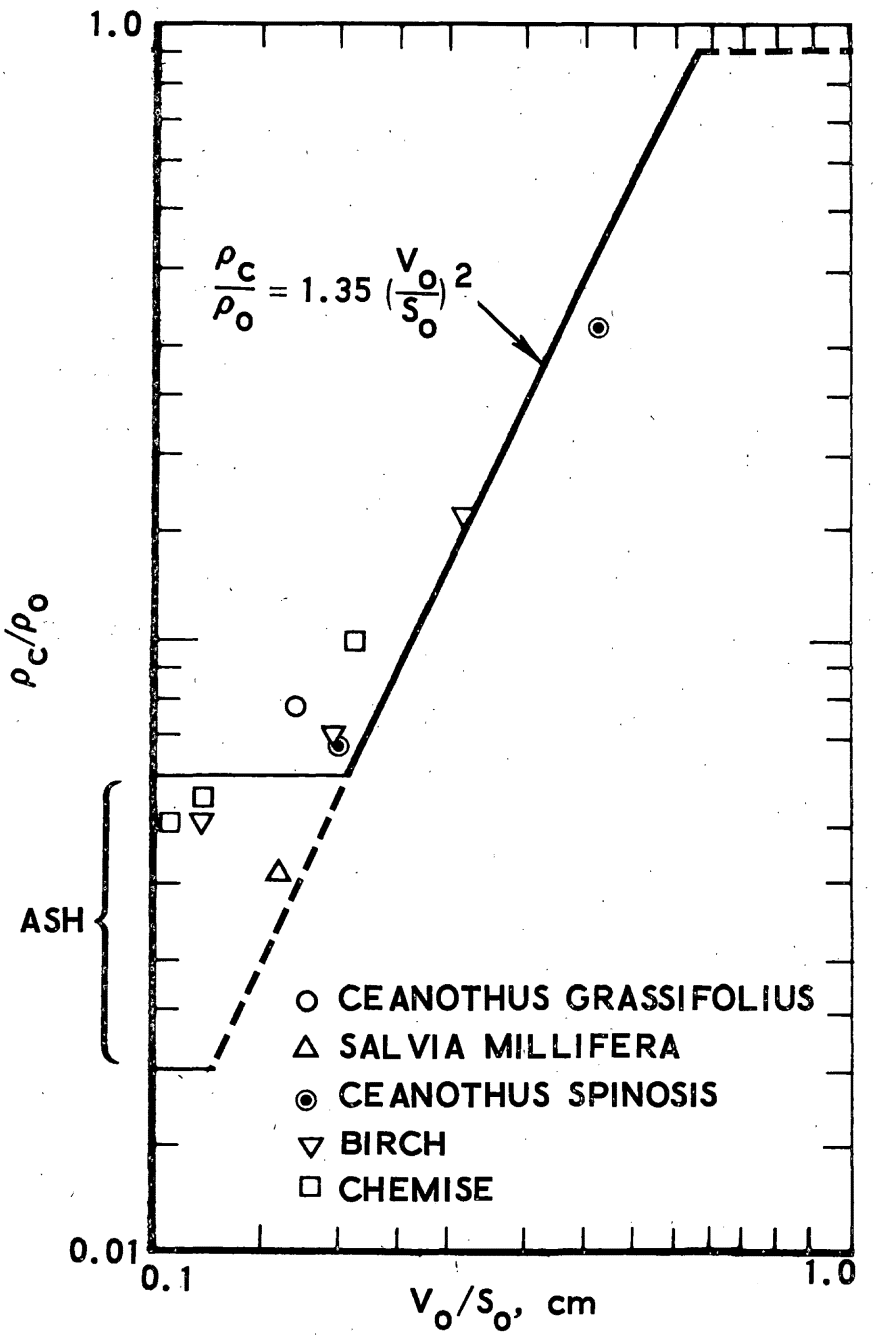

Fig. 17. Density at Burnout (Natural Fuels)

valid for $0.06\ \rho_o < \rho_c < \rho_o$, gives a reasonable correlation. The method of determination of V_o/S_o for natural fuels which were of irregular shapes (leaves, twigs, chips) is described in Appendix A. Values calculated from Eq. (35) were used subsequently in Eq. (33a) to determine the rate of burning with the lower limit for ρ_c set at $0.06 \cdot \rho_o$ which represents the average ash density. It should be noted that Eq. (35) indicates that for max $\rho_c/\rho_o = 1$, a cylindrical sample diameter is ~ 3.4 cm, which means that cylinders of that and larger size should not continue auto-burning with a significant mass loss in quiescent air once the source of external heat is removed.

Experimental data showing $\rho - \rho_c/\rho_o - \rho_c$ versus $t/D_o K$ are plotted for wood cylinders in Fig. 18. While the spread of data appears considerable, two observations should be made: one is that below $\rho/\rho_o \sim 1/3$ which for a 1 cm diameter cylinder would correspond to $\rho - \rho_c/\rho_o - \rho_c = 0.29$, a break point in the pyrolysis process should be expected with a resulting change in the constant K; the second is that fissures and cracks formed randomly in the later stages of burning affect the rate of mass loss and cause appreciable volume changes of the sample such that the substitution of density for mass is no longer valid. With these observations in mind, it is considered that Eq. (33) represents reasonably well the rate of auto-burning of wood mass loss, at least to the value of $\rho/\rho_o \geq 1/3$, and that the mean value of constant K = 55 sec/cm is close to the value of 60.6 derived from reaction kinetics.

The validity of Eq. (33) with a constant K = 55 sec/cm will be therefore limited to $\rho \geq 0.3\ \rho_o$ and to $D_o < D_{crit.}$ whose $D_{crit.} \sim 3.4$ cm corresponds to $\rho_c = \rho_o$ from Eq. (35). At $\rho \leq 0.3\ \rho_o$, the value of K will be less than 55 and it can no longer be assumed constant.

Similar measurements were made for wood spheres and these are shown in Fig. 19. Since the ratio of V_o/S_o for the sphere is 2/3 of a cylinder of the same diameter, a smaller value of K should be expected with a resulting steeper slope of the correlation curve. While Fig. 19 shows that many points are indeed below the K = 55 slope, there were not enough data available to make a more accurate prediction.

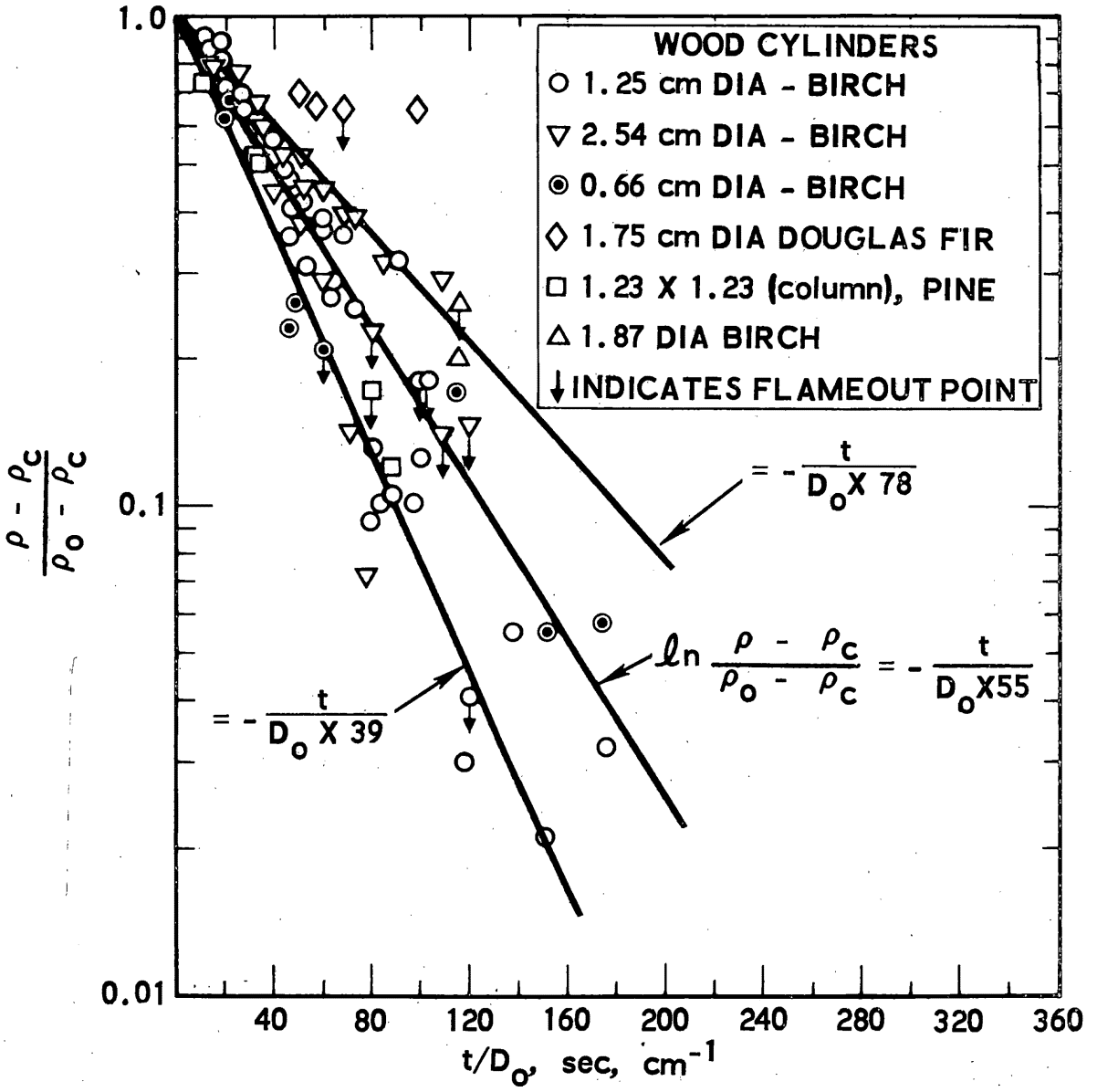

Fig. 18. Mass Loss Rate During Ground Burning

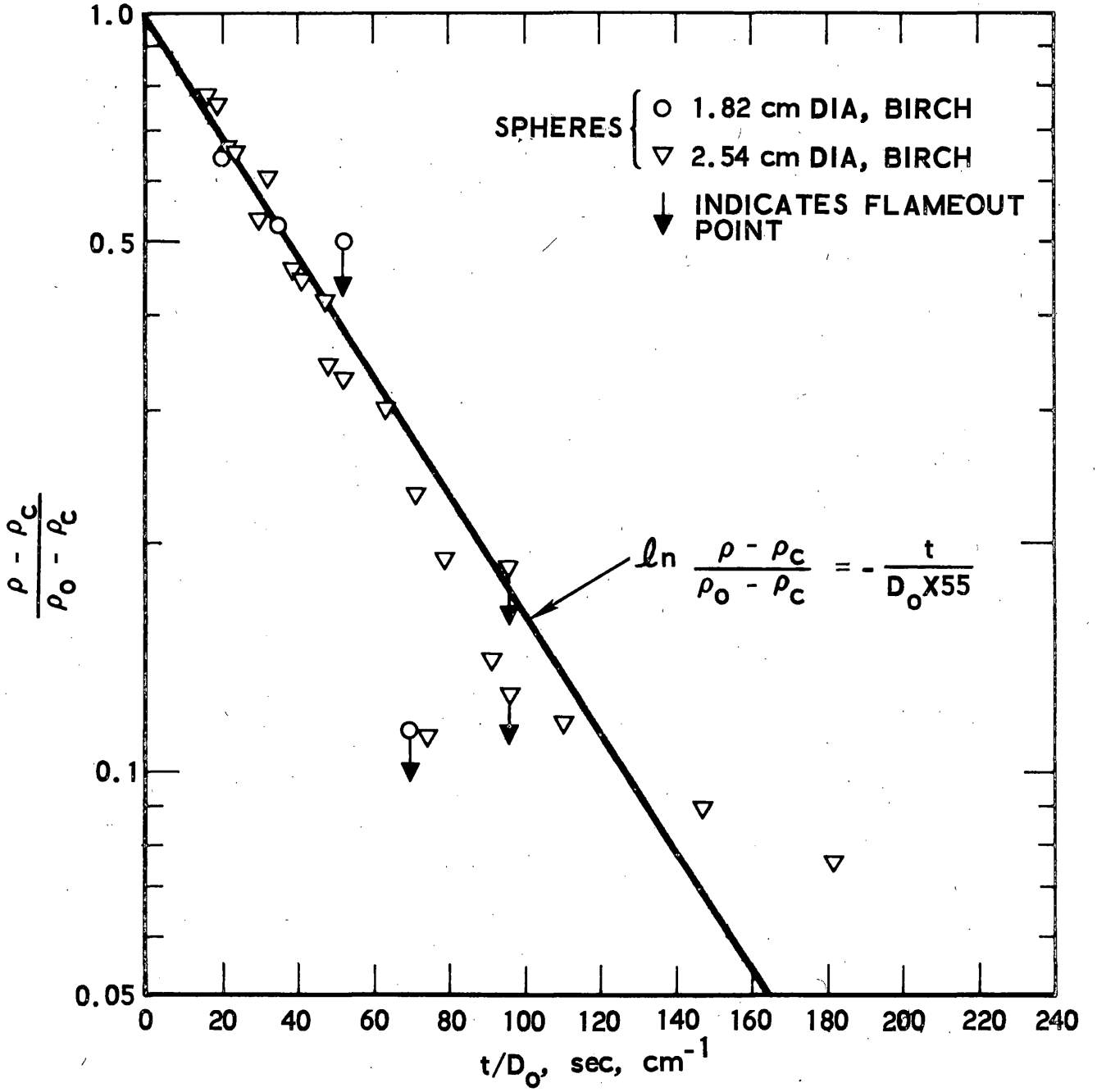

Fig. 19. Mass Loss Rate During Ground Burning

Data from Ref. 30 were plotted in a manner similar to that in Figs. 18 and 19 and show good correlation down to $\rho/\rho_o \geq 0.3$.

If the firebrand has at impact some density $\rho_i < \rho_o$ and diameter $D_i < D_o$, Eq. (33) will be modified to

$$\frac{\rho - \rho_c}{\rho_i - \rho_c} = \exp\left(-\frac{t}{D_i K}\right) \tag{33a}$$

and Eq. (35) to

$$\rho_c = \rho_o \cdot 1.35\left(\frac{V_i}{S_i}\right)^2 \tag{35a}$$

to define its burning process in quiescent air. Values ρ_i and D_i are defined from the trajectory program previously described. The constraints on the validity of Eq. (33) apply also to Eq. (33a).

To assess the ability of a burning firebrand to ignite a neighboring fuel element, it is necessary to define the firebrand flaming time as a function of impact condition and also the flame envelope.

Martin distinguished in the already quoted Ref. 31 a range of transient flaming, sustained flaming, and glowing as a function of Fourier number and radiant energy exposure. The author has modified the energy scale from Ref. 31 to correspond with observations made with piloted ignition, as shown by Fig. 20, reproduced from Emmons[36]. Transient flaming is defined here as the burn period which terminates with incomplete consumption of the solid. It is characteristic for thicker samples and is usually followed by a period of glowing before extinction. Permanent flaming, on the other hand, results in complete flaming combustion of the solid to a near-ash level.

The observation of flaming time, t_{fl}, of various <u>virgin</u> wood samples led to an equation

$$t_{fl} = 80 \cdot D_o^{1.25} \tag{36}$$

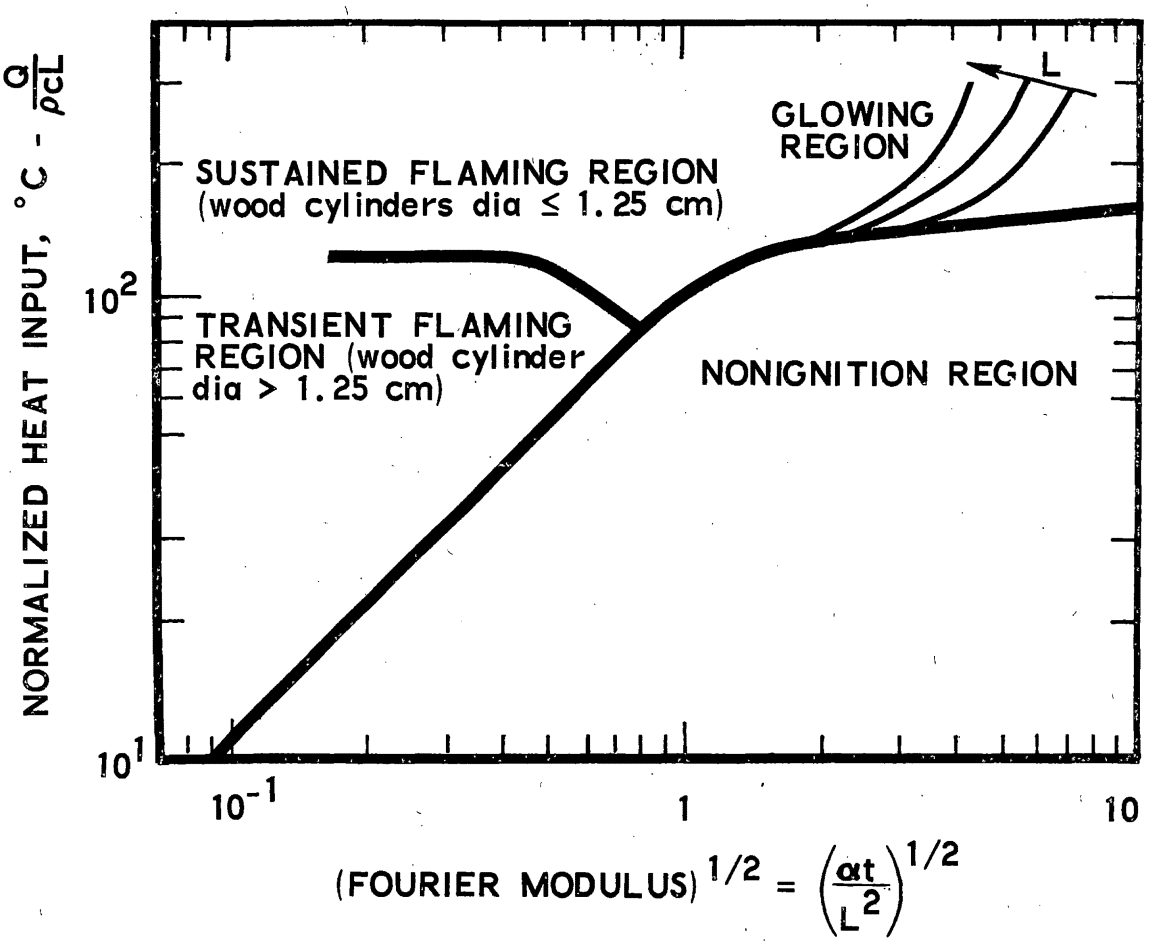

Fig. 20. Generalized Flame Ignition Behavior of Cellulose Fuels

Figure 21 presents experimental data for fabricated wood cylinders and shingles. The equivalent diameter, D_o, for shingles was obtained from volume and surface measurements $D_o = 4 \cdot (V_o/S_o)$. Note that data for Douglas fir cylinders (DF points in Fig. 21) have shown great variation in flaming time and lie outside of the Eq. (36) correlation. The reason for this is unknown. Figure 22 shows similar data for natural fuels converted to D_o in the same way as described above. The author believes that Eq. (36) is valid for all diameters less than approximately 3 cm and that a progressive and rapid drop in flaming time above this diameter should occur. This was partially verified experimentally by burning birch cylinders of 3.25 cm diameter. The measured flaming time was 120-150 sec, while Eq. (36) predicted 342 sec. On the other hand, for 2.5 cm cylinders, the flaming times were 250-280 sec while the calculated value for Eq. (36) was 251 sec.

The density of the wood at the end of the flaming time can be calculated from Eq. (33) by substituting t_{fl} for t

$$\frac{\rho_{fl} - \rho_c}{\rho_o - \rho_c} = \exp\left(-\frac{t_{fl}}{D_o \cdot K}\right) \qquad (33b)$$

The flaming density ratio ρ_{fl}/ρ_o calculated from Eq. (33b) and ρ_c/ρ_o from Eq. (35) are plotted as a function of D_o in Fig. 23. It can be seen that as $D_o \rightarrow 3.4$ cm, $\rho_{fl} \rightarrow \rho_o$ or $t_{fl} \rightarrow 0$. As it was stated before for values of ρ_{fl}/ρ_o less than approximately 0.3, at which a possible break point and change of slope in the pyrolysis curve of wood occurs, Eq. (33b) with a constant K = 55 will not be valid. However, calculations were performed down to $D_o = 0.2$ cm and are shown with a dotted line in Fig. 23.

Experimental observations of flaming time made down to $D_o = 0.48$ cm indicated reasonable agreement with the values calculated from Eq. (36), but the calculated values of ρ_{fl}/ρ_o from Eq. (33b) were higher than experimental data for $\rho_{fl}/\rho_o < 0.35$ (see Fig. 23).

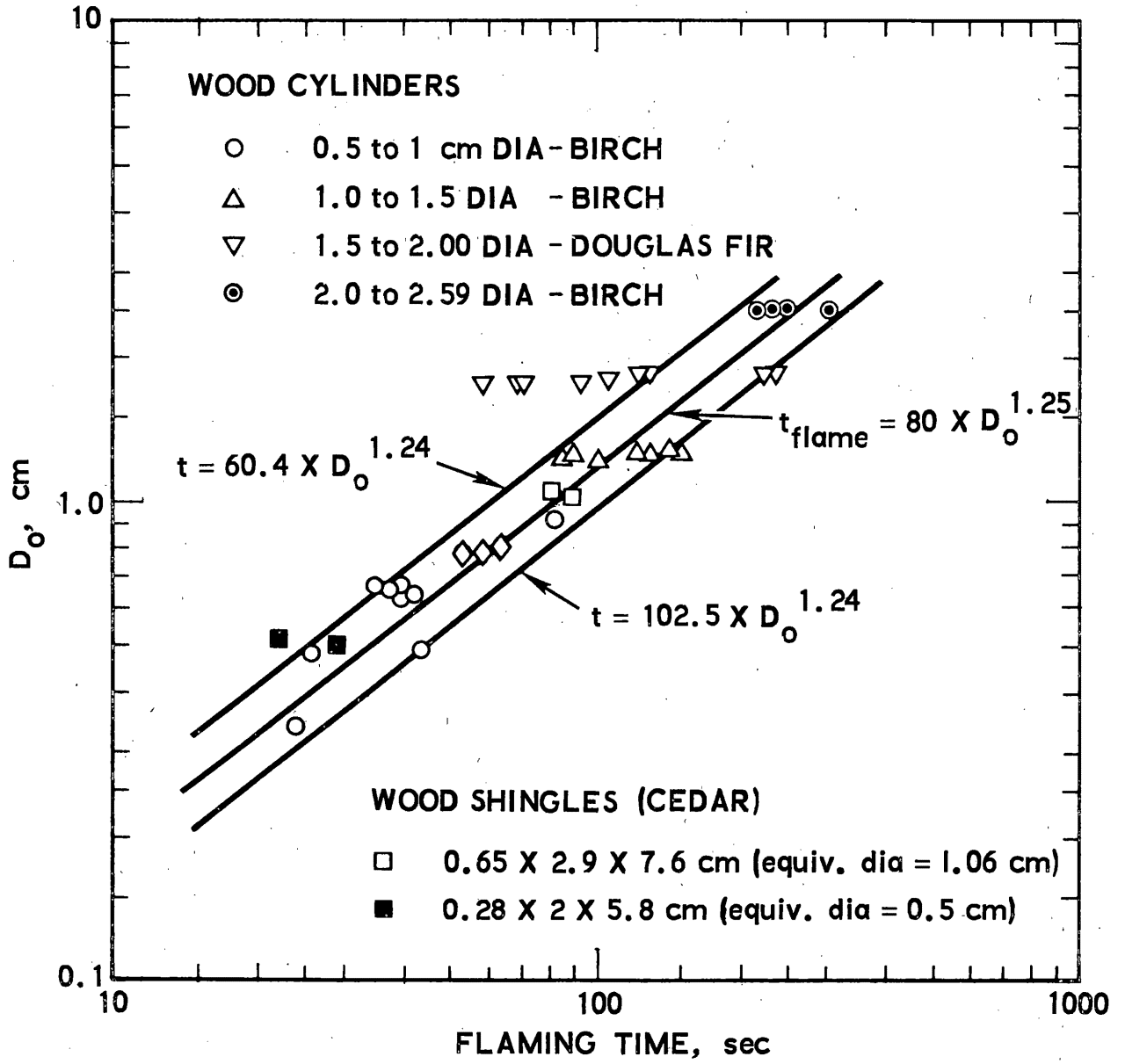

Fig. 21. Firebrand Flaming Time (Moisture 0 to 5%)

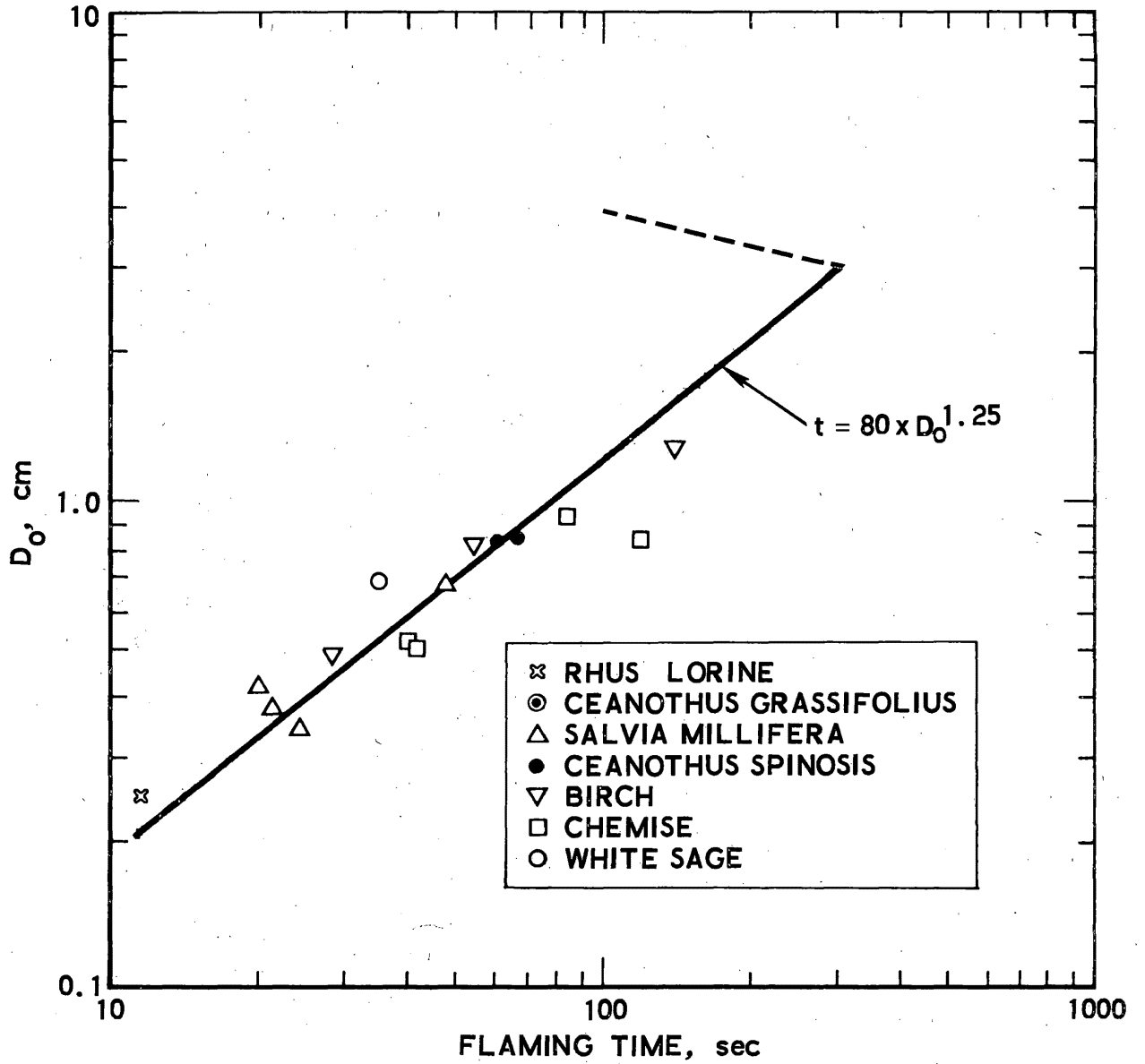

Fig. 22. Flaming Time (Natural Fuels)

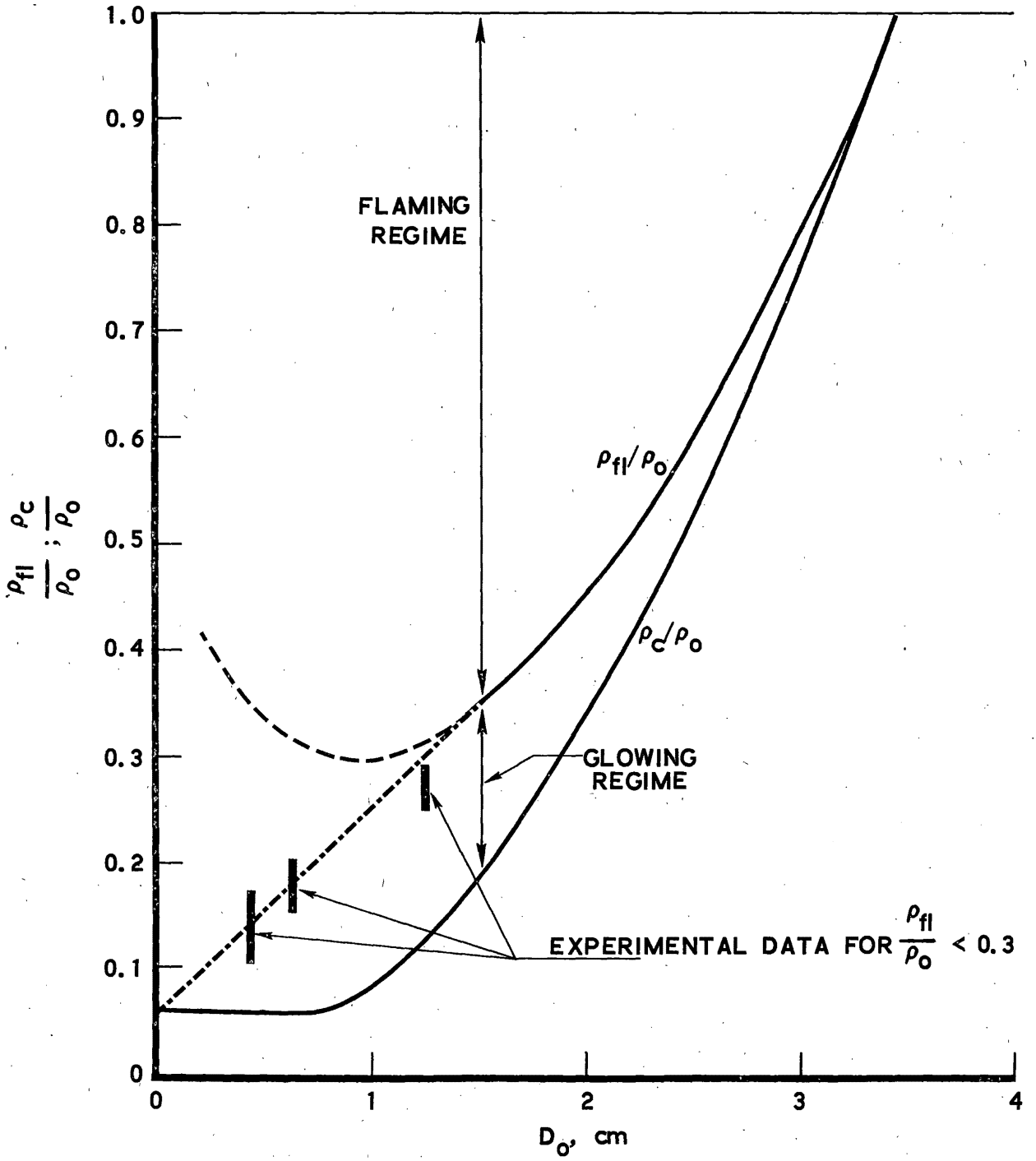

Fig. 23. Flaming and Glowing Regimes of Firebrands as a Function of Initial Diameter

In the case of a firebrand impacting after a certain period of burning in flight, its remaining flaming time after impact will be, of course, less than that calculated from Eq. (36) and it will be a function of firebrand impact diameter, D_i, and density, ρ_i.

By combining Eqs. (33a) and (33b), and substituting ρ_{fl} for ρ and t'_{fl} for t in Eq. (33a) the remaining flaming time, t'_{fl}, is

$$t'_{fl} = t_{fl} - D_i K \ln \frac{\rho_o - \rho_c}{\rho_i - \rho_c} \tag{37}$$

where ρ_c is calculated from Eq. (35a). The flaming time will vary for a given diameter from t_{fl} when $\rho_i = \rho_o$, to $t'_{fl} = 0$ when $\rho_i = \rho_{fl}$. A plot of flaming time as a function of impact density (ρ_i/ρ_o) is shown for different sizes of firebrands in Fig. 24. It has to be borne in mind that for $\rho_{fl}/\rho_o \leq 0.3$, value K is no longer = 55. For instance, for D = 0.5 cm, a value of K = 30 appears to fit the data. Comparison of the flaming time against the time required for ignition of virgin fuel (which is treated in Section 4.3) will provide one of the criteria for spot fire generation.

The effect of firebrand attitude on its flaming/glowing time was not examined in detail; however, some general observations were made. Most of the experimental work supporting this study was carried out with wood cylinders in a horizontal position. A few tests were performed in which the cylinders were placed, after initial ignition in the horizontal position, in a vertical position and the measurements of the flaming time were made. It was concluded from these tests that provided the cylinders were ignited uniformly throughout their length, no significant change in the flaming time was observed between horizontal and vertical position. A similar observation was made[1a] in which firebrands were burning in a fixed position and in a free moving state. It was reported there that no significant differences in the firebrand burning mechanism were observed.

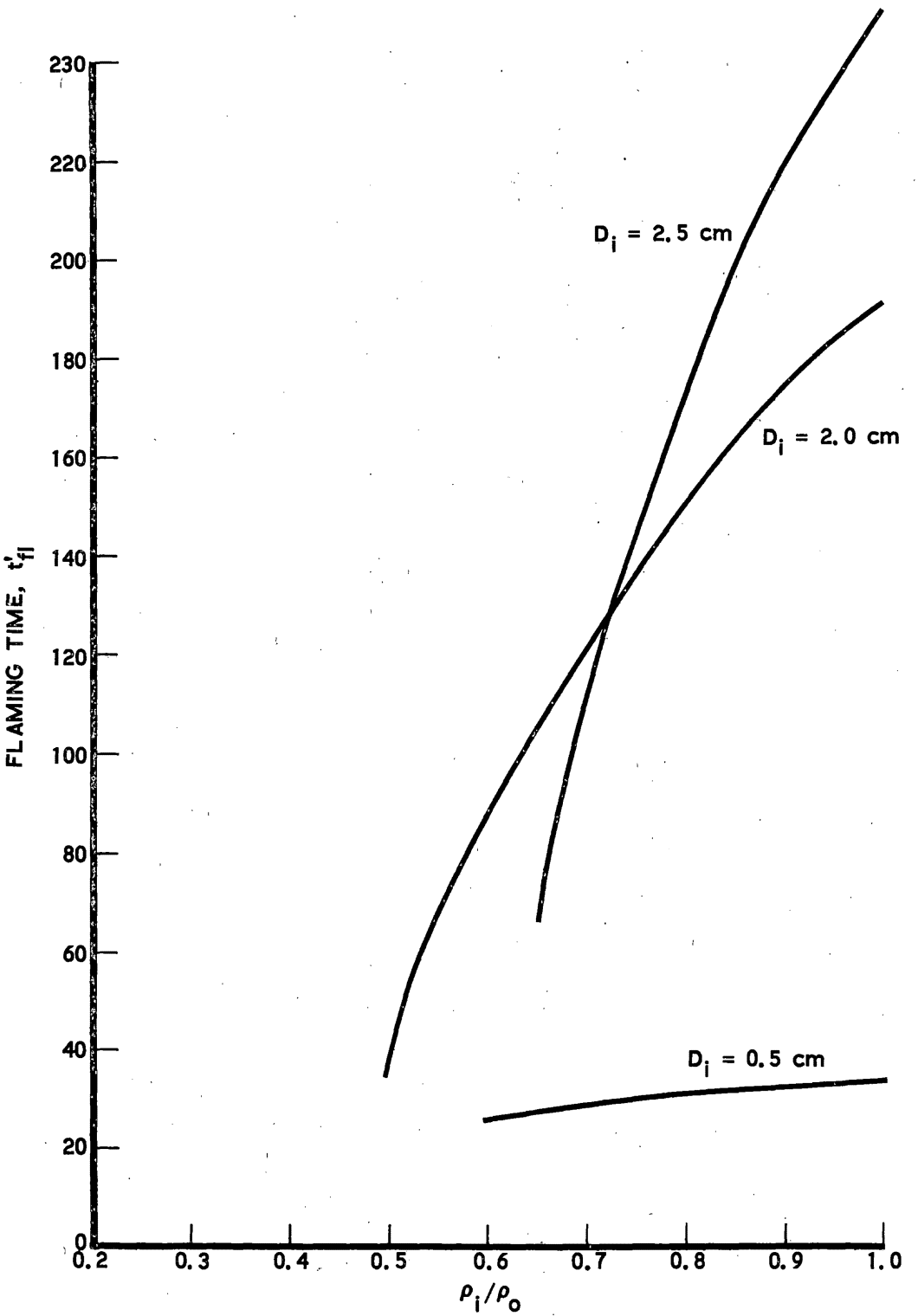

Fig. 24. Flaming Time of Cylindrical Firebrands as a Function of Impact Density and Size

It is necessary now to consider the problem of flame height of a burning firebrand on the ground since this information will be required in the statistical evaluation of the spot fire hazard.

Thomas[13] addressed the problem of flame sizes from line source and defined flame height by Eq. (10) which indicates it to be proportional to $\dot{m}^{2/3}$ where $\dot{m}$ was fuel mass burn rate per unit of fire front. Kosdon[33] found that the flame height for vertical alpha cellulose cylinders was proportional to $\dot{m}^{0.48}$. In the author's experimental work the flame height data for horizontal fuel cylinders are plotted in Fig. 25 and can be approximated by

$$h = 163 \cdot \dot{m}^{0.662} \tag{37a}$$

where h is flame height (cm) measured from the bottom of the cylinder, $\dot{m}$ is unit length rate of firebrand mass loss in g/cm-sec. The $\dot{m}$ exponent is similar to that arrived at by Thomas. The value $\dot{m}$ can be calculated from Eq. (32) by multiplying it by the cylinder unit length volume. With regard to the flame width, the maximum width was found to be approximately $1.2 \cdot D_o$ for horizontal or near horizontal cylindrical firebrands.

The effect of moisture on firebrand burning was not evaluated. The moisture will affect both the ignition time of a firebrand and the burning process itself. The effect of moisture on ignition of virgin fuels is dealt with in the next section, and comments made there are, in general, applicable to firebrand ignition. The qualitative assessment of firebrand ignition time in a fire front is difficult to make since the magnitude of heat flux is an unknown variable. This flux will be generally higher than that in the case of a single burning firebrand igniting a specimen of virgin fuel. Therefore, the ignition time in a flame front will be shorter than that calculated for the latter case. It was tacitly assumed that firebrands burning after impact in a flaming state must have low initial moisture (< 10 percent) and that they are formed from dead fuels. Consequently, with high heat fluxes available for the ignition in the flame front, the change in the ignition time with moisture should be small.

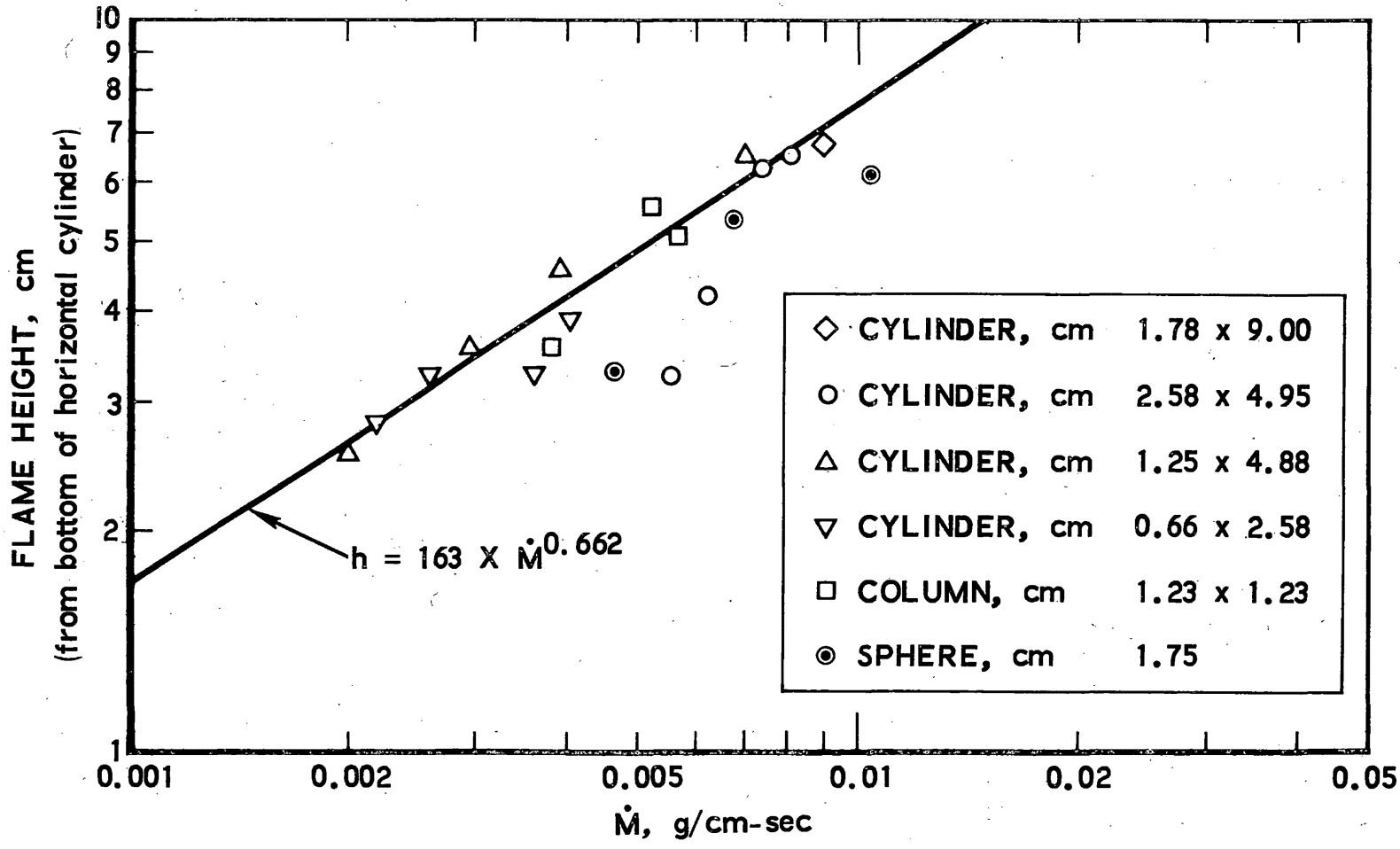

Fig. 25. Flame Height as a Function of Mass Loss Rate for Horizontal Cylinders and Spheres

The effect of moisture (which was varied from 3 to 10 percent) on the burning rate appears from the few tests made to slow down the rate of mass loss, which is to be expected. Not enough experiments were performed to offer a qualitative assessment.

The author's conclusions are not in complete agreement with Ref. 1a which stated that "moisture content exerts a very strong influence on the ignition process of the firebrands, but after ignition its influence is not very important, at least for not very large firebrands."

It is apparent that more experimental work is required on the moisture effect on firebrand ignition and burning under simulated flight conditions.

4.3 VIRGIN FUEL IGNITION

A firebrand which we consider as a spot fire hazard can be at impact in a state of either flaming or glowing combustion. As it was stated before, the problem addressed here is the case of flaming firebrands, considering a fuel specimen close enough and small enough to be engulfed in a flame in a part of its length and be subjected to both convective and radiative heat input. It was further assumed that in view of the limited flaming time of partially spent firebrands (see Fig. 24), we should be mainly concerned with easily ignitable virgin fuels with a low moisture content (< 10 percent), which implies dead fuels.

It is realized that the case of glowing combustion of a fallen firebrand cannot be neglected. It is quite possible for a glowing ember to fall directly on a litter composed of small size dead fuels (dry needles, leaves, etc.), and by conduction and radiation initiate slow glowing burning which may be followed by flaming combustion. Only very thin (< 0.1 cm) and dry fuel particles will have a chance of ignition from a glowing ember because surface temperatures will be lower than those recorded in flaming combustion, 600°C[14,21] versus 850-900°C[38,39], with correspondingly higher heat input rates.

When considering flame radiation in a fuel element immersed in that flame, we consider the flame to be a solid surface of temperature T_{fl} and emissivity ϵ.

Then the net radiative heat flux, $\dot{q}_r$ (cal/cm^2-sec) received at the element surface can be calculated as the difference

$$\dot{q}_r = \epsilon\beta \cdot \delta T_{fl}^4 - \epsilon_s \cdot \delta T_s^4 \qquad (38)$$

assuming the view factor equals unity

β = element surface absorptivity
δ = Stefan-Boltzmann constant = $1.36 \cdot 10^{-12}$ cal/cm^2-sec-$^oK^4$
ϵ = flame emissivity
ϵ_s = element surface emissivity
T_{fl} = flame temperature, ^oK
T_s = surface temperature, ^oK

Flame emissivity values, ϵ, reported for pine woods[40] varied between 0.16 and 0.28 for moisture content between 0 and 15 percent and in Ref. 42 it was assumed 0.227. Reference 52 calculated total flame emissivity as a function of soot content and flame thickness. For thin flames ($\sim$1 cm) dealt with here, the soot particle radiation will be predominant and for volume fraction occupied by soot particles varying between $0.1 \cdot 10^{-4}$ to $0.3 \cdot 10^{-4}$ flame emissivity would vary between 0.15 and 0.35. A value of $\epsilon = 0.23$ was assumed here as an average. Fuel surface absorptivity, β, reported in the literature,[50] varied from 0.45 to 0.77. A value of 0.6 was accepted here. A fuel element surface emissivity, ϵ_s, was assumed as 0.7 during the pre-ignition period.

The fuel surface temperature will vary as a function of heating time until ignition occurs. We have assumed, in accordance with previously reviewed data, surface ignition temperature with pilot ignition of 327^{o}C (600^{o}K).

The convection heat transfer to a fuel element immersed in the firebrand flame should be calculated from forced convection equations

$$N_{Nu} = B(R_e)^n$$

where N_{Nu} is the Nusselt number, R_e the Reynolds number for a fuel element of a given diameter, D_o, and B and n are constant depending on the value of Reynolds number. The difficulty in applying this equation is in the determination of gas velocity at the fuel element location. To obtain the order of magnitude values, flame tip velocities were calculated using Thomas' equation from Section 2 for flame heights from Fig. 25. Reynolds numbers calculated for small fuel elements (0.5 cm diameter) were of the order of 20-30 and for the larger diameter (3 cm) 130-230. This resulted in Nusselt numbers of approximately 2.6 and 7.7, respectively. Subsequent calculations performed with free convection columns have shown similar results, particularly when Eq. (40) was used. Consequently, in view of the R_e uncertainty, free convection calculation presented below was used for ignition time determination.

The convection heat transfer in a free convection in which fluid motion is induced by buoyancy forces only leads to the calculation of the film transfer coefficient h(cal/cm^2-sec-^{o}C) as follows:

$$N_{Nu} = 0.52 \sqrt[4]{N_{Gr} \cdot N_{Pr}} \quad \text{(Ref. 43)} \tag{39}$$

where

$$N_{Nu} = \frac{h \cdot D_o}{k} \quad \text{(Nusselt Number)}$$

$$N_{Gr} = \frac{gD^3 \cdot (T_{fl} - T_s)}{\nu^2 \cdot T_1} \quad \text{(Grashof Number)}$$

$$N_{Pr} = \frac{\nu}{\alpha} = \frac{\mu c}{k} \quad \text{(Prandtl Number)}$$

k = gas thermal conduction, cal/cm-sec-^{o}C
T_1 = ambient air temperature, ^{o}K
α = gas thermal diffusivity, cm^2/sec
μ = gas dynamic viscosity, g/cm-sec
ν = gas kinematic viscosity, cm^2/sec

The flame temperature, T_{fl}, based on the literature data and on the author's measurements, was determined to be an average of 1100°K (827°C). The author's measurements were done with unshielded 1/64-inch Chromel-Alumel thermocouples and the flame temperatures for various woods varied between 750 to 850°C. The gas properties were assumed to be equal to the air properties at the flame temperatures: c_p = 0.274 cal/g-°C, k = 1.48 · 10^{-3} cal/cm-sec-°C, μ = 0.036 centipose, ν = 0.85 cm^2/sec and α = 1.28 cm^2/sec.

The value h was obtained for a given diameter once the value of N_{Nu} was calculated from Eq. (39). Mean values of $T_{fl} - T_s$ were used in the calculation of the Grashof number. Table 2 gives the results of the calculation.

Table 2. Convective Heat Transfer Coefficient

Dia., cm	N_{Pr}	N_{Gr}^*	$N_{Gr} \cdot N_{Pr}$	N_{Nu}	h, cal/cm^2-sec-°C x 10^{-4}
0.2	0.664	25.6	17.01	1.056	7.83
0.5		399.8	265.85	2.100	6.23
1.0		3198.3	2126.9	3.530	5.23
2.0		25586.4	17015.0	5.940	4.41
3.0		86354.1	57425.0	8.050	3.98
4.0	0.664	204691.2	136119.6	9.990	3.70

*Calculated with an average value of $\overline{T_{fl} - T_s}$ = 700°C

Equation (39) is generally applicable in the range $10^3 < N_{Gr} \cdot N_{Pr} < 10^9$; consequently, an error is expected in the calculation of h for 0.5 and 0.2 cm diameters.

Weinberg (Ref. 44) suggested an alternate equation which would more accurately cover the whole range of sizes.

$$N_{Nu} = \exp\left[0.15 + 0.0971\ln\left(N_{Gr} \cdot N_{Pr}\right) + 0.0073\left(\ln N_{Gr} \cdot N_{Pr}\right)^2\right] \quad (40)$$

Weinberg has shown that calculation of heat transfer coefficient using Eq. (40) over the range of diameters in Table 2 resulted in an error of < 2 percent when compared with other data, and that Eq. (39) gave for diameters 0.2 and 0.5 cm errors of -28 and -16 percent, respectively.

The total heat flux at the surface of a fuel specimen will consist of a sum of radiant and convective fluxes, $\dot{q}_t = \dot{q}_r + \dot{q}_c$ where $\dot{q}_c = h(T_{fl} - T_s)$. This heat flux is transferred into the solid fuel during the pre-ignition period mainly by conduction through the solid.

The regime in which internal convection versus conduction heat transfer predominates can be defined by the value of Peclet number $N_{Pe} = c_f \cdot \dot{m} \cdot D/k_f$, where c_f is specific heat of fuel, $\dot{m}$ (g/cm^2, $< sec$) pyrolysis rate, D fuel diameter, and k_f fuel thermal conductivity. For $N_{Pe} \ll 1$ convection effects will be small compared to conduction while for $N_{Pe} \gg 1$ the convective term is not negligible (Ref. 45). For the sizes of fuels considered here (from near 0 to 3 cm diameter), Peclet number during the flaming period varies from near 0 to approximately 3.0 which is a "grey area" for significance of the internal convection term. However, during the pre-ignition period the mass rate of pyrolysis is small and Peclet number will be $\ll 1$. This allows the use of conduction heat transfer mechanism for fuel preheating and in many data presented by various research workers the time to ignition data calculated from a simple semi-infinite conduction slab model agreed well with the experimental data[45,46].

The transient conduction heat transfer into an infinitely long cylinder is expressed by

$$\frac{\partial T}{\partial t} = \alpha_f \cdot \frac{\partial^2 T}{\partial R^2} + \frac{\alpha_f}{R} \cdot \frac{\partial T}{\partial R} + \frac{\dot{Q}}{\rho_f c_f} \quad (41)$$

where R is cylinder radius, ρ_f, c_f, α_f are fuel density, specific heat and thermal diffusivity, respectively. The $\dot{Q}$ is the rate of heat required for moisture evaporation per unit of volume. In treating the moisture effect, it was assumed that with the moisture M expressed as a weight fraction of dry fuel it will be distributed uniformly through the fuel and that the density and specific heat of the fuel will be a function of the moisture such that

$$\rho_f = \rho_{fo}\,(1 + M) \qquad \text{(Ref. 47)}$$

$$c_f = c_{fo} + M \qquad \text{(Ref. 48)} \tag{42}$$

where ρ_{fo} and c_{fo} are the density and specific heat values for dry fuel. We have neglected for c_f the heat of the absorption of bond water which results in an error of < 10 percent. Thermal conductivity change of fuel with moisture is also defined[47,48], but we have assumed it to be constant in the small range of moisture from 0 to 10 percent.

Since a computer program was available to solve this problem numerically by finite elements technique with boundary conditions such that at $t = 0$, $T = T_1$, $R = R_o$, $\dot{q}_t = -k \cdot \partial T/\partial R$ where $\dot{q}_t$ is total rate of heat flow into the cylinder per unit area, temperature profiles and times for ignition were calculated for various diameter wood cylinders. An example of the temperature profile calculated in this manner is shown in Fig. 26.

Following the general objective of this work to use approximate closed form solutions wherever possible, the computed results with dry fuel were compared with the no-heat loss semi-infinite slab solution for ignition time using the Carslaw and Jaeger equation

$$t_{ign} = \frac{(T_s - T_1)^2 \cdot k_{fo} \cdot c_{fo} \cdot \rho_{fo} \cdot \pi}{4\bar{\dot{q}}_t^2} \tag{43}$$

The value of average total heat flux is $\bar{\dot{q}}_t = \bar{\dot{q}}_r + \bar{\dot{q}}_c$ where $\bar{\dot{q}}_r$ is mean radiation flux calculated from Eq. (38) and $\bar{\dot{q}}_c$ is mean convection flux calculated from known h.

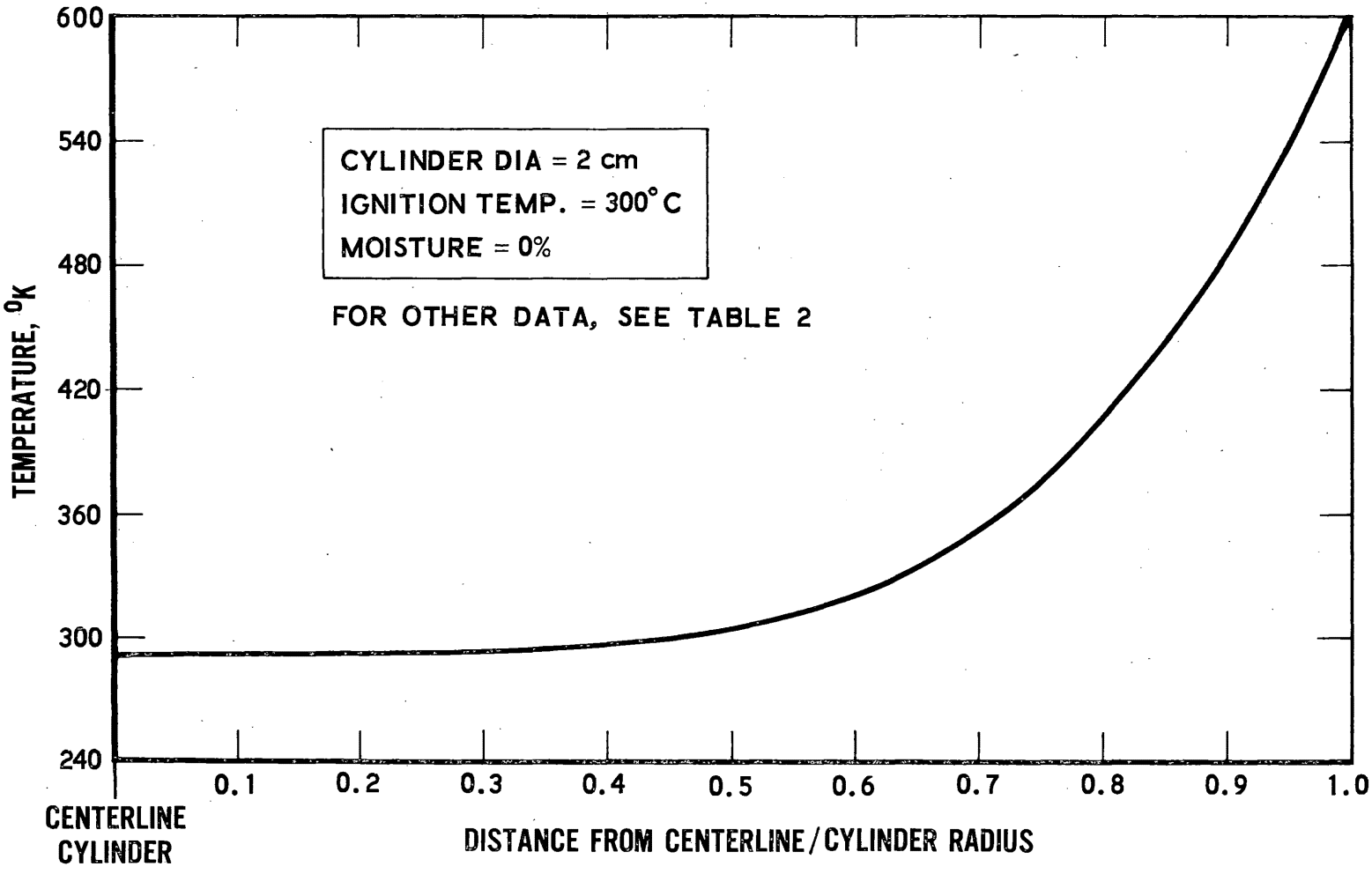

Fig. 26. Temperature Profile at Ignition in Wood Cylinder Heated in Firebrand Flame

It is known that Eq. (43) will not apply to small diameter fuel elements in which the centerline temperature will increase above ambient during the pre-ignition heating period. In Ref. 46, a constant (modifying factor) was used for correlation with experimental data but it appears that the modifying factor should be a function of fuel element diameter. Consequently, a correction is proposed to Eq. (43) in the form of

$$t'_{ign} = t_{ign}\left(\frac{D}{1.16}\right)^{0.5} \quad \text{for } D \leq 1.16 \text{ cm} \tag{43a}$$

For $D > 1.16$ cm, $t'_{ign} = t_{ign}$ calculated from Eq. (43). The moisture problem was also treated in a simplified way. The penetration distance, δ(cm), in which the temperature is raised above ambient can be calculated from

$$\delta = \sqrt{6\alpha_{fo} t'_{ign}} \quad \text{(Ref. 49)} \tag{44}$$

and the amount of moisture contained in it per unit of surface area is

$$W_M = M \cdot \delta \cdot \rho_{fo}$$

The additional time required to heat and evaporate W_M of water when the heat flux is $\bar{\dot{q}}_t$, is

$$\Delta t_{ign} = \frac{M \cdot \delta \cdot \Delta H_M \cdot \rho_{fo}}{\bar{\dot{q}}_t \cdot B} \tag{45}$$

where M is moisture fraction, ΔH_M is enthalpy increase of water, including latent heat of evaporation, and B is a correlation constant determined to match the computer calculation to be equal to 3. Consequently, for moisture function, M, the time to ignition will be

$$t''_{ign} = t'_{ign} + \Delta t \tag{46}$$

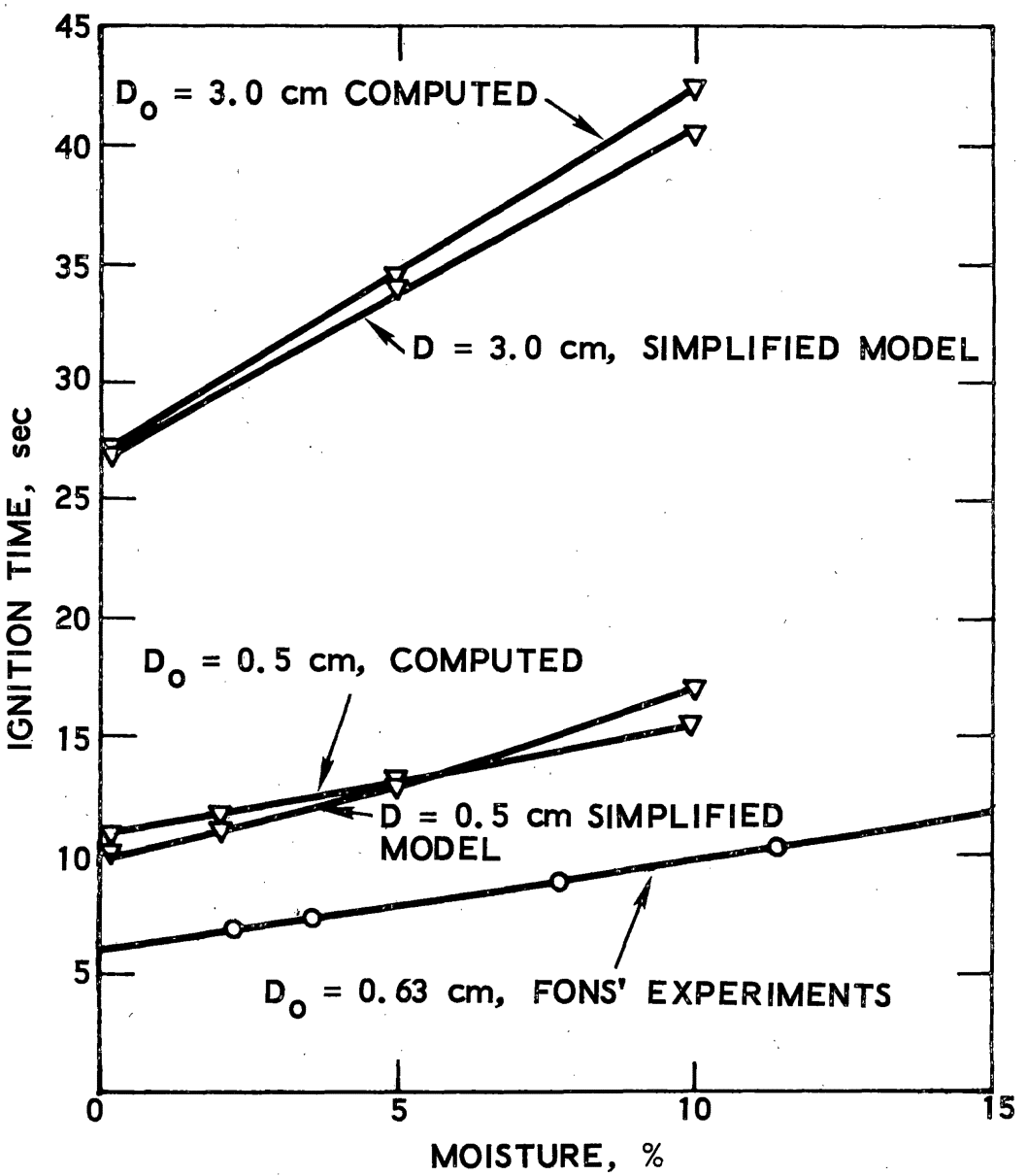

Fig. 27. Effect of Moisture on Ignition Time

5. STATISTICAL MODEL OF THE SPOT FIRE HAZARD

5.1 REVIEW OF PAST WORK

The objective of the work described in the preceding chapters was to develop analytical models of the various phases of firebrand phenomenology that enter into a statistical model of the spot fire hazard generated by firebrands.

Characterization of convection columns created above wild fires, the in-flight firebrand burning mechanism, and the trajectory was necessary to determine the impact point and the firebrand condition at the impact point. The spot fire hazard at any given distance from the fire front will be a function of the rate of firebrands impacting at that distance, of their lethality condition at impact (flame volume, duration), and of the virgin fuel ignitability at the impact point, which in turn will be a function of fuel type, size, loading, and moisture content.

The review of literature has not shown any detailed work done on this problem, although Berlad[53] presented general postulates of the spotting process. He postulated the autoignition temperature, T_c, of fuel as a significant parameter. If the array of fuel was at temperature $T > T_c$, then the descending firebrands would have a small effect on the fire spread, since the heat release rate from another source was already quite high. If, on the other hand, firebrands descend into a fuel array at $T < T_c$, they may create a spot fire if one assumes that the burning firebrand temperature $T_{frb} > T_c$. The firebrand will then make a significant contribution to the total energy release term. The relative importance of firebrands according to Berlad depends on the concentration of firebrands and on fuel ignition delay time. If the delay is relatively long, the firebrands may not be "terribly significant in the practical sense."

Berlad[54] addressed also the problem of long-range spotting and concluded that long-range firebrands (several miles) can be generated if there are strong convection columns that can carry the firebrands to altitudes as

Values for t_{ign} from the computer program, t_{ign} from Eq. (43) and values of t'_{ign} and t''_{ign} are shown in Table 3. The agreement between the two sets of data is reasonable.

The comparison of the ignition times calculated from Eqs. (43) and (46) with Fons' data from Ref. 51 is shown in Fig. 27. Fons' experiments were made with ponderosa pine which has lower density (~ 0.51 g/cm^3) and lower conductivity ($\sim 3 \cdot 10^{-4}$ cal/cm-sec-^{o}C) than the values for chaparral shown in Table 3. Furthermore, Fons carried out the ignition experiment in a heated furnace (1150^{o}F) and not by pilot ignition. However, his ignition surface temperature of 343^{o}C (650^{o}F) is close to 327^{o}C assumed for pilot ignition and applying correction factor of 0.6 (to account for density and conductivity difference) brings the calculated ignition values for an 0.5 cm cylinder close to his measured values for an 0.63 cm cylinder.

The equations and correlations presented heretofore will now permit the construction of a statistical model for spot fire hazard.

Table 3. Calculation of Fuel Ignition Time

		COMPUTER CALCULATIONS					SIMPLIFIED CALCULATIONS								
		t_{ign}, sec								M=0.02		M=0.05		M=0.10	
Dia., cm	$\bar{q}_t$, cal/cm^2, sec	M=0	M=0.02	M=0.05	M=0.10	δ, cm	t_{ign}, sec	t'_{ign}, sec	δ, * cm	Δt_{ign}	t''_{ign}	Δt_{ign}	t''_{ign}	Δt_{ign}	t''_{ign}
0.2	0.740	4.82	5.22	5.35	6.94	>0.10	11.47	4.76	0.195	0.80	5.56	2.00	6.76	4.00	8.76
0.5	0.635	10.74	11.66	13.08	15.60	>0.25	15.58	10.23	0.285	1.36	11.59	3.42	13.65	6.84	17.07
1.0	0.570	16.87	18.33	20.65	24.78	>0.50	19.34	17.95	0.378	2.00	19.95	5.00	22.95	10.00	27.95
2.0	0.518	23.45	25.67	29.00	35.31	0.57	23.42	23.42	0.432	2.54	25.96	6.35	29.77	12.70	36.12
3.0	0.488	27.51	30.21	34.53	42.29	0.75	26.40	26.40	0.459	2.86	29.26	7.16	33.56	14.32	40.72
4.0	0.470	30.38	33.49	38.94	47.96	0.76	28.44	28.44	0.476	3.08	31.52	7.71	36.15	15.42	43.86

ρ_{fo} = 0.75 g/cm^3 (chaparral)

c_{fo} = 0.34 cal/gm-^oC

k_{fo} = $3.4 \cdot 10^{-4}$ cal/cm-sec-^oC

α_{fo} = $1.33 \cdot 10^{-3}$ cm^2/sec

T_s = T_{ign} = 600^oK

T_l = 293^oK

$^*\delta = \sqrt{6 \cdot \alpha_{fo} \cdot t'_{ign}}$

high as 10,000 ft, if there is a strong wind, and if the burning firebrands can ignite fuel upon impact. These conclusions are in agreement with those expressed by the author in previous sections of this report.

Interesting experimental work on firebrand generation from wood-shingled roofs and other types was described in Ref. 55. Data presented on various sizes of firebrands collected (most of them with an area < 9 in.^{2}) indicated that wood-shingled roofs produced a greater number of brands, and that firebrand generation rate was greatly increased with increasing wind speed. It is also of interest to note that firebrands produced in the experiment appeared to be in a state of glowing combustion at the time of their generation or shortly thereafter.

An original probability model of the firebrand-created spot fire hazard was proposed by A. M. Rodriguez[56], and some of the methodology used in his work has been adopted in the model described below. Rodriquez made use of the author's experimental work on flaming duration and flame height, and taking into account the recipient bed fuel characteristics, constructed expressions for spot fire probability.

5.2 APPROACH TO THE MODEL

Firebrand generation depends on lifting forces produced by strong winds with an uplifting component. Such winds may be due to thermal buoyancy forces creating an uplift velocity as discussed in the two-dimensional convection column system, and/or pressure gradient forces associated with vortex flow, which was not dealt with here. The lifting of firebrands will also depend on the resistance offered by the attachment and weight of the firebrand, as well as its drag coefficient, which will depend on its size and shape.

It appears that the thermal buoyancy forces by themselves, i.e., without a pressure gradient, will probably not be large enough to create an updraft sufficient to lift large firebrands (diameter $\geq$ 2.5 cm). Consider, for instance, the Romero fire mentioned before and its maximum calculated

buoyant velocity of 13.34 m/sec (approximately 30 mph). The intensity of that fire at fuel loading of 1.6 lb/ft^2 and fire spread rate of 73 ft/min (see Table 1) was approximately 15,000 Btu/ft-sec. This can be considered a high-intensity fire, since according to Byram[57], intensities of the order of 20,000 to 30,000 Btu/ft-sec are associated with violent "blow-up fires." Even if the maximum fire spread rate were twice that of the Romero fire, the uplift velocity would increase only by a factor of $2^{1/3}$ or to 16.8 m/sec, and it would not be large enough for instance to lift 5 cm diameter pine cylinders. A second factor limiting the potential firebrand size which could be lifted by a two-dimensional column is a low uplift velocity near the ground at heights less than, say, 10 meters where, presumably, most of the potential firebrands will be situated. Thus, lifting of larger firebrands must be associated with transient gusts appearing at the fire front as a result of local accumulation of particularly flammable fuel, or as a result of locally-created vortices.

5.2.1 Firebrand Generation Function

If we denote:

P_l = gust probability

P_{lg} = lifting probability

P_g = lifting probability with gust present

P_{lng} = lifting probability without gust

then

$$P_l = P_{lg} \cdot P_g + P_{lng}(1 - P_g)$$

We can define the lifting probabilities as exponential functions

$$P_{lng} = 1 - \exp\ -k\left(\frac{\bar{v}^2}{v_{ic}^2} - 1\right) \qquad (47)$$

$$P_{lg} = 1 - \exp\left[-k_1\left(\frac{\bar{v}_g^2}{2 v_{ic}} - 1\right)\right] \qquad (48)$$

where

$\bar{v}$ = convection column uplift velocity at fuel bed maximum height

$\bar{v}_g$ = the average gust uplift velocity at fuel bed maximum height

$\bar{v}_{ic}$ = the lift velocity of firebrand size i

$$\left(\text{For cylindrical firebrands, } v_{ic} = \sqrt{\frac{\pi g}{2} \cdot \frac{\rho_{io}}{\rho_a} \cdot \frac{D_{io}}{C_D}}\right)$$

If $\bar{v}$ or $\bar{v}_g \leq v_{ic}$, P_{lng} or $P_{lg} = 0$. The k and k_1 are constants to be determined experimentally (they will probably be of the order 0.005 to 0.02).

The probability of gust P_g cannot be at present expressed analytically. If we equate gusts mainly to vortices referred to as fire whirls, then it is known that certain atmospheric and topographic conditions must exist to make the occurrence of vortices possible. It is proposed in our further work to define these conditions with an objective of real time "rating" of a fire front for fire whirl generation. The rating figures could be then associated with probability of occurrence.

The value of $\bar{v}_g$ will be determined from the fire whirl characterization. To calculate the probable rate of firebrands lifted, the total number of firebrands of size i has to be calculated for the fuel array from its known loading density and known dead fuel size distribution.

Denote:

D_{io} = initial firebrand diameter, cm

k_i = ratio of length/diameter of an average fuel element size i

W_i = weight per unit area of dead fuel size i in the fire front, g/cm^2

σ_i = ratio of fuel size i surface to volume, 1/cm

ρ_{io} = initial dead fuel (firebrand) density, g/cm^3

Assuming that all fuel of size i is composed of average size elements, then N_i, the number of potential firebrands per unit area of the burning zone, is equal to

$$N_i = \frac{1}{\pi \cdot 16 \cdot k_i} \cdot \sigma_i^3 \cdot \frac{W_i}{\rho_{io}}, \ 1/cm^2 \tag{49}$$

and

$$\dot{N}_i''' = N_i \cdot R, \ 1/cm\text{-}sec \tag{50a}$$

is the rate of potential firebrand per unit of flame front, if R = flame spread rate, cm/sec. The probable rate of firebrand generation per unit length of flame front is

$$\dot{N}_i'' = \dot{N}_i''' \cdot P_1, \ 1/cm\text{-}sec \tag{50b}$$

If the maximum trajectory range of firebrand size i is $X_{i\ max}$, and k_2 is a fraction of firebrands which impact the ground before burning out (determined from the trajectory and the shape of convection column), then

$$\dot{N}_i' = \dot{N}_i'' \cdot \frac{1}{X_{i\ max}} \cdot k_2, \ 1/cm^2\text{-}sec \tag{50c}$$

is the rate of firebrand falling per unit area ahead of the flame, assuming a uniform distribution of falling firebrands.

For a fuel cell of area A covered by fuel fraction $F = A_{fuel}/A$

$$\dot{N}_i = AF \cdot \dot{N}_i', \ 1/sec \tag{50d}$$

is the probable rate of firebrand impacting fuel in the cell A.

5.3 CRITERIA FOR VIRGIN FUEL IGNITION

5.3.1 Criterion of Firebrand Flaming Time

The flaming time of firebrand i after impact, when the diameter decreased from initial D_{io} to D_i and density from initial ρ_{io} to ρ_i must be greater than the ignition time of virgin fuel of size j. The flaming time of a firebrand can be calculated from Eq. (37), and the ignition time of fuel size j from Eq. (46). If $t_{fl(i)} < t_{ign(j)}$, no ignition will occur. If the j size was the smallest size of fuel in the recipient cell, then the firebrand of diameter D_i and density ρ_i will not present a fire hazard, and firebrands of larger diameter or greater density at impact have to be considered. If j was not the smallest size of fuel, the next smaller size will be considered in a similar manner. If $t_{fl(i)} > t_{ign(j)}$, firebrand flame volume and fuel "porosity" have to be compared.

5.3.2 Criterion of Firebrand Flame Volume

Fuel "porosity" defined as a volume fraction occupied by fuel size j

$$f_j = \frac{W_j}{\rho_j h_f} \tag{51}$$

where h_f = average bed height, cm, W_j = weight of dead fuel size j per unit area, g/cm^2, and ρ_j = density of virgin dead fuel size j, g/cm^3.

The flame volume can be calculated using Eq. (37a) flame height $\bar{h}_{fl\ i}$

$$V_{fl\ i} = 1.2\ D_i \cdot \bar{h}_{fl\ i} \cdot k_i D_i \cdot k_4 = 1.2 \cdot D_i^2 \cdot \bar{h}_{fl\ i} \cdot k_i \cdot k_3 \tag{52}$$

where $\bar{h}_{fl\ i}$ = average flame height of firebrand during the fuel heating period, cm, and k_3 = length fraction of burning firebrand.

We shall assume that the virgin fuel of diameter D_j will have a chance to be ignited if at least a length of it equal to its diameter[56] is immersed in flame. Then, the smallest fuel element volume of fuel size j

The probability of at least one spot fire is

$$P = 1 - \exp(-\lambda) \tag{57}$$

An example of a spot fire hazard calculation for the Romero fire (without gust) is presented in Appendix B.

The calculations have shown that with several values of constants assumed, a two-dimensional convection column associated with a fairly large Romero type fire can support flight of only smallest size firebrands (0.2 cm). These firebrands can ignite only smallest size dead fuels at short distances ahead of the fire front (20 m); but the probability of a spot fire at that distance is close to unity.

The approach presented here requires experimental verification. The main thrust of the experimental work should be in defining the firebrand generation parameters. The relationships between fuel type and size on one hand, and the convection column uplift velocity in firebrand formation on the other, is of particular importance in the whole analysis of the spot fire hazard.

If $V_{fl\ j} > V_{fl\ i}$, then $m_{jj} > m_{ij}$ and the probability of fire spreading in fuel size j will be at least as high as the probability of ignition. If $V_{fl\ j} < V_{fl\ i}$, then $m_{jj} < m_{ij}$. Only the smaller of the two, m_{jj} or m_{ij} will enter into the measure of the spot fire probability.

5.4 SPOT FIRE PROBABILITY

The expected number of spot fires per unit time $\dot{\lambda}$ in a fuel cell of area A is obtained by summation of all firebrand sizes multiplied by the expected number of fuel elements which can be ignited by each firebrand.

$$\dot{\lambda} = \sum_{i=1}^{I} \left[\dot{N}_i \cdot \sum_{j=1}^{J} \left\{ m_{jj}, m_{ij} \right\}_{min} \right] \tag{54}$$

where I and J are numbers of firebrand and recipient cell fuel size categories, respectively.

If we consider the flaming zone which may have a mosaic of different fuels and is, therefore, divided into fuel cells of width (perpendicular to the fire front) L, then burning time of that cell

$$t_B = \frac{L}{R} \tag{55}$$

If we consider that there may be a transient gust of duration t_g (sec), then the total expected number of fires during the burning time of a fire front L is

$$\lambda = \dot{\lambda} (t_B - t_g) + \dot{\lambda}_g \cdot t_g \tag{56}$$

where $\dot{\lambda}_g$ is calculated in a similar manner to $\dot{\lambda}$, except that because of greater uplift velocities, larger sizes of firebrands will be carried ahead of the main fire front over larger than X distances X_g. If a recipient fuel cell is located at distance X' such that $X < X' < X_g$, $\dot{\lambda}$ becomes zero, and the only firebrands will be those generated by the gust.

The probability of at least one spot fire is

$$P = 1 - \exp(-\lambda) \tag{57}$$

An example of a spot fire hazard calculation for the Romero fire (without gust) is presented in Appendix B.

The calculations have shown that with several values of constants assumed, a two-dimensional convection column associated with a fairly large Romero type fire can support flight of only smallest size firebrands (0.2 cm). These firebrands can ignite only smallest size dead fuels at short distances ahead of the fire front (20 m); but the probability of a spot fire at that distance is close to unity.

The approach presented here requires experimental verification. The main thrust of the experimental work should be in defining the firebrand generation parameters. The relationships between fuel type and size on one hand, and the convection column uplift velocity in firebrand formation on the other, is of particular importance in the whole analysis of the spot fire hazard.

6. CONCLUSIONS

1. An analytical method was proposed for prediction of spot fire hazard caused by flying firebrands. The analytical treatment included all phases of firebrand history although it was confined only to the flaming combustion of the firebrand as being more hazardous. Outside of the computer trajectory program, the methodology applied was based on approximate but simple analytical expressions. Using these expressions, an example of spot fire probability for the Romero fire was calculated in Appendix B.

2. The two-dimensional convection column generates buoyancy forces which, even for large fires, are not strong enough to lift firebrands larger than, say, one-inch diameter. The impact distance of small firebrands left with sufficient burning time to ignite the recipient fuel will, in most cases, be limited to a few hundred feet. However, the probability of at least a single spot fire from the shower of small brands will be very high.

3. There is a need for further analytical and experimental work in at least the following areas:

   a. It is necessary to establish the relationship between the rate, and size of firebrand generation on one hand and the fuel type and convection column characteristics on the other. Experimental data in this area are mandatory to verify firebrand generation functions.

   b. The process of burning of firebrands in flight should be further explored experimentally to establish the relationship between the change in the firebrand mass and size with time as a function of its initial size, fuel type and relative velocity.

   c. The regime of glowing versus flaming combustion time of firebrands should be explored experimentally and recipient fuel ignition criteria with glowing firebrands should be postulated.

   d. Fire-created vortices (fire whirls) should be characterized in simple terms and these terms should be verified experimentally. This is of particular importance for long range spotting since from past observations of various fires, fire whirls can lift large size brands to considerable heights.

APPENDIX A

NATURAL WOOD SURFACE DETERMINATION AND FLAMING TIME COMPARISON

Natural wood's surface determination is necessary because of the importance of surface to volume ratio on the burning rate. The natural woods have mostly irregular shapes in the form of tapering branches with attached twigs, leaves, etc. The method used in this work consisted of immersion, after weighing, of the specimen in molten wax (we used Parawax at $100^{\circ} \pm 1^{\circ}C$), lightly shaken off after immersion, letting it solidify, and then weighing it again.

The thickness of the solidified wax layer was determined from wax immersion of fabricated wood shingles and cylinders of known surface and volume. Equivalent diameter of a shingle was calculated as $D = 4V/S$.

WAX LAYER THICKNESS

	Dia · Length, cm	Wax Thickness, cm	Fuel Type
Cylinders	2.5 · 10.38	0.01465	Birch
	1.78 · 7.50	0.01455	Douglas Fir
	1.25 · 7.60	0.01350	Birch
	0.64 · 4.90	0.0128	Birch
Shingle	0.26 · 3.55 · 6.1 (Equiv D = 0.47 cm)	0.0140	Cedar

For the cylindrical samples, the wax thickness appears to be a weak function of cylinder diameter, but in further experiments with natural fuels which had equivalent diameter ($D = 4V/S$) less than 0.5 cm a wax layer thickness of 0.013 cm was assumed. The total surface of the specimens was determined by dividing wax weight by wax density ($0.895\ g/cm^3$) and by wax layer thickness. The specimen volume was calculated from its known weight and known fuel density.

The shortcoming of this method was that wax-treated specimens could not be used in burn experiments and it was, therefore, necessary to always provide two "similar" specimens of which one was used for surface determination and the other one for the burning test. There was, of course, an error introduced in the degree of "similarity" of the specimens which could only be assessed visually and by weighing.

All specimens, cylinders, flat plates and natural woods were reduced to the equivalent diameter, D = 4V/S, and flaming time calculated from Eq. (36). The $t_{fl} = 80 \cdot D^{1.25}$ was then compared against experimental values. The table below shows some of the results.

FLAMING TIME BASED ON EQUIVALENT Dia = 4V/S

Type of Wood	Shape	Equivalent Dia, cm	Measured* Flaming Time, sec	Calculated Flaming Time, sec
White Sage	Irregular	0.38	22	23.9
Chemise	Irregular	0.20	26	11.0
Cedar	Shingle	1.06	80	86.0
Cedar	Shingle	0.50	28	33.0
Birch	Cylinder	0.66	40	47.6
Birch	Cylinder	1.25	125	105.0
Birch	Cylinder	2.54	230	256.0
Pine	Square Column	1.23	100	103.0
Birch	Sphere	2.50**	230	256.0

*Average from several samples

**Equivalent diameter for sphere, D = 6V/S

Thus, it appears that flaming times of various shapes of most wood specimens can be calculated by the formula for f_t quoted above when the equivalent diameter is defined as D = 4V/S. Chemise, however, had a longer flaming time than calculated.

APPENDIX B

EXAMPLE CALCULATION FOR ROMERO FIRE SPOT FIRE HAZARD ASSESSMENT

The calculation is made for a two-dimensional convection column characterized for one phase of the Romero fire with no gust.

Starting with the smallest fuel size, (fuel was chaparral), with surface to volume ratio $\sigma = 640/ft^{-1}$:

Calculated mean diameter: $D_o = 4/\sigma = 0.2$ cm

Critical lift velocity:

$$v_{ic} = w_f = \sqrt{\frac{g}{C_D} \cdot \frac{\rho_f}{\rho_a} \cdot \frac{\pi}{2} \cdot D_o}$$

$$= \sqrt{\frac{981}{2.0} \cdot \frac{0.73}{1.2 \cdot 10^{-3}} \cdot \frac{3.14}{2} \cdot 0.2} = 306 \text{ cm/sec}$$

$C_D = 2$, $\rho_f = 0.73$ g/cm^3, $\rho_a = 1.2 \cdot 10^{-3}$ g/cm^3

The convection column vertical velocity at height of fuel array, $h_f = 7.5$ ft = 228.6 cm, is

$$u_f = u_o\sqrt{\frac{h_f}{L_o}} = 1334\sqrt{\frac{228.6}{3780}} = 328 \text{ cm/sec}$$

Comparing w_f with u_f, it can be seen that the smallest size fuel can just be lifted and that the next size (0.96) cm dead fuels could not be lifted.

At a distance "a" 20 m from the column front, and flight duration of 5 sec, firebrands 0.2 cm will impact with approximately the same diameter but with the density reduced from the original value of 0.73 g/cm^3 to $\rho_i = 0.29$ g/cm^3. The remaining flaming time from Eqs. (36) and (37) is

$$t'_{fl} = t_{fl} - D_i \cdot K \cdot \ln \frac{80 - \rho_c}{\rho_i - \rho_c}$$

The value of K for 0.2 cm is not 55 but 17 (see Fig. 23). The ρ_c - burn out density for the 0.2 cm size is $0.06 \cdot \rho_o = 0.044$ g/cm^3.

$$t'_{fl} = 10.7 - 0.2 \cdot 17 \cdot \ln \frac{0.73 - 0.044}{0.29 - 0.044} = 10.7 - 3.5 = 7.2 \text{ sec}$$

At approximately "b" distance 75 m from the column, the firebrand density is down to 0.19 g/cm^3 with the diameter reduced to 0.16 cm. The remaining flaming time after impact calculated in a manner similar to the above is

$$t_{fl_b} = 8.0 - 3.9 = 4.1 \text{ sec}$$

The ignition time of the smallest size dead fuel in the recipient bed ($\sigma = 640\,\text{ft}^{-1}$, $D_o = 0.2$ cm) can be calculated from Eq. (46), or read from Table 3 as $t'_{ign} = 4.74$ sec.

Comparing the flaming and ignition time, it appears that any firebrands falling at 20 m ahead of the fire may be able to ignite the smallest dead fuel sizes ($t'_{fl} > t_{ign}$) and that 0.2 cm firebrands falling at 75 m or beyond will not have sufficient flaming time left for fuel ignition.

The average flame height h_{fl} can be calculated from Eq. (37a)

$$\bar{h}_{fl} = 163 \cdot \bar{\dot{m}}_i^{0.662}$$

where

$$\bar{\dot{m}}_i = \frac{\pi D_i^2}{4} \cdot (\rho_i - \rho_{fl}) \cdot \frac{1}{t'_{fl}}$$

where ρ_{fl} is the flame density from Fig. 23 equal to $0.1\rho_o = 0.073$ g/cm^3 and flame volume from Eq. (52) is

$$V_{fl} = 1.2 \cdot D_i^2 \cdot \bar{h}_{fl} \cdot k_i \cdot k_3 = 1.2 \cdot 0.2^2 \cdot 1.62 \cdot 0.5 \cdot 10 = 0.39 \text{ cm}^3$$

where k_4 = length fraction of the burning firebrand, assumed = 0.5 and k_i = firebrand length to diameter ratio, assumed = 10. For the recipient dead fuel size j = 0.2 cm (the only one that could be ignited), the fuel "porosity" factor [see Eq. (51)]

$$f_j = \frac{W_j}{\rho_j \cdot h_f} = \frac{0.194}{46 \cdot 7.5} = 5.62 \cdot 10^{-4}$$

where W_j, ρ_j, h_f is obtained from Romero fuel bed data.

The minimum volume of dead fuel element of size j which must be ignited is

$$V_j = \frac{\pi}{4} \cdot D_j^3 = \frac{\pi}{4} \cdot 0.2^3 = 6.28 \cdot 10^{-3} \text{ cm}^3$$

The flame volume V_{fl} must be greater than the fuel element volume and this condition is satisfied in the above example. The expected number of fuel size j ignited by one firebrand i [Eq. (53)]

$$m_{ij} = \left(\frac{V_{fl} \cdot 4}{D_i^3} - 1 \right) \cdot f_j = 0.034$$

In order to calculate the probable number of firebrands, the firebrand generation function proposed before is used

$$P_{lng} = 1 \exp \left[-k \left(\frac{\bar{V}^2}{V_{ic}^2} - 1 \right) \right]$$

The k is an unknown constant, but if we assume that for $\bar{V} = 2V_{ic}$, 10 percent of potential firebrands will be lifted, then k = 0.035, and for the values established before $\bar{V}$ = 3.28 cm/sec and V_{ic} = 3.06 cm/sec.

$$P_l = P_{lng} = 1 - \exp \left[-0.035 \left(\frac{3.28^2}{3.06^2} - 1 \right) = 0.0052 \right]$$

The potential number of firebrands size i (0.2 cm) per unit area of the burning cell, Eq. (49)

$$N_i = \frac{1}{\pi \cdot 16 \cdot k_i} \cdot \sigma_i^3 \cdot \frac{W_i}{\rho_{io}}$$

Substituting values from available fuel bed data, we find

$$N_i = \frac{1}{\pi \cdot 16 \cdot 10} \cdot 640^3 \cdot \frac{0.194}{46} = 2199.4 \ 1/cm^2$$

The rate of potential firebrand [Eq. (50a)] per unit of flame front

$$\dot{N}_i''' = N_i \cdot R$$

where R is the fire spread rate (obtained from Rothermel's program) = 37.1 cm/sec and N_i''' = 81597.7 1/cm-sec. The probable rate of firebrand generation [Eq. (50b)]

$$\dot{N}_i'' = \dot{N}_i''' \cdot P_1 = 8.597.7 \cdot 0,0052 = 424.3, 1/cm\text{-}sec$$

The maximum distance which 0.2 cm firebrands can travel before burnout was calculated from the trajectory program as $X_{i\ max}$ = 229 m.

Rate of firebrands falling on recipient fuel unit area [Eq. (50c)]

$$\dot{N}_i' = N_i'' \cdot \frac{1}{X_{i\ max}} k_2 = 424.3 \cdot \frac{1}{22900} \cdot 0.6 = 0.0111, \ 1/cm^2\text{-}sec$$

where k_2 is the fraction of firebrands impacting the ground from trajectory program = 0.6. Recipient cell has an area of 100 · 100 cm and is covered with fuel throughout so that fuel fraction F = 1.

The probable rate of firebrands impacting the recipient cell

$$\dot{N}_i = A \cdot \dot{N}_i' = 0.0111 \cdot 1 \cdot 10^4 = 111, \ 1/\text{sec}$$

Expected rate of fuel size j ignited by firebrands size i in the fuel cell

$$\dot{\lambda} = \dot{N}_i \cdot m_{ij} = 111 \cdot 0.034 = 3.77, \ 1/\text{sec}$$

If the burning cell has the same width (L = 100 cm) as the recipient one, the burning time is

$$t_B = \frac{L}{R} = \frac{100}{37.1} = 2.69 \text{ sec}$$

and the number of fuel elements size j ignited

$$\lambda = \dot{\lambda} \cdot t_B = 3.77 \cdot 2.69 = 10.14$$

and the probability of at least one spot fire

$$P = 1 - \exp(-\lambda) = 0.99996$$

With the reservation that the several constant values are assumed quite arbitrarily, it appears that near the fire front the probability of spot fire by small flaming embers is very high. The results will not be significantly different even with considerable change in the constant values. They confirm the observations of a shower of sparks falling ahead of the fire front. If the convection column could support flight of larger size firebrands, their number would be significantly smaller than that of 0.2 cm size considered here, their trajectory would be much longer, and the calculated probability of a single fire would be of considerably lower value than that arrived at above.

REFERENCES

1a. Tarifa, C. Sanchez, "Transport and Combustion of Firebrands," Final Report of Grants FG-SP-114 and FG-SP 146 (Vol. II), Aeronautical Institute of Madrid, May 1965.

1b. Tarifa, C. Sanchez, "On the Flight Paths and Lifetimes of Burning Particles of Wood," Tenth Combustion Symposium (1964), The Combustion Institute, 1965, pp. 1021-1037.

2. Clements, H. B., "Lift-Off of Firebrands," Southern Forest Fire Laboratory, private communication.

3a. Lee, S. -L. and J. M. Hellman, "Study of Firebrand Trajectories in a Turbulent Swirling Natural Convection Column," Combustion and Flame, 13, 1969, pp. 645-655.

3b. Lee, S. -L and J. M. Hellman, "Firebrand Trajectory Study Using an Empirical Velocity-Dependent Burning Law," Combustion and Flame, 15, 1970, pp. 265-274.

4. Young, P. H., "Firebrand Trajectory Model," Aerospace Report No. ATR-73(8158)-1, The Aerospace Corporation, El Segundo, California, June 1973.

5. Stevenson, A. E. and D. A. Schermerhorn, "Aerial Fire Suppression Techniques Program - Forest Service, U. S. Department of Agriculture Forest Fire Model Evaluation Final Report, 13 April to October 1972," Aerospace Report No. ATR-73(7289)-2, The Aerospace Corporation, El Segundo, California, 20 October 1972.

6. Countryman, C. M., "Project Flambeau," Final Report, 1, Pacific Southwest Forest and Range Experiment Station, 1969.

7. Schmidt, W., "Turbulente Ausbreitung eines Stromes Erhitzer Luft," Zeitschrift fur Angewandte Mathematic und Mechanik, 21, 1941.

8. Rouse, H., C. S. Yih, and H. W. Humphreys, "Gravitational Cavitation from a Boundary Source," Tellus, 4(3), August 1952.

9. Taylor, G. I., "Fire Under Influence of Natural Convection," International Symposium on the Use of Models in Fire Research, National Academy of Sciences, National Research Council, 1961.

10. Morton, B. R., "Turbulent Gravitational Convection from Maintained and Instantaneous Sources," Proc. Roy. Soc., 234A, January 1956.

REFERENCES (Continued)

11. Morton, B.R., "The Ascent of Turbulent Forced Plumes in a Calm Atmosphere," Int. J. Air Pollution, 1, 1959.

12. Morton, B.R., "Modeling Fire Plumes," Tenth Symposium on Combustion (1964), The Combustion Institute, 1965.

13. Thomas, P.H., "The Size of Flames from Natural Fires," Ninth Symposium on Combustion (1962), The Combustion Institute, 1963.

14. Thomas, P.H., R. Baldwin, and A.J.M. Heselden, "Buoyant Diffusion Flames: Some Measurements of Air Entrainment, Heat Transfer, and Flame Merging," Tenth Symposium on Combustion (1964), The Combustion Institute, 1965.

15. Thomas, P.H., "Some Aspects of the Growth and Spread of Fire in the Open," Forestry, 40, 1967.

16. Putnam, A.A., "A Model Study of Wind-Blown Free Burning Fires," Tenth Symposium on Combustion (1964), The Combustion Institute, 1965.

17. Lee, Shao-Lin, and H.W. Emmons, "A Study of Natural Convection Above a Line Fire," J. of Fluid Mechanics, 11, 1961.

18. Albini, F.A., "A Physical Model for Fire Spread in Brush," Eleventh Symposium on Combustion (1966), The Combustion Institute, 1967.

19. Taylor, R.J., et al, "Convection Activity Above a Large Scale Brush Fire," CSIRO Division of Atmospheric Physics, Victoria, Australia.

20. Fons, W.L., "Project Fire Model," U.S. Department of Agriculture Forest Service, May 1960.

21. Stevenson, A.E., et al, "Computer Simulation of an Actual Forest Fire," Spring Meeting of the Western States Combustion Institute, April 1973.

22. Roberts, A.F., "A Review of Kinetics Data for the Pyrolysis of Wood and Related Substances," Combustion and Flame, 14, 1970.

23. Kung, Hsiang-Cheng and A.S. Kadelkaz, "On the Heat of Reaction in Wood Pyrolysis," Western Combustion Institute Spring Meeting, Tempe, Arizona, April 1973.

REFERENCES (Continued)

24. Kanury, A. Murty, "Thermal Decomposition Kinetics of Wood Pyrolysis."

25. Kanury, A. Murty, "Ignition of Cellulosic Solids - A Review," Fire Research Abstracts and Reviews, 14(1), 1972.

26. Tinney, E. Roy, "The Combustion of Wooden Dowels in Heated Air," Tenth Symposium on Combustion, The Combustion Institute, 1965.

27. Alvarez, N. J. and S. B. Martin, "Mechanism of Ignition of Thermally Irradiated Cellulose," Thirteenth Symposium on Combustion, The Combustion Institute, 1971.

28. Simms, D. L., "Ignition of Cellulosic Materials by Radiation," Combustion and Flame, iv(4), December 1960.

29. Blackshear, P. L. and A. M. Kanury, "On the Combustion of Wood. I. A Scale Effect in the Pyrolysis of Solids," Combustion Science and Technology, 2, 1970.

30. Blackshear, P. L. and K. A. Murty, "Heat and Mass Transfer To, From and Within Cellulosic Solids Burning in Air," Tenth Symposium on Combustion, The Combustion Institute, 1965.

31. Martin, S., "Ignition of Organic Materials by Radiation," Fire Research Abstracts and Review, 6, 1964.

32. Martin, S., "Diffusion-Controlled Ignition of Cellulosic Materials by Intense Radiant Energy," Tenth Symposium on Combustion, The Combustion Institute, 1969.

33. Kosdon, F. J., F. A. Williams and C. Boman, "Combustion of Vertical Cellulosic Cylinders in Air," Twelfth Combustion Symposium, The Combustion Institute, 1969.

34. Clements, H. B. and A. Alkidas, "Combustion of Wood in Methanol Flames," USDA Forest Service, Macon, Georgia, October 26, 1972.

35. Roberts, A. F., "Problems Associated with the Theoretical Analysis of the Burning of Wood," Thirteenth Symposium on Combustion, The Combustion Institute, 1971.

36. Emmons, H. W., "Fundamental Problems of the Free Burning Fire," Tenth Symposium on Combustion, The Combustion Institute, 1965.

37. Baumford, C.H., J. Crank, and D.H. Molan, "The Combustion of Wood, Part I," Proceedings of Cambridge Philosophical Society, 42(2), June 1946.

38. Anderson, H.E., et al, "Mechanisms of Fire Spread Research Progress Report No. 2," U.S. Forest Service Research Paper INT-28, 1966.

39. Fons, W.L., H.B. Clements and P.M. George, "Scale Effects on Propagation Rate of Laboratory Crib Fires."

40. Anderson, H.E., "Heat Transfer and Fire Spread," USDA Forest Service Research Paper INT-69, 1969.

41. Fons, W.L., "Analysis of Fire Spread in Light Forest Fuels," Journal of Agricultural Research, 72(13), February 1946.

42. Byram, G.M., et al, "Thermal Properties of Forest Fuels," U.S. Department of Agriculture, Division of Fire Research, October 1952.

43. Jakob, Max, Heat Transfer, Vol. I, John Wiley and Sons, New York, 1967.

44.* Weinberg, E.K., "Parametric Study for Determining Total Flame Heat Transport to Fine Natural Fuel Twigs and Branches," Report No. ATM-73(8158)-2, The Aerospace Corporation, 8 March 1973.

45. Kanury, A.M. and P.L. Blackshear, Jr., "On the Combustion of Wood, II: The Influence of Internal Convection on the Transient Pyrolysis of Cellulose," Combustion Science and Technology, 2, 1970.

46. Koohyar, A.N., J.R. Welker, and C.M. Sliepcender, "The Irradiation and Ignition of Wood by Flame," Fire Technology, 4, 1968.

47. Simms, D.L. and M. Law, "The Ignition of Wet and Dry Wood by Radiation," Combustion and Flame, 11, 1967.

48. Sauer, F.M., "The Charring of Wood During Exposure to Thermal Radiation," U.S. Department of Agriculture, Division of Fire Research, Interim Technical Report AFSWP-868, August 1956.

*Aerospace internal correspondence. Not available for external distribution.

REFERENCES (Concluded)

49. Goodman, T. R., Application of Integral Methods to Transient Nonlinear Heat Transfer, Academic Press, 1964.

50. USDA Forest Service Research "Moisture Content Influences Ignitability of Slash Pine Litter," Note SE-173, May 1972.

51. Fons, W. L., "Heating and Ignition of Small Wood Cylinders," Industrial and Engineering Chemistry, 42(10), November 1950.

52. Felske, J. D. and C. L. Tien, "Calculation of the Emissivity of Luminous Flames," Combustion Science and Technology, 7, 1973.

53. Berlad, A. L., "Fire Spread in Solid Fuel Arrays," Combustion and Flame, 14, 1970.

54. Berlad, A. L. and S. L. Lee, "Long Range Spotting," Combustion and Flame, 12, 1968.

55. Waterman, T. E., "Experimental Study of Firebrand Generation," Report NRDL-TRC-69-19, January 1969.

56.* Rodriguez, A. M., "Probability Model for Fire Spreading by Fallout of Lofted Debris," Aerospace IOC A73-5414.5-01, The Aerospace Corporation, El Segundo, California, 30 January 1973.

57. Byram, G. M., "Forest Fire Behavior," Forest Fire, Control and Use, McGraw-Hill Book Co., 1959.

*Aerospace internal correspondence. Not available for external distribution.

SYMBOLS

a	pre-exponential constant, sec^{-1}
A	firebrand maximum cross-section, cm^2
A	convection column width at height y, cm/sec
A_g	$2\ b_g$ - convection column width on the ground, cm
A_o	$2\ b_o$ - convection column width at height L, cm
b_g	half width of convection column at the ground, cm
b_o	half width of convection column at height L, cm
B	constant
c_f	specific heat of fuel, cal/g-^oC
c_{fo}	specific of dry fuel, cal/g-^oC
c_p	air (gas) specific heat, cal/g-^oC
c_r	radiation loss factor
C_D	drag coefficient
D	firebrand or fuel diameter, cm
D_i	firebrand impact diameter, cm
D_{io}	initial firebrand diameter, cm initial L size firebrand diameter, cm
D_j	recipient fuel size j diameter, cm
D_o	initial firebrand or fuel diameter, cm
E	activation energy, cal/g-mole
f_j	volume fraction occupied by fuel j
F	fuel fraction

SYMBOLS (Continued)

g	gravitational constant, cm/sec^2
h	firebrand flame height, cm
h_f	average fuel bed height, cm
h_{fl}	average flame height, cm
$h_{fl\ i}$	average flame height of firebrand during fuel heating period, cm
$h_{fl\ j}$	flame height of fuel size j, cm
h_g	height for constant velocity u_g, cm
H	heat release per unit of length, Btu/cm
H_{comb}	heat of fuel combustion, cal/g
k	shape factor
k	gas thermal conductivity, cal/cm-sec, ^oC
k_f	thermal conductivity of fuel (wood), cal/cm-sec, ^oC
k_{fo}	thermal conductivity of dry fuel (wood), cal/cm-sec, ^oC
k_i	ratio of length/diameter fuel element size i
k_2	fraction of firebrand impacting the ground
k_3	length fraction of burning firebrand
K	constant, cm/sec
L	flame height or length, cm
L	width of a fuel cell, cm
L_o	initial firebrand length, cm
m	firebrand mass, g
$\dot{m}$	firebrand mass loss rate, g/cm-sec

SYMBOLS (Continued)

m_{ij}	number of fuel elements size j in the flame of firebrand i
M	moisture fraction
$\dot{M}_{air}$	entrained air mass flow rate per unit of flame front, g/cm-sec
$\dot{M}_f$	fuel mass flow rate per unit of flame front, g/cm-sec
$\dot{M}_t$	total mass flow rate per unit of flame front, g/cm-sec
N_{Gr}	Grashof Number
N_i	number of potential firebrands per unit area, cm^{-2}
$\dot{N}_i$	probable rate of firebrand in fuel cell, sec^{-1}
$\dot{N}_i'$	probable rate of firebrand in fuel cell, sec^{-1}
$\dot{N}_i''$	rate of firebrand per unit of flame front, cm^{-1}, sec^{-1}
$\dot{N}_i'''$	rate of potential firebrand per unit of flame front, cm^{-1}, sec^{-1}
N_{Nu}	Nusselt Number
N_{Pe}	Peclet Number
N_{Pr}	Prandtl Number
P	probability of one spot fire
P_g	gust probability
P_l	lifting probability
P_{lg}	lifting probability with gust
P_{lng}	lifting probability without gust
$\dot{q}_c$	net convective heat flux, cal/cm^2-sec
$\dot{q}_r$	net radiative heat flux, cal/cm^2-sec
$\dot{q}_t$	total heat flux, cal/cm^2-sec

SYMBOLS (Continued)

Q	constant
$\dot{Q}$	heat rate moisture evaporation
$\bar{r}$	mean fuel radius, cm
R	universal gas constant, 1.987 cal/g-mole-^{o}K
R	flame spread rate, cm/sec
R	radius of wood cylinder
S	surface, cm^2
S_i	firebrand surface at impact, cm^2
S_o	initial firebrand surface, cm^2
t	burn time, sec
t_b	gust duration, sec
t_B	burning time of fuel cell, sec
t_{fl}	flaming time of virgin firebrand, sec
t'_{fl}	flaming time of firebrand at impact condition, sec
t_{ign}	time to firebrand (wood) ignition, sec
t'_{ign}	corrected time to ignition, sec
t''_{ign}	ignition time of moist fuel, sec
T	pyrolysis or gas temperature, ^{o}K
T_1	ambient air temperature, ^{o}K
T_{fl}	characteristic flame temperature, ^{o}K
T_s	surface temperature, ^{o}K
u	wind velocity, cm/sec

SYMBOLS (Continued)

u	vertical gas velocity at height y, cm/sec
u_f	vertical gas velocity at height of fuel array, cm/sec
u_g	vertical gas velocity at the ground, cm/sec
u_o	vertical gas velocity at height L, cm/sec
v	absolute velocity of a firebrand, cm/sec
v	entrained air velocity at height y, cm/sec
$\bar{v}$	convection column velocity at fuel bed height, cm/sec
$\bar{v}_g$	average gust velocity at fuel bed height, cm/sec
$\bar{v}_{ic}$	lift velocity of firebrand size i, cm/sec
V	volume, cm^3
V_{fl}	flame volume
V_{fli}	flame volume of firebrand size i, cm^3
V_{flj}	flame volume of a fuel size j, cm^3
V_i	firebrand volume at impact, cm^3
V_j	volume of fuel element j, cm^3
V_o	initial firebrand volume, cm^3
w	firebrand velocity relative to wind, cm/sec
w_{fo}	initial firebrand fall velocity, cm/sec
$w_{f(t)}$	firebrand fall velocity at time t, cm/sec
W_i	dead fuel weight size i per unit area, g/cm^2
W_j	dead fuel weight size j per unit area, g/cm^2
W_n	fuel bed loading for one size fuel, g/cm^2

SYMBOLS (Continued)

α	angle, deg
α	air entrainment coefficient
α	gas thermal diffusivity, cm^2/sec
α_f	fuel thermal diffusivity, cm^2/sec
α_{fo}	thermal diffusivity of dry fuel, cm^2/sec
β	surface absorptivity
σ	Stefan-Boltzmann constant = $1.36 \cdot 10^{-12}$ $cal/cm^2\text{-}sec\text{-}^oK^4$
δ	heat penetration distance, cm
ΔH_M	enthalpy increase of heated water, cal/g
ϵ	flame emissivity
ϵ_s	surface emissivity
θ	angle of plume tilt from vertical, deg
λ	number of expected spotfires in a fuel cell
$\dot{\lambda}$	rate of expected spot fires in a fuel cell, sec^{-1}
μ	gas dynamic viscosity, g/cm-sec
μ_a	absolute viscosity
ν	gas kinematic viscosity, cm^2/sec
ρ	firebrand or wood density, g/cm^3
ρ	gas density in the convection column, g/cm^3
ρ_a	air density
ρ_c	final density of firebrand, g/cm^3
ρ_F	density of fuel (wood), g/cm^3

SYMBOLS (Concluded)

$\rho_{f\ impact}$	density of fuel and at impact, g/cm^3
ρ_{fl}	gas density, g/cm^3
ρ_{fl}	density of firebrand at the end of flaming, g/cm^3
ρ_{fo}	density of dry fuel, g/cm^3
ρ_g	gas density in the convection column at the ground, g/cm^3
ρ_i	firebrand impact density, g/cm^3
ρ_{io}	initial dead fuel (firebrand) density, g/cm^3
ρ_j	density of dead fuel size, j, g/cm^3
ρ_o	initial firebrand (wood) density, g/cm^3
$\rho_{(t)}$	firebrand (wood) density at time t, g/cm^3
ρ_{wo}	virgin wood density
ρ_l	ambient air density, g/cm^3
σ_i	ratio of fuel size i surface to volume, cm^{-1}
τ_{res}	flame residence time, sec